LIFETIME ANALYSIS OF SKELETAL MUSCLE PATHOLOGY IN THE MUSCULAR DYSTROPHY X-LINKED MOUSE

A Dissertation

by

RYAN THOMAS MASSOPUST

Submitted to the Office of Graduate and Professional Studies of
Texas A&M University
in partial fulfillment of the requirements for the degree of

DOCTOR OF PHILOSOPHY

Chair of Committee,	Jennifer Dulin
Committee Members,	Dylan McCreedy
	Uel J. McMahan
	Mendell Rimer
Interdisciplinary Program Chair,	Michael Smotherman

May 2020

Major Subject: Neuroscience

ABSTRACT

Duchenne muscular dystrophy (DMD) is an X-linked muscle wasting disease that affects 1:3500 males at birth. Mutations in the *DMD* gene alter the reading frame, preventing expression of functional dystrophin protein. Dystrophin functions to connect the intracellular cytoskeleton to the extracellular matrix, facilitating lateral transmission of force during muscle contraction. Without dystrophin, skeletal muscles are susceptible to repeated cycles of contraction-induced damage and repair. Eventually, repair mechanisms fail and muscle is replaced by fibrotic and adipose tissue, leading to muscle weakness, loss of ambulation and premature death.

The muscular dystrophy X-linked mouse (mdx) is the most commonly used preclinical model for DMD. Although disease progression in the mouse does not perfectly model the human disease, it shares many of the same pathological features. Early characterizations of the model reported severe pathology through early adulthood followed by disease stabilization. As a result, research in the mdx mouse has largely neglected to describe pathology in aged animals.

The overarching goal of these studies is to improve the understanding of the mdx mouse model by tracking pathological features of the disease throughout life. We performed a thorough characterization of myofiber pathology in mdx mice from 2 weeks to 2 years of age. Using unique preparations to analyze mdx tissue from a new perspective, we identify a previously underappreciated feature of mdx pathology and extend the knowledge of hallmark features by tracking them throughout life. We report

that individual mdx muscle fibers undergo progressive hypertrophy that continues through the lifespan. Despite massive hypertrophy on the myofiber level, we report no hypertrophy on the muscle level. These seemingly contradictory findings are explained by previously underappreciated myofiber loss in mdx mice. We therefore conclude that the utility of the mdx mouse in testing therapeutics is target dependent. Specifically, the mdx mouse is an excellent model for a therapeutic intending to prevent myofiber loss, but a poor model for one aimed at inducing myofiber hypertrophy. During the generation of these findings we improved the utility of tissue clearing techniques in skeletal muscles by characterizing compatibility with neuromuscular junction markers useful for the study of neuromuscular disease.

DEDICATION

This dissertation is dedicated to my parents in gratitude for the lessons they taught me by example. My father taught me that it is a privilege to have potential, but there is no substitute for hard work. My mother taught me that compassion and service are keys to building a meaningful life.

ACKNOWLEDGEMENTS

I have deep gratitude for the mentorship I received from Dr. Wesley J. Thompson. His genuine love of science was infectious. I would like to think I have gained a measure of the curiosity and dedication that made him such a high caliber scientist. He was not only a mentor to me but also a friend. I am very thankful for the time we shared.

My thanks go out to my current committee chair, Dr. Jennifer Dulin, for her time and guidance in navigating unforeseen challenges and for always pointing me in the right direction. Thanks to Dr. Dylan McCreedy for making me at home in his lab and for his incredible generosity of time and resources. Thanks to Dr. Uel J. McMahan for his insightful teaching and challenging questions and Dr. Mendell Rimer for his calm presence, vast knowledge and superb advice. You have all made me a better scientist. Thanks to the Texas A&M Institute for Neuroscience for bringing me into this community and allowing me to develop my skills as a scientist.

My time here was made much richer by my lab-mates. Dr. Young il Lee, Ian Smith, Seth Haddix, and Robert Louis Hastings, you all provided insight, advice and conversation that improved the quality of my projects and my days. Dr. Young il Lee deserves special recognition for his invaluable guidance and contribution to my development as a scientist as well as leadership in the lab, especially over the last year.

I would also like to recognize my girlfriend, Sara, who has made my life immeasurably better. Thank you for you unwavering patience, support, and encouragement when I was down and for celebrating with me when times were good.

Finally, thank you to my family for consistent support and encouragement not only through my PhD but also throughout my entire life. Your unfaltering belief in me has kept me going at times when I was unsure of myself.

CONTRIBUTORS AND FUNDING SOURCES

Contributors

This work was supervised by a dissertation committee of Professors Jennifer Dulin, Dylan McCreedy, and Uel Jackson McMahan of the Biology Department, and Professor Mendell Rimer of the Department of Neuroscience and Experimental Therapeutics.

Experimental design for Section 2 was discussed between Dr. Wesley J. Thompson, Dr. Young il Lee and Ryan Massopust. Experimental design for Section 3 was done by Ryan Massopust. Experimental design for Section 4 was discussed between Dr. Jen Dulin, Dr. Dylan McCreedy, and Ryan Massopust. All sections were improved by valuable input from the dissertation committee as well as lab members Dr. Young il Lee, Ian Smith, Seth Haddix and Robert Louis Hastings.

Confocal images presented in Sections 2 were in part collected by Dr. Wesley J. Thompson. Light sheet images presented in Sections 3 and 4 were in part collected by Dr. Dylan McCreedy. The CUBIC experiment in chapter 4 was carried out by Theodore Margo.

All other work conducted for the dissertation was completed by Ryan Massopust independently.

Funding Sources

This work was supported by National Institute of Health grant numbers R01 NS020480 and 1S10RR028951-0, and funds from Wesley J. Thompson's start up package awarded by Texas A&M University.

NOMENCLATURE

ABD1	Actin binding domain 1
AChE	Acetylcholinesterase
AChR	Acetylcholine receptor
BBT	Borate buffer triton
BTX	Bungarotoxin
CLARITY	clear lipid-exchanged anatomically rigid imaging/immunostaining compatible tissue hydrogel
CSA	Cross-sectional area
CUBIC	Clear unobstructed brain imaging cocktails and computational analysis
DGC	Dystroglycan complex
DMD	Duchenne muscular dystrophy
ECM	Extracellular matrix
EDL	Extensor digitorum longus
ETA	Epitrochleoanconeus
Fas2	Fasciculin II
FGF	Fibroblast growth factor
GRMD	Golden retriever muscular dystrophy
LRP4	Low-density lipoprotein receptor protein 4
mdx	Muscular dystrophy x-linked mouse

MEPP	Miniature endplate potential
MHC	Myosin heavy chain
MuSK	Muscle specific kinase
NMJ	Neuromuscular junction
PACT	Passive CLARITY technique
PBS	Phosphate buffered saline
PFA	Paraformaldehyde
RG	Red green
SC	Satellite cell
SOL	Soleus
STM	Sternomastoid
tSC	Terminal Schwann cell
WT	Wild type

TABLE OF CONTENTS

Page

LIST OF FIGURES

Page

1. INTRODUCTION

1.1. Duchenne muscular dystrophy

Duchenne muscular dystrophy (DMD) is an X-linked recessive muscle wasting disease that affects 1:3500 males at birth. The disease can be caused by several different mutations in the *DMD* gene, the largest gene in the human genome. The most common mutations seen in *DMD* are large deletions but large duplications and small mutations can also cause the disease (Darras et al., 1988; Passos-Bueno et al., 1992). Regardless of the type, mutations that cause DMD prevent translation of the protein product of the *DMD* gene, dystrophin (Hoffman et al., 1987).

Dystrophin is a 427kDa cytosolic protein that is expressed widely from brain to muscle. In muscle, dystrophin localizes to the sarcolemma of myofibers and functions to connect the intracellular cytoskeleton to the extracellular matrix (ECM) via connection with the dystrophin glycoprotein complex (DGC) (Bonilla et al., 1988; Porter et al., 1992). At its N-terminus, dystrophin binds directly to F-actin via its actin-binding amino-terminal domain (ABD1) linking it to the actin network. ABD1 also binds to intermediate filament proteins, linking dystrophin to the contractile machinery of the myofiber (Stone et al, 2005; Stone et al., 2007). The majority of dystrophin's size comes from its central rod domain, made up of 24 spectrin-like repeats. Within the rod domain, there is a second actin-binding domain that works in conjunction with ABD1 to bind strongly to actin filaments. The rod domain also interacts with microtubules and is required for normal microtubule organization in myofibers (Prins et al., 2009; Belanto et

al., 2014). The cysteine rich domain of dystrophin binds β-dystroglycan, a transmembrane protein of the DGC (Jung et al., 1995). β-dystroglycan binds α-dytroglycan, which binds to laminins in the ECM, completing the link from intracellular cytoskeleton to ECM. At the carboxy terminal domain, dystrophin proffers binding sites for dystrobrevin and syntrophins, localizing other DGC components to the sarcolemma (Sadoulet-Puccio et al., 1997) (Figure 1.1).

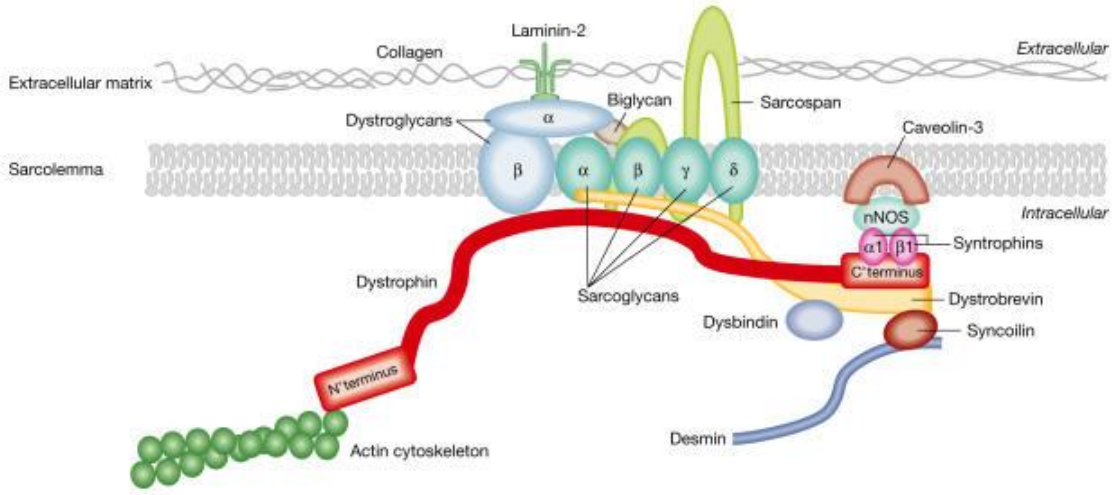

Figure 1.1. The dystrophin glycoprotein complex.
Dystrophin (red) links the intracellular actin cytoskeleton to the DGC by binding F-actin and β-dystroglycan respectively. The DGC plays an important role in sarcolemmal integrity by linking the actin cytoskeleton to the ECM. Reprinted from (Nowak and Davies, 2004).

Dystrophin is the key member of the DGC; without dystrophin several other proteins fail to localize to the membrane and the DGC fails to connect the intracellular cytoskeleton to the ECM. Failure of this link causes a loss of tensile strength, membrane leakage and progressive myofiber damage and prevents the DGC from fulfilling its role

in signaling (Moens et al., 1993; Straub et al., 1997; Blake et al., 2002). As the pathology progresses cycles of muscle fiber degeneration and regeneration ensue.

While DMD is primarily genetically inherited, sporadic cases occur at a rate of 1 in 10,000 sperm or eggs. Causes of the high rate of sporadic cases are unknown and make it challenging to manage DMD with genetic screening alone (Nowak and Davies, 2004). Some of the first recognizable symptoms in human patients are delayed motor development, hypertrophy of the calf muscles, and elevated creatine kinase (CK) levels. Symptoms start to develop around 2 years of age, but the average age of diagnosis is about 4.5 (van Ruiten et al., 2014). As the pathology advances, cycles of myofiber degeneration and regeneration give way to a failure of regeneration and muscle tissue is replaced with fibrotic and adipose tissue. While deposition of these alternative tissues can give the appearance of muscle hypertrophy, it leads to progressive muscle weakness and loss of ambulation by about 11 or 12 years of age (Ciafaloni et al., 2016). The average lifespan for DMD is about 21 years. The leading causes of death in DMD are cardiac and respiratory failure; the advent of mechanical ventilation has extended the lifespan of patients who can benefit from such support (Passamano et al., 2012). There is no cure for DMD and all treatments are palliative. Currently, standard treatment is administration of corticosteroids, which extend the ability to walk by 1 to 3 years (Manzur et al., 2008; Moxley et al., 2010).

Despite the lack of treatment options, there are numerous promising therapeutic strategies under development. Once the genetic cause of DMD was discovered, viral gene therapy seemed a promising therapeutic avenue. One of the largest challenges of

viral gene therapy is avoiding a strong immunological response. Fortunately, in DMD a small number of fibers express a truncated form of dystrophin caused by a natural occurrence of exon skipping. These revertant fibers do not elicit an immune response, providing a template for restoring dystrophin (Fall et al., 2006). However, viral delivery is also limited by the capacity of the vector and the *DMD* gene is the largest in the human genome. In response to these limitations, scientists have created mini- and micro dystrophin genes that have large deletions in the central rod domain in order to increase compatibility with viral delivery while maintaining partial functional rescue (Yue et al., 2003; Bachrach et al., 2004). A successful outcome of this therapy results in pathology similar to Becker muscular dystrophy, a milder form of dystrophy that is the result of mutations in the central rod domain that preserve the reading frame and cause expression of truncated dystrophin. Mini- and micro dystrophins showed efficacy in mdx mice, restoring truncated dystrophin expression to roughly half of muscle fibers (Dudley et al., 2004, DelloRusso et al., 2002). These results translated well in the golden retriever muscular dystrophy model (GRMD) and are currently in phase 1/2 clinical trials (Pichavant et al., 2010). Another promising therapeutic approach utilizes exon skipping to express a truncated, partially functional, dystrophin protein. Antisense oligonucleotides are utilized to delete a region of pre-mRNA that contains the mutation, skipping the mutated exon (Du and Gatti, 2009). Exon skipping therapies have shown promise in animal models of DMD and numerous treatments are in phase 2 clinical trials (Echevarria et al., 2018). Most recently a new gene editing technique, CRISPR/Cas9, is being used to correct mutations in the *DMD* gene. The technique works by viral delivery

of the bacterial DNA endonuclease enzyme Cas9 and guide RNAs that target the DNA of interest to confer a targeted mutation, such as a deletion or mutated or inserted sequence, into the genomic DNA. The efficacy of this technique has been demonstrated in mice and dogs and is working its way towards human clinical trials (Bengtsson et al., 2017). While these therapeutic avenues represent exciting advances in the race to cure DMD, we still lack a thorough characterization of the disease pathology that would inform translation of therapeutics from mouse to human.

1.2 The muscular dystrophy X-linked mouse

The muscular dystrophy X-linked mouse (mdx) was discovered as the result of a spontaneous mutation in a colony of C57BL/10 mice causing a histological and functional pathology characteristic of DMD (Bulfield et al., 1984). The model was initially characterized as having a comparatively mild phenotype relative to human DMD. Specifically, the mouse was reported to undergo a "crisis period" of muscle damage between 3 and 12 weeks of age, after which the disease progression stabilizes. Mdx mice develop normally up to about 20 days of age, at which point massive muscle necrosis occurs, resulting in decreases in muscle weight and tension output (Dangain and Vrbova, 1984). Prior to the onset of damage, there are no changes in body or muscle weight, or in the diameter, number or type of myofibers (Tanabe et al., 1986). During necrosis, there is substantial infiltration of immune cells and a progressive increase in the proportion of type 1 fibers. By 26 weeks of age, only 5% of original myofibers remain, but damaged myofibers are successfully replaced by a robust regenerative

response (Carnwath and Shotton, 1987). As a result of these findings, the mdx mouse was generally considered to be an excellent model of myofiber necrosis and repair but a poor model for human DMD pathology.

Shortly thereafter, dystrophin was identified as the product of the *DMD* gene and the homology of the mdx mutation to that causing DMD generated renewed interest in mdx mice as a model for DMD (Hoffman et al., 1987). As in DMD, mdx mice lack functional dystrophin protein. In light of these findings, aged mdx mice were analyzed and reports indicated a progressive pathology more similar to DMD. Specifically, beyond 15 months of age, muscles display progressive atrophy and branching. A high degree of fibrosis occurs in some muscles (soleus and plantaris) but not in others (extensor digitorum longus). In addition, hindlimb muscles display a loss of specific force throughout the first year of life (Pastoret and Sebille, 1993a; Pastoret and Sebille, 1993b). In aged mdx mice many of the pathological features of DMD were observed, such as postural abnormalities, cardiac dysfunction, motor weakness, and low body and muscle weights (Pastoret and Sebille, 1995). Mdx mice also have a reduced lifespan relative to WT, albeit a less severe reduction compared to patients with DMD (Lefaucheur et al., 1995; Chamberlain et al., 2007).

Salient morphological changes are evident at the neuromuscular junction (NMJ) of mdx mice, such as fragmentation of the acetylcholine receptor (AChR) aggregate and reduction in postsynaptic folds (Lyons and Slater, 1991). There is some evidence that these changes are also present in DMD (Theroux et al., 2008). While these morphological changes are agreed upon, whether they have consequences for synaptic

transmission is a topic of debate. Based on reports, it seems that there may be substantial intermuscular variation in the efficacy of synaptic transmission in mdx. In the diaphragm muscle of 37-week-old mdx mice, depressed resting membrane potential, MEPP amplitude, quantal content and AChR density were observed (Nagel et al., 1990). In the epitrochleoanconeus (ETA) muscle of 8-week-old mdx mice, reports indicate no change in miniature endplate potential (MEPP) frequency or amplitude, acetylcholine receptor density at the postsynaptic membrane or quantal content (Lyons and Slater, 1991). The issue was recently revisited and tested in the diaphragm of 2 to 6-month-old mdx mice. Changes in neuromuscular transmission, such as decreased miniature endplate potential amplitude, increased quantal content, and increased rundown were reported (van der Pijl et al., 2016). It is possible that these differences are due to the frequency of use of the muscle; the diaphragm is used constantly during respiration while the ETA is a forelimb muscle that is used sparingly by comparison. As respiratory failure is a leading cause of death in DMD (Passamano et al., 2012), it seems logical that the diaphragm is severely affected. It is also possible that variation exists both within and between colonies of mdx mice and account for some of the variability between reports.

Noticeable changes in the morphology of muscle fibers indicate that the mdx mouse undergoes cycles of myofiber degeneration and regeneration. Centrally positioned nuclei after initial development have long been appreciated as a marker of regenerated muscle fibers and are seen in DMD as well as mdx mice (Spiro et al., 1966). Strings of central nuclei run through the center of the myofiber, sometimes in short chains indicating a site of damage and repair, and other times in long chains running

most or all of the length of a myofiber, indicating that the myofiber was replaced. Mdx mice also replicate the extensive myofiber branching seen in DMD (Swash and Schwartz, 1977; Ontell, 1981). These branches are thought to be the result of improper fusion of myoblasts within the same basal lamina sheath during regeneration. Branch points on muscle fibers have been shown to be sites of mechanical weakness and therefore may contribute to continued myofiber turnover in the mdx and DMD (Chan et al., 2007). These morphological changes will be considered extensively in proceeding sections. While mdx mice do not perfectly replicate the human disease, it is clear that many pathological features are replicated.

1.3 Development and structure of skeletal muscle

During embryonic development, skeletal muscle originates from the tissue of the paraxial mesoderm. Specification of the paraxial mesoderm is controlled by numerous signaling molecules such Wnt and fibroblast growth factor (FGF) (Takada et al., 1994; Ciruna and Rossant, 2001). In response to precise gradients and timing of morphogen expression, the tissue becomes compartmentalized and the somites develop in the posterior area of the paraxial mesoderm (Hubaud and Pourquie, 2014). The somites are then organized corresponding to the muscle groups they will give rise to, but are not yet myogenically fated. The first indicator of myogenesis in the somites is activation of myogenic factor Myf5 (Ott et al., 1991). Skeletal muscle-fated cells begin to form in the myotome, indicated by expression of multiple isoforms of myosin heavy chain (MHC) and actins that will come to make up the contractile units of muscle fibers (Sassoon et

al., 1988; Lyons et al., 1990). Myogenesis proceeds in a rostral to caudal direction; cells migrate into place and form muscle masses as the embryo elongates. The formation of these masses into myofibers is governed by transcription factor Pax3 and myogenic regulatory factors Myf5, MyoD, myogenin, and MRF4. These primary myofibers are few in number but take the form of rudimentary muscles and provide a template for subsequent myogenesis (Horst et al., 2006).

Secondary myogenesis begins in the embryo with expression of transcription factor Pax7 in a subset of myogenic progenitors. The precursor cells fuse together along the primary myotubes, forming new myotubes. While primary myotubes express only slow MHC, now fast MHCs are also expressed (Van Horn and Crow, 1989; Condon et al., 1990). After fusion, the nuclei are moved to the center of the myotubes and lined up (Kelly and Zachs, 1969). Myotubes mature into myofibers with the development of the myofibril network and myonuclei are transported to the periphery, directly beneath the sarcolemma (Figure 1.2) (Capers, 1960). Then nuclei are moved in order to maximize the distance between adjacent myonuclei (Bruusgaard et al., 2003). Maximizing distance between myonuclei is consistent with the myonuclear domain hypothesis, which posits that each nucleus is responsible for providing transcripts for their own specific volume of cytoplasm (Hall and Ralston, 1989; Pavlath et al., 1989). This wave of myogenesis is supported by proliferation of Pax7+ progenitor cells, a subset of which may become resident satellite cells along muscle fibers (Gros et al., 2004). Satellite cells will be discussed in proceeding sections. After secondary myogenesis the primary growth of

muscle tissue in healthy animals is through hypertrophy of muscle fibers via addition of myofibrils, rather than through addition of myofibers.

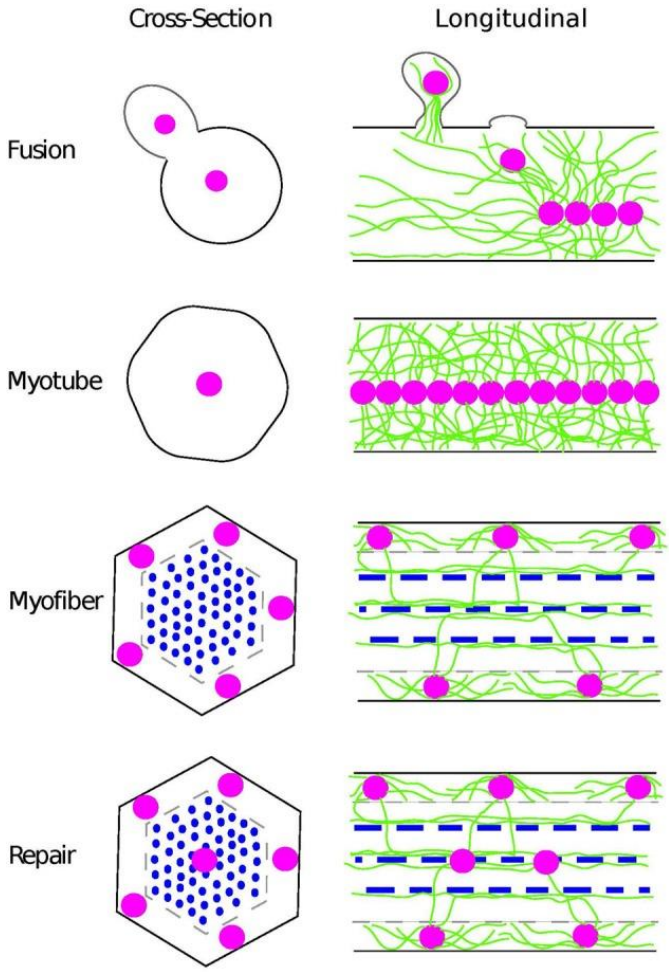

Figure 1.2 Position of nuclei during muscle development and repair.
Nuclei (pink) fuse into myotubes and line up in the center of the cell. As the myotubes matures the myofibril network (blue) is built and the nuclei are moved to the periphery and spaced out via their connections to the actin network (green). During muscle repair myonuclei fuse into the myofiber and are transported to the center of the cell. Reprinted from (Folker and Baylies, 2013).

The cellular unit of skeletal muscle is the myofiber. Each myofiber is an elongate syncytium containing the repetitively organized contractile machinery called the myofibril network. Each myofibril is composed of repeating units known as sarcomeres, containing myosin and actin filaments that slide past each other during contraction. Mammalian sarcomeres are about 2 μm long and shorten by about 30% on contraction (Au, 2004). The myosin filaments are anchored in the center of the sarcomere (M line) and the actin filaments are anchored at the edges of the sarcomere (Z lines) (Figure 1.3). During muscle contraction myosin binds to actin and pulls actin towards the M line in an adenosine triphosphate mediated interaction. This interaction is tightly regulated by calcium, which is released by the sarcoplasmic reticulum in response to an action potential. In relaxed muscle the myosin binding sites on actin are blocked by tropomyosin via steric blocking (Lehman et al., 1995). These binding sites become accessible when rising cytosolic calcium binds to troponin, causing a conformational change that displaces tropomyosin and reveals the myosin binding sites on actin. The end result of these interactions causes the Z lines of the sarcomere to be pulled towards the M line, inducing muscle contraction.

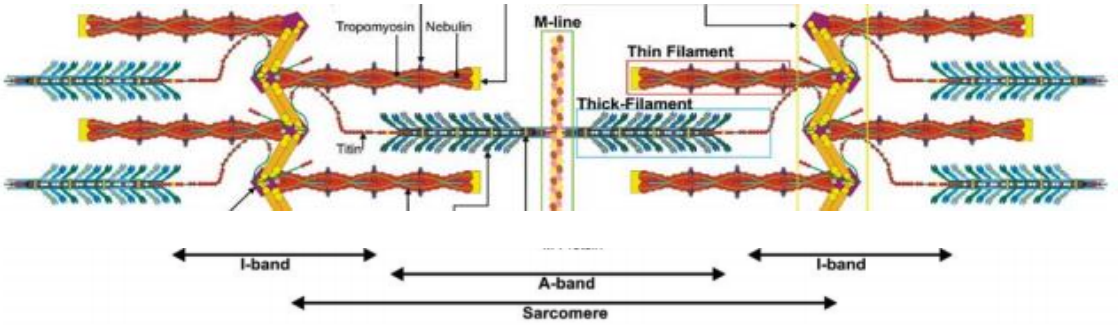

Figure 1.3 Sarcomere structure.
Myosin (thick filaments) is anchored to the M-line. Actin (thin filaments) is anchored to the Z-line. During muscle contraction myosin binds actin and pulls it towards the M-line in a cyclic process mediated by adenosine triphosphate. Edited from (Au, 2004).

During the maturation from myotube to myofiber, motor endplates are formed and innervated. Each myofiber is innervated by a single motor neuron and each motor neuron innervates many individual muscle fibers. These groups are called motor units, and vary widely in the number of muscle fibers included. When a motor unit is activated its myofibers contract. In this way, the nervous system has greater control of the intensity of contraction, allowing for finer motor control. Fibers in a motor unit are all of the same type; in humans there are three fiber types. Type 1 fibers are slow twitch fibers, named for their contraction speed and time to fatigue relative to fast twitch fibers. Fast twitch fibers are broken down into several types; type 2A and 2X are seen in humans with an additional type, 2B, seen in mice. All fast twitch fibers are fast to fatigue and fast to contract but differ in their MHC expression and metabolism (Talbot and Maves, 2016). Also during the maturation from myotube to myofiber, the basal lamina is assembled and satellite cells (SC), myogenic stem cells, take their place between the sarcolemma and the basal lamina. Each myofiber is enclosed in connective tissue called

endomysium, which is connected to the basal lamina. Myofibers are organized into fascicles, groups of myofibers wrapped in connective tissue called perimysium. Finally, skeletal muscles are bound in another layer of connective tissue, the epimysium (Gillies and Lieber, 2011). The organization of skeletal muscle fibers is largely stable, but damaging events can cause profound changes to their structure.

1.3.1 Skeletal muscle repair processes

Skeletal muscle injury occurs regularly throughout life, caused by numerous sources ranging from disease to the muscle's own contractions. Depending on the scale and severity of damage, one of two repair processes are initiated. The primary repair process is satellite cell mediated repair, a process that shares many similarities with muscle development. The second repair process, the dysferlin mediated repair process, specializes in quick repair of small membrane injuries. Early muscle regeneration experiments were performed by removing the muscle, cutting it in to small pieces and then replacing it in the muscle bed. Even after such a severe and large-scale injury, skeletal muscles regenerate (Studitsky et al., 1964). In the mdx mouse it is estimated that 95% of the muscle fibers are replaced in the first 26 weeks of life (Carnwath and Shotton, 1987).

In severe injury, the myofiber sarcolemma is compromised and the myofiber cytosol is no longer contained. One of the first markers of this type of damage is elevated creatine kinase level in serum. Elevated creatine kinase is an early sign of DMD but is not reliable marker since it is a general indication of muscle damage and does not

indicate the severity of damage (Zats et al., 1991). In this early phase of degeneration the muscle is infiltrated by immune cells, triggering an inflammatory response. Neutrophils are the dominant cell seen in the first hours after injury, arriving via the bloodstream. They are followed by macrophages that act to phagocytose cellular debris and remove damaged tissue from the area. Additionally, these immune cells play an essential signaling role in initiating the myogenic regenerative response (McClung et al., 2007).

Satellite cells are thought to be remnants of the myogenic precursor cells that drive embryonic muscle development. A population of these progenitors express Pax3 and Pax7 but do not express myogenic regulatory factors. There is some evidence suggesting these cells become SCs and take the sublaminar but extracellular position that is their namesake, downregulating Pax3 in the process (Kassar-Duchossoy et al., 2005). However, others maintain that SCs have a distinct lineage from embryonic progenitor cells (Hutcheson et al., 2009). Expression of Pax7 is the hallmark of SCs and is required for their development. It also drives expression of myogenic factor Myf5 and correlates with a committed but not differentiated myogenic state (Olguin et al., 2007). After the surge of postnatal growth is complete, SC number drops precipitously and the remaining cells enter a quiescent state.

Skeletal muscle regeneration is a strictly ordered process, beginning with activation of SCs. Regeneration fails in Pax7 depleted muscles, indicating that SCs are required for repair and other cell types cannot perform the same function (Lepper et al., 2011). The damaged muscle releases transcription factors that are involved in SC activation, such as MRF4, myogenin, MyoD, and Myf5. SCs enter the cell cycle and

proliferate to give rise to myogenic precursor cells. These cells migrate to the injury site and upregulate myogenic regulatory factors, becoming myoblasts. Macrophages release pro-inflammatory cytokines that play a role in myoblast differentiation by repressing Pax7 expression (Palacios et al., 2010). Myoblasts begin to fuse at the site of damage to repair injury or move into the vacant basal lamina sheaths and begin to fuse to form new myofibers (Snow, 1977). Newly formed fibers express embryonic myosin heavy chain, indicating that they are entirely new fibers, rather than repaired (Whalen et al., 1990). In addition, many regenerated myofibers are branched, which is likely the result of incomplete fusion of myofibers within the same basal lamina sheath (Blaveri et al., 1999). When regeneration is complete the myofibers are larger than they were prior to injury and contain central nuclei as well as peripheral nuclei (Figure 1.2).

In instances of smaller physical injury to the sarcolemma, the satellite cell mediated repair process is not necessary. A faster acting membrane repair process mediated by dysferlin is better suited to handle these injuries. Dysferlin is a 230 kDa protein that is localized to the sarcolemma; mutations in the encoding gene cause limb-girdle muscular dystrophy, which is characterized by muscle wasting in proximal limb muscles such as those in the shoulders and thighs (Doherty et al., 2003; Han and Campbell, 2007). When injury occurs to the sarcolemma, calcium floods the cell and creates an area of high calcium density, activating proteases that cleave cytoskeletal elements and inducing aggregation of dysferlin repair vesicles to the injury site (Hernandez-Deviez et al., 2008). In the presence of high calcium these vesicles fuse into

the membrane and reseal the cell. This process occurs on the scale of seconds and is capable of repairing injuries of up to about 1000 μm^2 (McDade et al., 2014).

1.4 Structure and function of the neuromuscular junction

The NMJ is a tripartite synapse composed of the motor nerve terminal, acetylcholine receptor aggregate, and terminal Schwann cells (tSC) (Sanes and Lichtman, 1999). The acetylcholine receptor aggregate, or motor endplate, lies in the myofiber sarcolemma and is closely apposed on the presynaptic side by the motor nerve terminal. Terminal Schwann cells cap the synapse and play numerous roles in NMJ development and maintenance (Figure 1.4) (Ko and Robitaille, 2015). The NMJ connects the central nervous system to skeletal muscles and functions to convert action potentials of lower motor neurons into chemical signals received by the innervated muscle fiber. In mammals the primary neurotransmitter at the NMJ is acetylcholine. In response to acetylcholine, the muscle fiber depolarizes and generates an action potential that runs from the NMJ to the distal ends of the muscle fiber to induce muscle contraction and thus, voluntary movement. The structure of this synapse provides a robust safety factor for synaptic transmission.

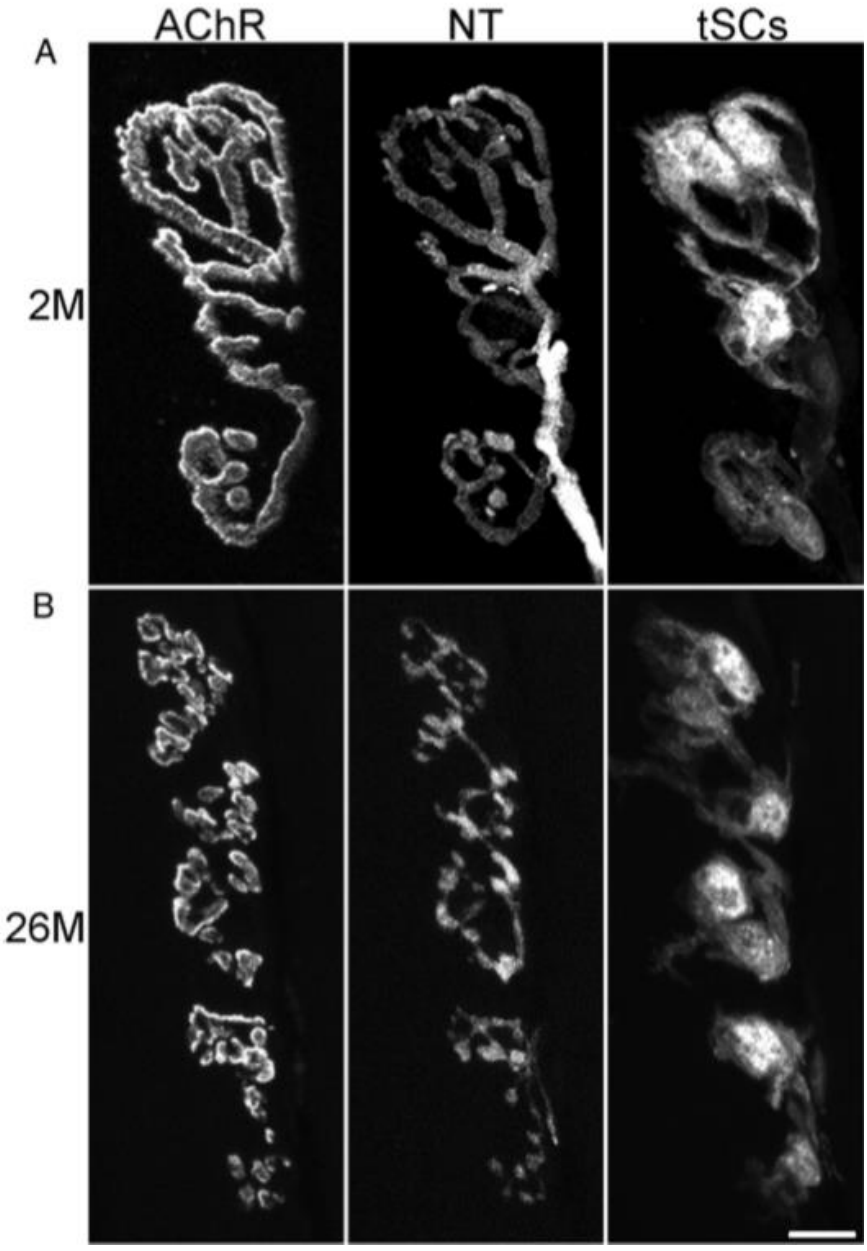

Figure 1.4. Components of the neuromuscular junction in young and aged mice. A) Components of the NMJ from a 2-month-old mouse. The endplate displays the canonical pretzel morphology, precisely apposed by the nerve terminal. Terminal Schwann cells cap the synapse. B) Components of the NMJ from a 26-month-old mouse. The endplate and nerve terminal display fragmented morphology. Terminal Schwann cells cap the synapse. Scale bar = 10 μm. Reprinted from (Li et al., 2012).

The NMJ is more than an order of magnitude larger than most central nervous system synapses, providing a substantial investigative advantage. As a result, the structure and function of this synapse has been studied extensively. On the postsynaptic side, about 10,000 AChRs per μm^2 aggregate at the synapse to form the motor endplate, responsible for converting chemical signals released by the motor neuron into electrical signals that induce muscle contraction (Hall and Sanes, 1993). The endplate goes through a series of conformational changes throughout the lifespan, starting as plaque of receptors innervated by several motor neurons. Coincident with synapse elimination, the plaque becomes perforated, and ultimately takes on the singly innervated "pretzel" shaped adult morphology (Figure 1.4A) (Slater, 1982; Marques et al, 2000). In mice this process is typically complete by the third postnatal week. Beyond this point, the morphology of the endplate is quite stable but can become altered in disease and old age as the result of injury, among other causes. In these instances, the endplate becomes fragmented; the continuous gutters of the pretzel are broken up into punctate structures resembling islands (Figure 1.4B). The motor nerve terminal closely apposes the endplate, matching the conformational changes throughout the lifespan. In between the two, the ECM plays a stabilizing role, connecting to the postsynaptic sarcolemma via the DGC and the presynaptic nerve terminal (Nishimune et al., 2004).

Directly beneath the motor endplate, synaptic myonuclei are tethered to the sarcolemma by Syne-1, a nuclear envelope protein. In WT mice there are typically 3 to 6 myonuclei at a given synapse. In transgenic mice designed to prevent Syne-1 function, synaptic myonuclei do not cluster beneath the endplate, demonstrating that Syne-1 is

essential for localization of synaptic myonuclei; however, synaptic myonuclei are not required for normal maturation of the synapse (Englander and Rubin, 1987; Grady et al., 2005). These nuclei are transcriptionally distinct and have been shown to provide transcripts for AChR subunits (Sanes et al., 1991; Simon et al., 1992), AChE and muscle-specific kinase (MuSK) as well as possible retrograde signals involved in presynaptic differentiation (Jevsek et al., 2006a; Jevsek et al., 2006b). Dysregulation of synaptic nuclei has been correlated to neuromuscular disease.

The forces that drive synapse formation and maturation are numerous (Thompson et al., 1983; Burden et al., 2018; Li et al., 2018). Release of neural agrin from the presynaptic motor neuron induces NMJ development (McMahan, 1990) through its interaction with low-density lipoprotein receptor-related protein 4 (LRP4). Agrin binds to LRP4, which induces phosphorylation of MuSK. The MuSK/LRP4 complex is in the synaptic cleft, bound to the postsynaptic membrane and transcripts for this complex are produced in the myofiber (Kim et al., 2008a; Kim et al., 2008b). This series of interaction induces clustering of AChRs. Signals driving synaptic maturation are required from not only the neuron but also the muscle to induce canonical synapse formation (Ruegg et al., 1992; Ferns et al., 1993; Yumoto et al., 2012). In the myofibers, rapsyn binds directly to AChRs and is necessary for clustering (Apel et al., 1997; Moransard et al., 2003; Gautam et al., 1995). The tSCs also play an active role in synapse elimination, providing general competition and stress to the innervating motor neurons to drive competition. Terminal Schwann cells have been shown to intercalate process into motor nerve terminals and phagocytize pieces of the nerve terminal. In

response to this stress, some motor axons retract, leaving behind vacant receptor patches on the muscle fiber surface. These patches can either become innervated by remaining nerve terminals or are lost. These processes are in part responsible for the unique shapes of adult motor endplates (Figure 1.5) (Smith et al., 2013).

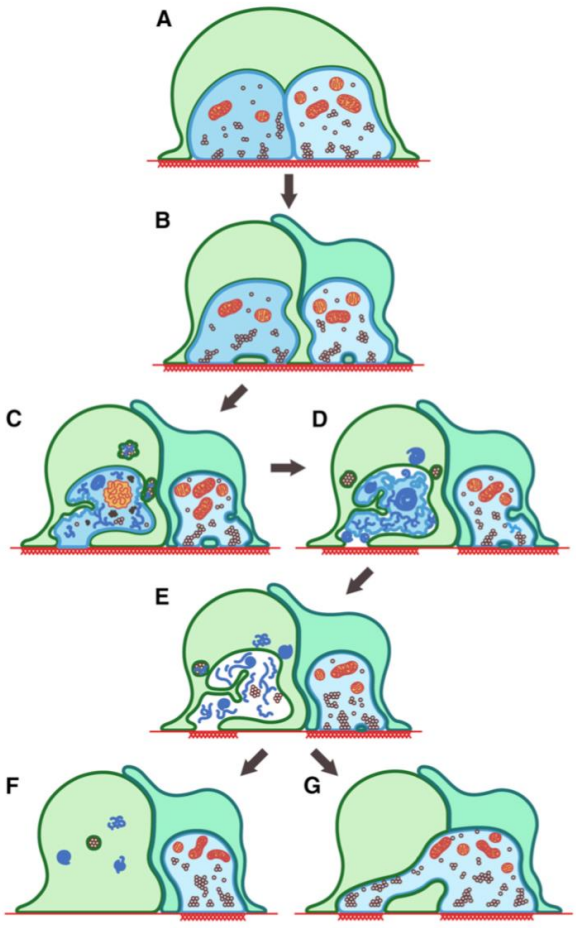

Figure 1.5 Schematic of terminal Schwann cell's role in synapse elimination. Terminal Schwann cells (green) drive synapse elimination by intercalating processes into nerve terminals (blue) and competing for the AChR dense postsynaptic membrane (red). Reprinted from (Smith et al., 2013).

Acetylcholine receptors are constructed of 5 subunits to form a pentameric cation channel. The receptors lie in a trough on the muscle fiber membrane, called the synaptic gutter. Within the gutter, narrow pits called junctional folds project down into the muscle. AChRs line the edges of the folds and are apposed presynaptically by the active zones of the motor nerve terminal. A dystrophin homolog, utrophin, is also expressed at crests of junctional folds and is involved in the NMJ development (Sanes and Lichtman, 1999). Voltage gated sodium channels are densely packed in the bottom of junctional folds, contributing to the generation of action potentials. When acetylcholine binds AChRs, the channels open and sodium ions rush across the membrane, depolarizing the cell. If the depolarization reaches threshold, an action potential is triggered and runs down the sarcolemma. In order for the action potential to reach the inner myofibrils, it runs along a transverse structure called the T-tubule system. The action potential reaches the sarcoplasmic reticulum triggering the release of calcium into the cell. Calcium binds to troponin inducing a conformational change that reveals binding sites for myosin to bind actin and muscle contraction ensues.

1.4.1 Remodeling at the neuromuscular junction

Like skeletal muscle, the NMJ possesses great capacity for repair after insult. As discussed previously, regeneration of skeletal muscles occurs primarily as a result of satellite cell proliferation and fusion of the myogenic cells either at the site of injury or to replace lost myotubes. In the either case it has been shown in the frog that the nerve terminal remains at the synapse while the muscle fiber regenerates and that the new

synapse is formed in the same location (Burden et al., 1979). Interestingly, the synapse reforms at the original location even when both the axon and myofiber are injured, indicating the presence of signals with the basal lamina that instruct synaptic localization (Marshall et al., 1977). In the mouse NMJ, the motor nerve terminal has been shown to behave differently in some cases. In the instance of a crushing injury on the muscle near the synaptic site, the nerve terminal retracts (Rich and Lichtman, 1989). Following laser ablation of muscle fibers in the synaptic area, the nerve terminal remains at the synaptic site (Li and Thompson, 2011). The severity of injury may determine the response of the nerve terminal, however, in either case the synapse is reformed at the original synaptic site.

Upon regeneration after damage, the structure of the NMJ is often altered, sometimes dramatically. It has been shown that in normal aging, as well as in dystrophy, damage at the site of the NMJ induces fragmentation of the synapse (Lyons and Slater, 1991; Li et al., 2011; Haddix et al., 2018). That is not to say that fragmentation is exclusively caused by myofiber damage. Alterations in all three parts of the NMJ can induce endplate fragmentation. Overexpression of rapsyn induces endplate fragmentation, possibly by interrupting transportation of AChRs to the sarcolemma (Han et al., 2000). On the presynaptic side, vesicular acetylcholine transporter overexpression increases the amount acetylcholine loaded in synaptic vesicles and results in premature endplate fragmentation (Sugita et al., 2016). The activity of tSCs also plays a role in synaptic remodeling. Overexpression of neuregulin 1 type III in motor neurons increases tSC activity and induces fragmentation (Lee et al., 2016). Conversely, there are

numerous reports demonstrating factors that have a protective effect on synaptic aging. For example, exercise, calorie restriction, and the muscle-secreted factor fibroblast growth factor binding protein 1 protect the synapse from premature aging (Valdez et al., 2010; Taetzch et al., 2017). Given the number of causes for fragmentation, it would be challenging to determine the cause of fragmentation in a given case. Fortunately, in the case of muscle damage, the repaired myofiber contains central nuclei and therefore damage is easy to detect. Central nuclei are a strong indicator that a damage event has occurred, and may be the cause of remodeling (Lyons and Slater, 1991; Wada et al., 2008).

In cases of repeated myofiber damage and repair, changes also occur within the synaptic cleft (Patton et al., 1999). When myofibers degenerate, much of the original ECM is retained, however, regenerating myofibers produce their own ECM. The result is a thicker layer of ECM, which may provide an explanation for the increased width of the synaptic cleft in dystrophy (Lyons and Slater, 1991). A widened synaptic cleft and thicker ECM could have a dramatic effect on signaling that occurs in the cleft, such as the agrin LRP4/MuSK interaction among many others. This is an area deserving of more research.

In the case of axonal injury, the distal nerve and nerve terminal degrade and the proximal portion of the axon retracts. Depending on the severity of injury, the axon regrows to innervate the original synaptic site. Both the endoneurial tube and the Schwann cells take part in guiding the axon back to its original synapse (Rich and Lichtman, 1989; Son and Thompson, 1995; Ngyuen et al., 2002; Kang et al., 2003).

Schwann cells play a diverse role, phagocytizing the axonal debris and providing a path to reinnervate the muscle (Kang and Lichtman, 2013). In cases of more severe injury, a new axon may come to innervate the muscle fibers. Regardless, the axons reinnervate the original synaptic site without inducing fragmentation. However, the longer it takes for the axon to reinnervate the endplate, the more likely some synaptic remodeling occurs (Kang et al., 2014).

It is clear that NMJ remodeling occurs as part of the aging process, in disease, as a result of injury, as well as from alterations of protein expression in the nerve terminal and muscle. However, the consequence or benefit of this remodeling remains unclear. Recordings from fragmented junctions of aged wild type mice show no perturbation of synaptic transmission, and may actually be more robust (Willadt et al., 2016). There is physiological precedent for this idea; myofibers are rebuilt stronger after injury. In many cases the biological response to insult is to rebuild a more robust structure. However, in cases such as dystrophy where repeated bouts of remodeling occur, reports indicate muscle dependent dysfunctions in synaptic transmission, as discussed previously (Nagel et al., 1990; Lyons and Slater, 1991; van der Pijl, 2016). It is important to note that these studies did not determine the morphology of the NMJ they were recording from, but in adult dystrophic mice the majority of NMJs are remodeled. It may be that repeated instances of damage and repair begin to interfere with synaptic transmission for reasons other than fragmentation, such as a widening of the synaptic cleft. Regardless, changes in transmission are minor and unlikely in themselves to drive large scale changes that impact quality of life in disease and aging.

1.5 Sarcopenia in aging and similarities to muscular dystrophy

Sarcopenia is a hallmark of aging mammalian muscle. Defined as the loss of muscle mass as a direct consequence of aging, sarcopenia is a normal part of the aging process. Its causes are numerous but generally divided into two categories: changes that induce muscle atrophy and changes that induce myofiber loss. Humans may begin to lose muscle mass each decade starting at age 30 (Fisher, 2004). The rate of loss is variable and often increases in old age. People with a sedentary lifestyle are at higher risk for sarcopenia. Exercise, especially resistance training, helps delay onset and severity. Sarcopenia is considered to be a biomarker for aging, a way to distinguish biological age as opposed to chronological age (Fisher, 2004). As sarcopenia progresses it results in progressive muscle weakness that leads to loss of balance and mobility in old age. This leads to a loss of independence as well as a tremendous financial burden, costing more than 12 billion dollars per year in the United States alone (Janssen et al., 2004).

In humans, myofiber loss is a major contributor to sarcopenia. The onset of fiber loss is contested. One report indicates that myofiber loss begins around 25 years of age, and humans lose 40% of their muscle fibers between ages 24 and 77 (Lexell et al., 1986; Lexell et al., 1988). Others report a later onset of myofiber loss, around age 50 (Faulkner et al., 2007). Atrophy of fibers also plays a role in sarcopenia but to a lesser degree than myofiber loss. The trend of these findings is generally replicated in mice; however, the consistency of these results is clouded by muscle group and biological sex differences. Early reports on fiber loss in the mouse demonstrated these differences, reporting fiber

loss in male but not female Biceps brachii and female but not male extensor digitorum longus (EDL) and soleus (SOL) (Rowe, 1969). In C57/BL6J mice, loss of muscle mass with age is a muscle group dependent feature. As they age from 6 to 24 months, they lose substantial muscle mass in the EDL and SOL but not the sternomastoid (STM) (Sheard and Anderson, 2012). This is likely driven by significant myofiber loss in the EDL and SOL that is not seen in the STM. Myofiber atrophy may also play a role in this process, but cross-sectional area (CSA) does not change significantly with age in these mice (Sheard and Anderson, 2012). Myofiber loss is a major feature of both sarcopenia and DMD, and whether this feature is replicated in the mdx mouse is a topic central to this dissertation.

Because sarcopenia occurs as a direct result of the aging process it can be challenging to distinguish sarcopenia from disease related pathology like cancer cachexia or muscle wasting in dystrophy. One hallmark of sarcopenia is fiber size variability, a feature shared in DMD and the mdx mouse, but that differentiates it from cancer cachexia (Engel and Ozawa, 2004; Hepple, 2012). Muscles from sarcopenic humans also display extensive fiber type grouping. In normal muscles, different fiber types are interspersed, but in cases of damage and disease, fibers of the same type are clustered together. This phenomenon is thought to occur as the result of repeating neuromuscular damage leading to reinnervation of neighboring muscle fibers by the same motor neuron (Anderson, 2003). Fiber type grouping has also been reported in DMD (Engel and Ozawa, 2004). Another shared characteristic of DMD and sarcopenia is coexpression of multiple myosin heavy chain isoforms in myofibers (Andersen et al.,

1999; Marini et al., 1991). These shared histopathological features hint at a common mechanism - cycles of myofiber degeneration/regeneration. Fragmentation on the motor endplate is a hallmark of dystrophic muscle as discussed above and is another shared feature of sarcopenia. There is evidence that degeneration and subsequent regeneration of the muscle fibers drive this process in both aging and dystrophy (Lyons and Slater, 1991; Li et al., 2011). In sarcopenia there is substantial evidence for motor neuron loss via a decline in motor neuron cell body counts in the spinal cords of aged humans (Kawamura, 1977). Motor neuron loss and denervation is reported in aged mice as well (Stanmore et al., 1978; Valdez et al., 2010). It is possible that motor neuron death may be caused by muscle fiber loss, inducing an eventual retraction and apoptosis. However, there is little evidence for motor neuron loss in DMD (Tomlinson et al., 1974). Therefore, it seems unlikely that loss of myofibers drives the death of motor neurons.

2. ANALYSIS OF MDX PATHOLOGY IN ISOLATED MYOFIBERS

2.1 Research rationale

The mdx mouse is the most widely used preclinical model for DMD, but there is still much to learn about the degree to which the model mimics the human disease. This is especially true in old age, as most reports focus on the first 6 months of life. Many features of DMD are also present in the mdx mouse. For example, presence of central nuclei, muscle hypertrophy, muscle fiber branching and shortened lifespans are features of both the human disease and the mouse model (Bulfield et al., 1984; Lyons and Slater, 1991; Minatel et al., 2003; Chan et al., 2007; Chamberlain et al., 2007). On the other hand, synaptic function, muscle strength and mobility are less severely affected in mdx as compared to DMD (Nagel et al., 1990; Pastoret and Sebille, 1993a; Lefaucher et al., 1995; van der Pijl, 2016). Few reports track these features beyond 6 months of age in the mdx mouse model, and several of these features, such as central nuclei and myofiber branching, are challenging to track due to historical limitations of histological analysis techniques. To fill this void, we tracked hallmark features of dystrophy in isolated muscle fibers from the mdx mouse from 2 weeks to 2 years of age in order to characterize the degree to which the model mimics the human disease. Identifying which aspects of mdx pathology mimic DMD is essential in determining which therapeutic targets show the most promise to translate from mouse to human.

2.2 Materials and methods

2.2.1 Mouse strains

C57BL/10ScSn-*Dmd*^{mdx}/J mice (mdx, RRID:IMSR_JAX:001801) and C57BL/10ScSnJ (BL/10J, RRID:IMSR_JAX:000476) mice were purchased from Jackson Laboratory and bred in house. Use of these mice has been previously reported and all mice are available from Jackson Laboratory. Three male mice per genotype and age were used for each experiment, totaling 42 mice for the experiments performed in this chapter. All experimental procedures were approved by the Texas A&M University Institutional Animal Care and Use Committee (2016-0158 or 2019-0179) and in full compliance with the NIH Guidelines for the Humane Care and Use of Laboratory Animals.

2.2.2 Single myofiber isolation

Mice were sacrificed via intraperitoneal injection of 0.15 mL of Euthosol (Med-Pharmex). Following sacrifice, myofibers were isolated as previously described (Wada et al., 2003). Briefly, the hindlimb of the mouse was skinned and EDL muscles were dissected in a calcium chelating solution (137 mM NaCl, 5.4 mM KCl, 5 mM MgCl2, 4 mM EGTA, 5 mM HEPES, pH 7.0) to prevent contraction. Immediately after dissection muscles were pinned in Sylgard-lined dishes and stained with α-bungarotoxin (BTX) (1 mg/ml) conjugated to Alexa Fluor^{TM} 555 (Thermo Fisher Scientific Cat# B35451) diluted 1:500 in calcium chelating solution for 2 hours to label AChRs. After staining, the muscles were washed in calcium chelating solution 3 times for 5 minutes per wash.

The muscles were then fixed in calcium chelated 4% paraformaldehyde for 48 hours at room temperature. After fixation, the muscles were washed in calcium chelating solution 3 times for 5 minutes per wash. Muscles were then bathed in 40% NaOH for 3 hours at room temperature to degrade connective tissue. DAPI (1 mg/ml) (Thermo Fisher Scientific Cat# D3571) diluted 1:2000 in phosphate buffered saline (PBS) was applied to label nuclei for 20 minutes. Muscles were gently shaken for 8 minutes in PBS on a rocking platform. Forceps and a dissecting microscope were used to mount individual muscle fibers onto slides in anti-fade fluorescence mounting medium.

2.2.3 Muscle preparations

To compare single muscle fibers to larger groups of myofibers, whole mount preparations were used. Animals were euthanized as described above. The STM, SOL and EDL muscles were dissected, pinned at resting length in a sylgard-lined dish and fixed with phosphate buffered 4% paraformaldehyde for 30 minutes. After fixation, muscles were washed three times in phosphate buffered saline (PBS) and labeled with α-bungarotoxin conjugated to Alexa Fluor™ 555 diluted 1:500 in PBS for 2 hours. Nuclei were labeled with DAPI, diluted 1:2000 in PBS. Muscles were washed 3 times in PBS before a longitudinal bundle of myofibers was dissected from tendon to tendon and mounted on a microscope slide in anti-fade fluorescence mounting medium.

2.2.4 Image Acquisition and Analysis

Whole mounts were analyzed using a Leica DMRX epifluorescence microscope with a 40X oil objective (NA 1.0). Junctions were considered fragmented if they had 5 or more separate receptor rich areas upon visual inspection. Fragmentation analysis was done using the threshold function and then the automated count function in ImageJ. The minimum object area was set to 5 μm^2. Isolated myofibers were imaged with a Leica TPS II SP5 or Zeiss LSM 780 confocal microscope. Confocal image stacks were collected throughout the entire volume of each fiber using a 20X (NA 0.4 - 0.8) objective with a 1.5 µm z-step size. The AChRs and synaptic nuclei were imaged with a 40X (NA 1.4) oil immersion objective with a 0.3 µm z-step size. ImageJ was used for all measurements. Adobe Photoshop was used to stitch the images of entire myofibers from overlapping maximum projections of the image stacks. Myofiber length and diameter were measured using the ImageJ segment tool. Measurements of the diameter were taken in the XY and Z direction at 3 equidistant points along the length of the muscle and averaged. Volume was calculated by using the formula $V = \pi r^2 \text{ x } l$. Nuclear number, number of central nuclei, and number of branches were quantified from confocal stacks. Myonuclear domain was calculated by dividing myofiber volume by total number of nuclei. Synaptic nuclei were counted by hand and categorized as synaptic if they met the following 2 criteria: they were within 1 µm of the sarcolemma and they were directly beneath the AChRs.

2.2.5 Statistical Analysis

For analysis of whole mounts, N=3 animals were used per age group and 100 junctions were analyzed per muscle for a total of 300 junctions per group. Junctions were considered fragmented if they had 5 or more separate receptor rich areas within the junction. Counts were transformed into relative frequencies and averaged by group. For analysis of single fibers, 360 total myofibers from 36 mice were analyzed. Mice were grouped by age (2, 6, 12, 24, 52, 104 weeks) and genotype (mdx or C57BL10J). Two way ANOVA with Tukey *post hoc* analysis was used to assess significance between groups. All statistical analyses were performed using Prism GraphPad 7 software. Statistical significance was set at $P < 0.05$.

2.3 Results

2.3.1 Mdx mice undergo progressive myofiber hypertrophy and hypernucleation

One of the signature features of DMD is muscle hypertrophy that occurs in the early stage of the disease, followed by muscle atrophy as the disease advances (Reimers et al., 1996; Kornegay et al., 2012). In order to determine if mdx mice follow the same pattern of growth we isolated single myofibers (Figure 2.1) and tracked three aspects of myofiber size - length, diameter, and volume - throughout the lifespan. Myofiber length develops normally in mdx mice, showing no difference from WT through the first year of life. However, at 2 years of age mdx myofibers are longer than WT, likely due to

complex branching architecture seen at high rates in aged mdx mice (Figure 2.2A). Myofiber diameter also develops normally in mdx mice through the first 12 weeks of life, however, by 24 weeks, mdx mice have significantly larger diameters than WT and this increase persists through the lifespan (Figure 2.2B). Myofiber volume develops normally in mdx mice through the first 12 weeks of life, but beyond that myofibers become progressively hypertrophic (Figure 2.2C). By 2 years of age mdx myofibers are 155% larger than age-matched WT myofibers (Figure 2.2C). Between 1 and 2 years of age WT myofibers lose an average of 27% of their volume while mdx myofibers increase in volume by an average of 18%. While the loss of volume in WT individual myofibers is not significant, it likely contributes to significant sarcopenia on the muscle level (Sheard and Anderson, 2012). Interestingly, mdx myofibers do not seem to be susceptible to atrophy associated with sarcopenia. These results indicate that the myofiber hypertrophy seen in mdx is progressive and does not follow the pattern seen in DMD. Previous reports demonstrate that hypertrophy induced in WT muscles is preceded by an increase in myonuclei (Bruusgaard et al., 2010). This is thought to be necessary to support the increased volume of the cell.

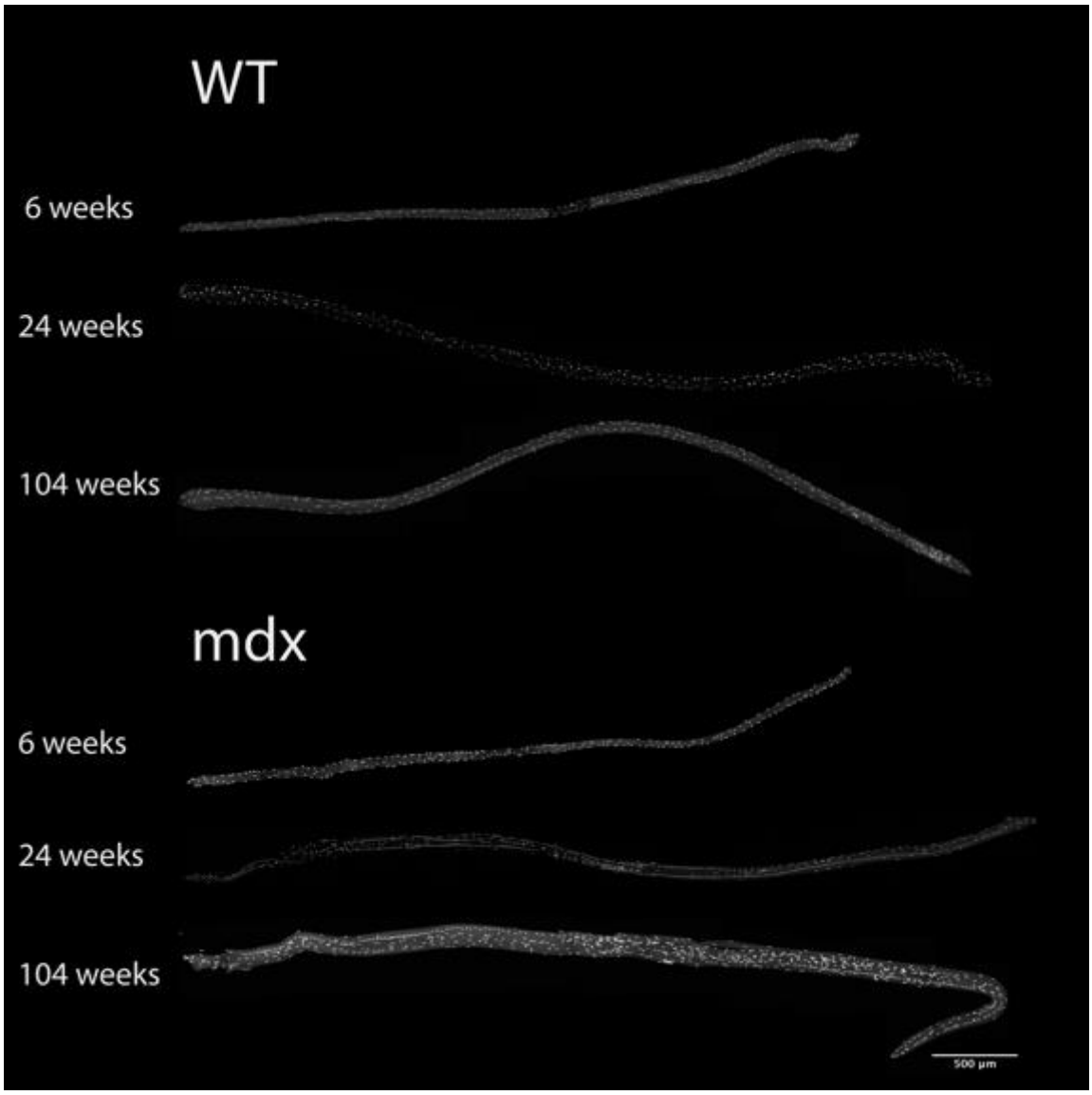

Figure 2.1 Isolated myofibers from WT and mdx EDL muscles at various ages. Representative images of myofibers throughout the lifespan stained with DAPI to visualize nuclei.

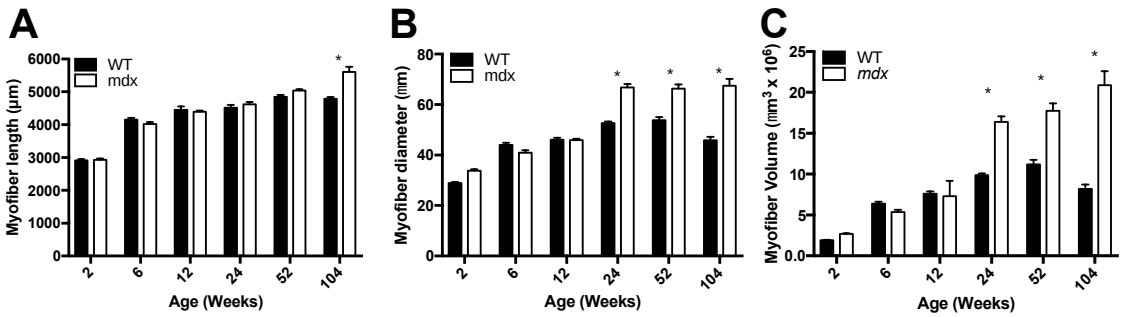

Figure 2.2 Measures of myofiber size in mdx and WT myofibers.
A) Myofiber length is not altered in mdx mice until 2 years of age, at which time extensive branching architecture occurs in mdx muscles. B) The diameter of mdx myofibers is larger than age-matched WT starting at 24 weeks and continuing through the lifespan. C) Mdx myofibers become progressively hypertrophic throughout the lifespan and are not susceptible to atrophy in old age. N = 3 mice and 30 myofibers per group. Analysis via two way ANOVA with Tukey *post hoc* test. * = $p < 0.05$.

The presence of central nuclei in myofibers has long been considered to be a marker of myofiber repair and is a hallmark of DMD pathology. We tracked the number and location of myonuclei throughout the lifespan of mdx mice. The number of nuclei in mdx myofibers is no different from WT for the first 6 weeks; however, starting between 6 and 12 weeks mdx myofibers become hypernucleated (Figure 2.3A). This hypernucleation increases throughout the first year of life and then decreases between 1 and 2 years of age. The increase in myonuclear number precedes myofiber hypertrophy as expected from previous reports on WT myofiber hypertrophy (Bruusgaard et al., 2010).

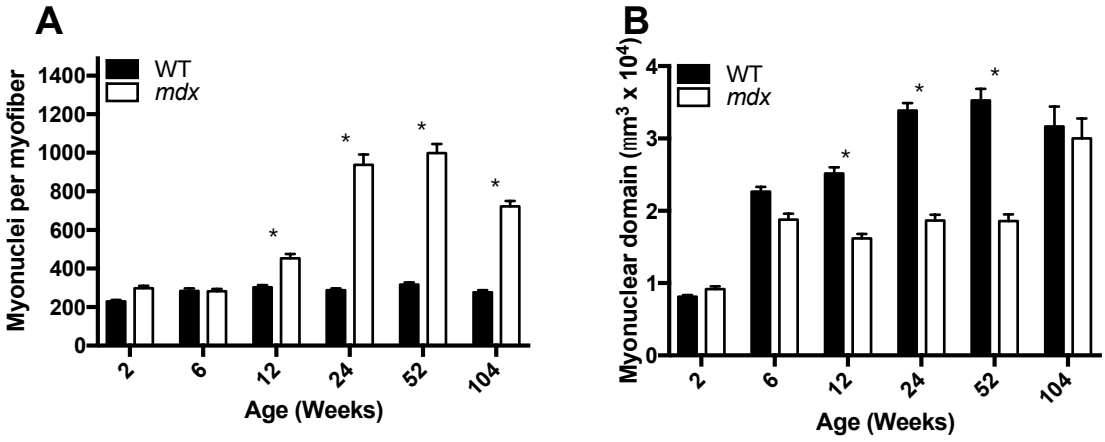

Figure 2.3 Myonuclear number and density in mdx and WT myofibers. A) Mdx myofibers become hypernucleated by 12 weeks of age demonstrating recruitment of new myonuclei prior to the onset of hypertrophy. Hypernucleation increases through the first year of life but decreases in severity in old age. B) The myonuclear domain of mdx mice is smaller than WT from 12 to 52 weeks of age indicating a higher density of myonuclei. N = 3 mice and 30 myofibers per group. Analysis via two way ANOVA with Tukey *post hoc* test. * = $p < 0.05$.

The relationship between myofiber volume and myonuclear number is accounted for in a statistic called myonuclear domain, which is the average volume of sarcoplasm per myonucleus. Dysregulation of the myonuclear domain is a pathological feature of human muscular dystrophies as well as spinal muscular atrophy (Tews and Goebel, 1997; Tews et al., 1997). In WT mouse myofibers the myonuclear domain increases steadily through the first year of life as a result of slow growth of the myofiber without the addition of myonuclei. Between 1 and 2 years of age, WT myonuclear domain decreases due to a loss of myofiber volume without a loss of myonuclei. This is in stark contrast to what we observe in mdx myofibers where there is growth of the myonuclear domain between 2 and 6 weeks followed by a preservation of the myonuclear domain

between 6 weeks and 1 year of age (Figure 2.3B). The mdx myonuclear domain is significantly smaller than WT at 12, 24, and 52 weeks indicating that there is a tight coupling between the addition of myonuclei and growth of the myofiber. The relationship breaks down in old age when mdx fibers continue to grow in size but lose myonuclei. The preservation of myonuclear domain size in mdx mice despite ongoing muscle fiber damage and repair indicates that processes within the myofiber regulate the myonuclear density. It is possible that the reduced myonuclear domain size in mdx mice corresponds to the increased protein demands of a cell tasked with repeated repair.

2.3.2 Myofiber branching and central nuclei contribute to hypertrophy and hypernucleation respectively

As referenced above, myofiber branching plays a significant role in myofiber hypertrophy (Faber et al., 2014). While no significant branching occurs in WT mice, we found that branching started in mdx EDL muscles between 6 and 12 weeks of age and increased in severity throughout the lifespan such that by 2 years of age the average mdx myofiber contained approximately 3 separate branches (Figure 2.4A). Branching architecture in these myofibers is complex and irregular, often branching several times in close proximity or rerouting the fiber in direction that is not parallel to the length of the muscle itself (Figure 2.4B-D). These branch points have previously been demonstrated to be sites of mechanical weakness and as such are likely to contribute to cycles of myofiber damage (Chan et al., 2007).

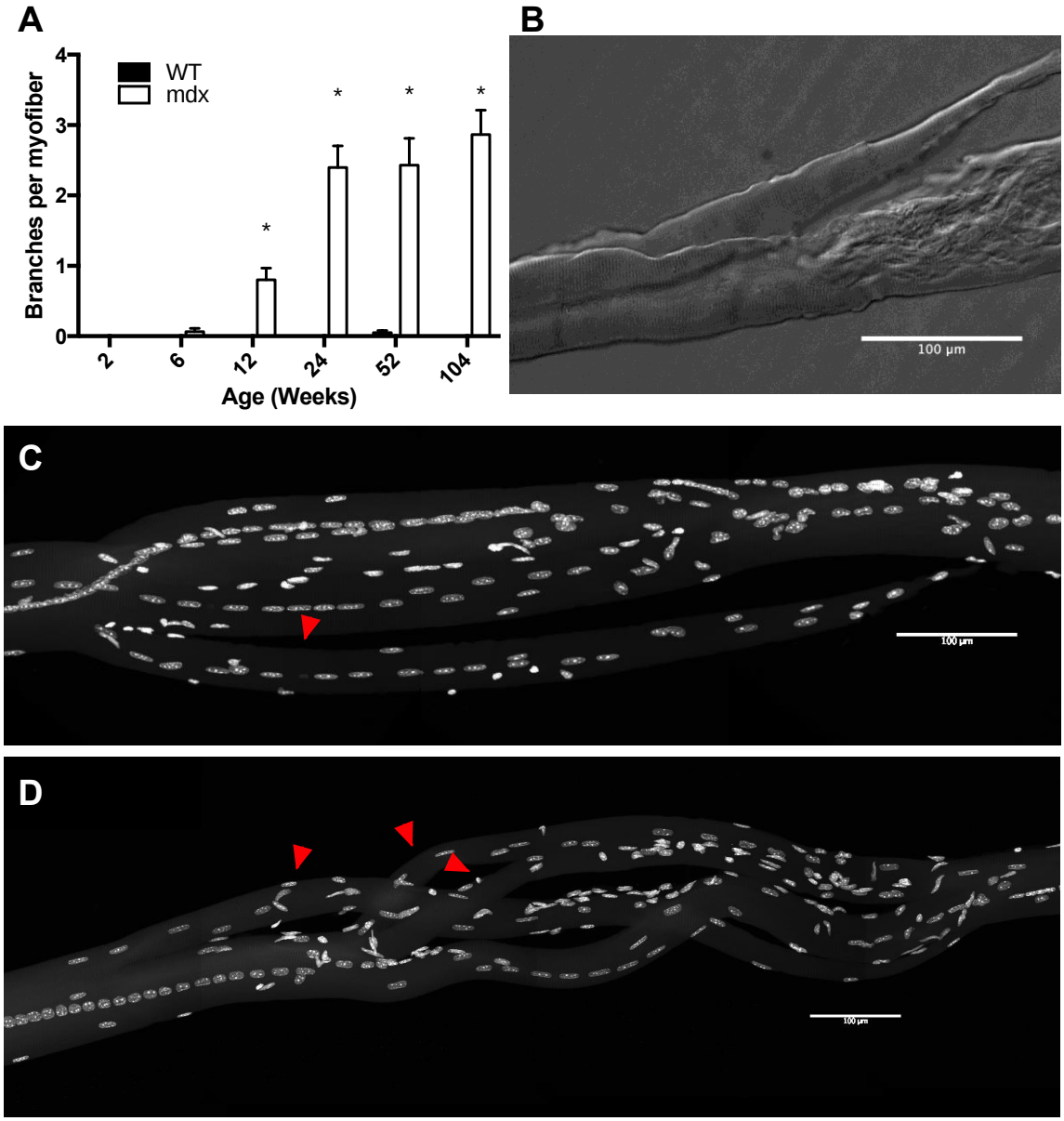

Figure 2.4 Myofiber branching in mdx myofibers.
A) Myofiber branching increases with age in mdx mice. No significant branches were observed in WT mice. B) Differential interference contrast image of a damaged myofiber with a branch from a 24-week-old mdx mouse. C) An example of a myofiber branch from a 52-week-old mdx mouse. Red arrowhead identifies the branch. D) An example of complex branching architecture seen in 104-week-old mdx mice. Red arrowheads identify branches. Scale bars = 100 µm. N = 3 mice and 30 myofibers per group. Analysis via two way ANOVA with Tukey *post hoc* test. * = $p < 0.05$.

The presence of central nuclei in myofibers is a marker of myofiber repair and has long been recognized as a sign of diseased muscle tissue (Jirmanova and Thesleff, 1972). Here, we categorized each myonucleus as central or peripheral based on its location relative to the sarcolemma. WT myofibers do not have significant numbers of central nuclei at any time point. However, mdx myofibers begin to accrue large numbers of central nuclei between 6 and 12 weeks, a hallmark of myofiber repair (Jirmanova and Thesleff, 1972). The number of central nuclei per myofiber increases through the first year of life, and then decreases between 1 year and 2 years of age, following the same pattern as total myonuclear number (Figure 2.5A). By 24 weeks of age, all myofibers analyzed contained central nuclei at some point along their length, indicating that 100% of myofibers underwent damage and repair in the first 24 weeks of life (Figure 2.5B).

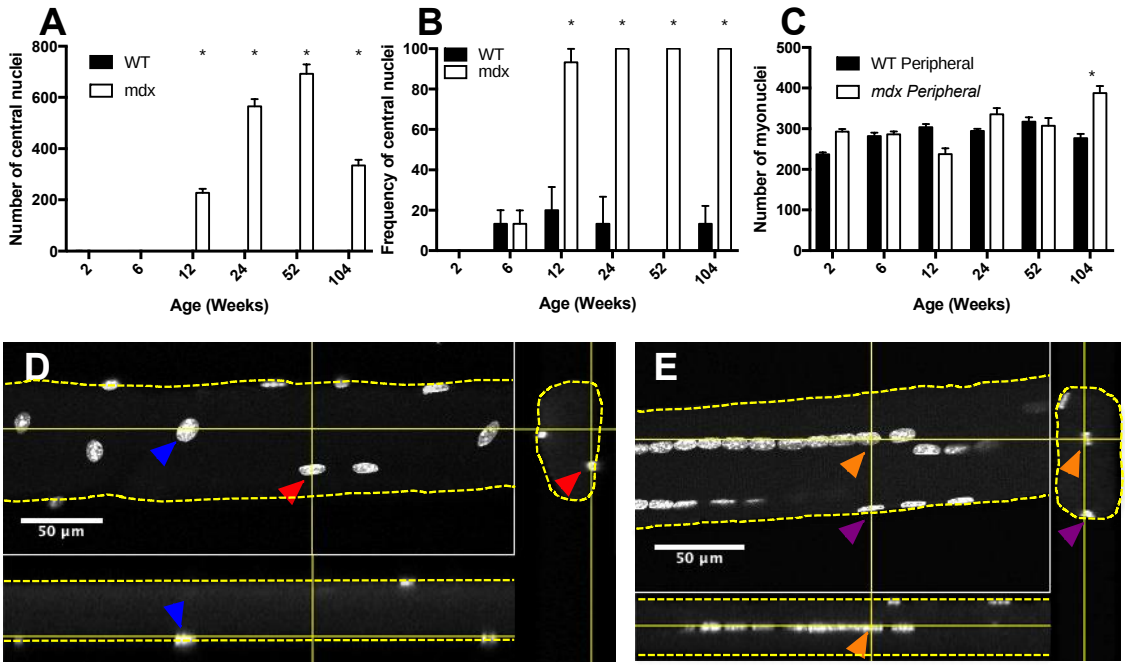

Figure 2.5 Number and location of myonuclei in mdx and WT myofibers.
A) Mdx myofibers accrue progressively more central nuclei throughout the first year of life. Central nuclei number decreases in the second year of life, coincident with a decrease in total myonuclear number. B) Frequency of myofibers containing central nuclei at any point along their length. By 24 weeks of age 100% of mdx myofibers contain central nuclei. C) Mdx and WT myofibers have same number of peripheral nuclei through the first year of life. This indicates that central nuclei in mdx account for hypernucleation. D) Confocal image of a 24-week-old WT myofiber containing peripheral nuclei with orthogonal views. Solid yellow lines indicate virtual slices. Dashed yellow lines outline myofibers. Color coated arrowheads identify the same myonucleus from different views. E) Confocal image of a 24-week-old mdx myofiber containing peripheral and central nuclei with orthogonal views. Solid yellow lines indicate virtual slices. Dashed yellow lines outline myofibers. Orange arrowheads identify a central nucleus from different views. Purple arrowheads identify a peripheral nucleus from different views. N = 3 mice and 30 myofibers per group. Analysis via two way ANOVA with Tukey *post hoc* test. * = $p < 0.05$.

We assessed the number of peripheral and central nuclei as separate populations and observed that the number of peripheral myonuclei in mdx myofibers is not different from the total number of myonuclei in WT myofibers until 2 years of age (Figure 2.5C). Therefore, the hypernucleation seen in mdx myofibers throughout the first year of life is completely accounted for by the presence of central nuclei. This replicates the finding first reported by (Duddy et al., 2015).

2.3.3 Mdx mice undergo progressive endplate fragmentation and accumulation of synaptic nuclei

Fragmentation of the NMJ may have important implications for synaptic transmission. There is some evidence of fragmentation of the AChR aggregate at the NMJ in DMD; however, the shape of the human NMJ is different than the mouse (Theroux et al., 2008). Fragmentation occurs in aging as well as in numerous disease states and has been induced by deliberate damage to muscles (Valdez et al., 2010; Li et al., 2011; Li and Thompson, 2011). In WT mice, fragmentation was first observed between 12 and 24 weeks; by 24 weeks about 6% of endplates were fragmented. The frequency of fragmentation increased through the lifespan such that, by 2 years of age roughly 26% of endplates were fragmented. In mdx, fragmentation first occurs between 2 and 6 weeks of age; by 6 weeks about 13% of endplates are fragmented. By 12 weeks the frequency of fragmented endplates jumps to 80% indicating that roughly 67% of myofibers underwent damage and repair to their NMJ during that 6-week period. At 24 weeks and beyond 100% of analyzed junctions were fragmented (Figure 2.6A). In order to assess the severity of fragmentation, we quantified the number of discrete fragments per endplate. There was no difference between mdx and WT in the first 6 weeks of life. By 12 weeks of age mdx junctions have significantly more fragments than WT (Figure 2.6B). Severity of fragmentation increases progressively in mdx mice through the first year of life but the number of fragments per endplate decreases between 1 and 2 years of age. This decline in old age is likely due to receptor and/or fiber loss as well as partial/full

denervation that occurs at this age. Regardless, the degree of NMJ fragmentation in mdx mice remains substantially greater than WT mice from 12 weeks of age onward.

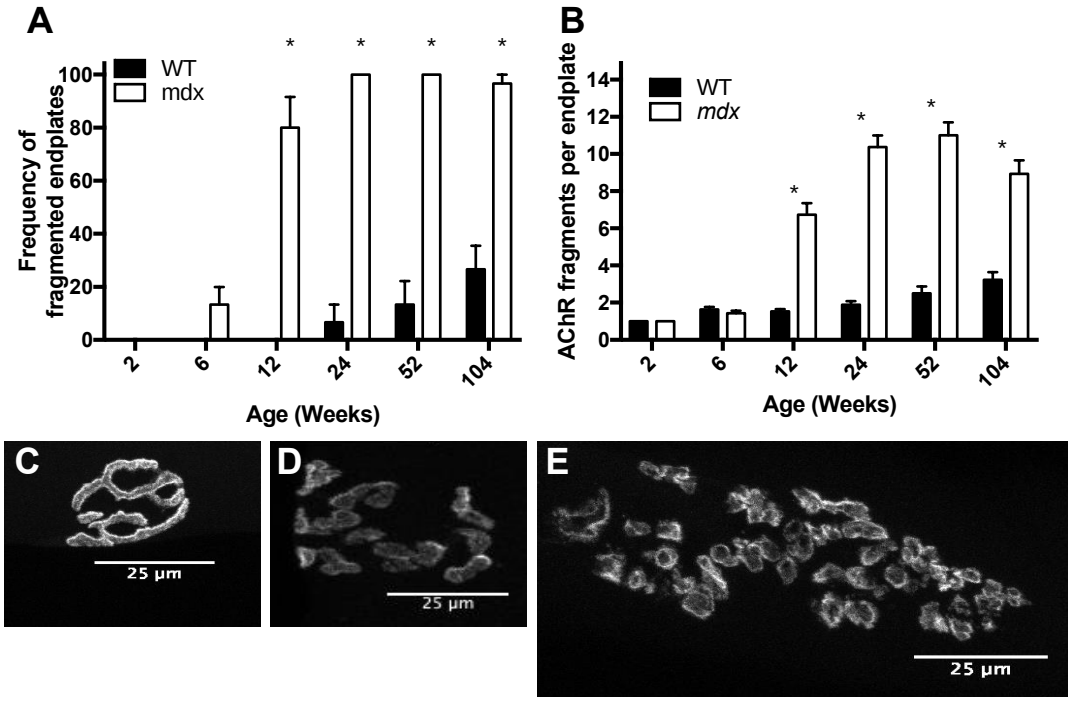

Figure 2.6 Frequency and severity of endplate fragmentation.
A) Rates of endplate fragmentation are elevated in mdx mice. By 24 weeks of age, every endplate analyzed was fragmented. B) The number of AChR fragments per endplate increases progressively through the first year of life. C) Endplate from a 12-week-old WT mouse stained with BTX demonstrating the continuous "pretzel" like morphology. D) Endplate from a 12-week-old mdx mouse stained with BTX demonstrating the fragmented phenotype. E) Endplate from a 52-week-old mdx mouse stained with BTX demonstrating the increase in severity of fragmentation with age. Scale is preserved between C, D and E. N = 3 mice and 30 myofibers per group. Analysis via two way ANOVA with Tukey *post hoc* test. * = $p < 0.05$.

Beneath each endplate lies a subpopulation of myonuclei known as synaptic nuclei. These nuclei are tethered to the sarcolemma by Syne-1 and provide the transcripts necessary to maintain the AChR aggregate (Grady et al., 2005). We assessed

the number of synaptic myonuclei beneath junctions to determine whether fragmentation of the AChR aggregate corresponds with changes in synaptic myonuclei populations. At WT neuromuscular junctions, there are approximately 5 synaptic myonuclei per junction at all time points assessed. However, in mdx mice, we observed a sharp increase in the number of synaptic myonuclei starting between 6 and 12 weeks of age. The number of synaptic myonuclei peaks at 24 weeks of age before steadily decreasing with age (Figure 2.7A). Even with the decrease in old age, mdx mice have elevated numbers of synaptic myonuclei relative to WT at 12, 24, 52, and 104 weeks. Interestingly, synaptic myonuclear numbers begin to tail off before the decline in total myonuclei.

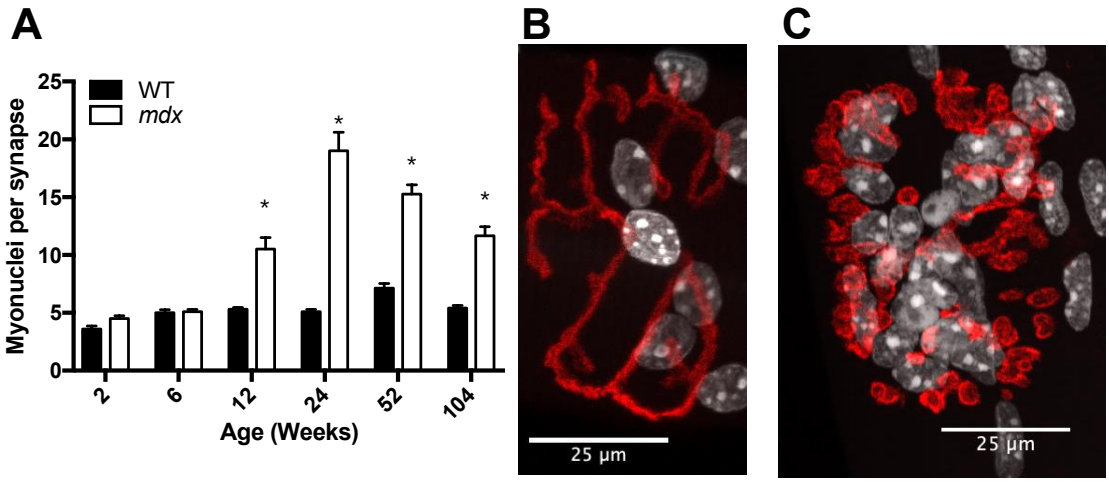

Figure 2.7 Mdx mice possess greater numbers of synaptic myonuclei beginning at 12 weeks of age.
A) Mdx NMJs have higher numbers of synaptic nuclei starting at 12 weeks of age and continuing through the lifespan. B) 24-week-old WT endplate and synaptic nuclei stained with BTX (red) and DAPI (white). C) 24-week-old mdx endplate and synaptic nuclei stained with BTX (red) and DAPI (white). Scale is preserved between B and C. N = 3 mice and 30 myofibers per group. Analysis via two way ANOVA with Tukey *post hoc* test. * = $p < 0.05$.

2.3.4 Endplate fragmentation rates in muscle whole mounts

The preceding data was collected by analysis of isolated single myofibers. It is therefore possible that the population of isolated myofibers is in some way biased by the preparation. Therefore, we analyzed the fragmentation rates of several muscles using the whole mount preparation technique to compare results with the single fiber analysis. As expected, there was no significant fragmentation in WT animals at the timepoints tested. However, in mdx there was a high rate of fragmentation in all three muscles at both 6 and 12 weeks (Figure 2.8). The results from the EDL muscle whole mounts are consistent with the data collected by single fibers, indicating that there is no significant bias in the sample of single muscle fibers with regard to damaged myofibers.

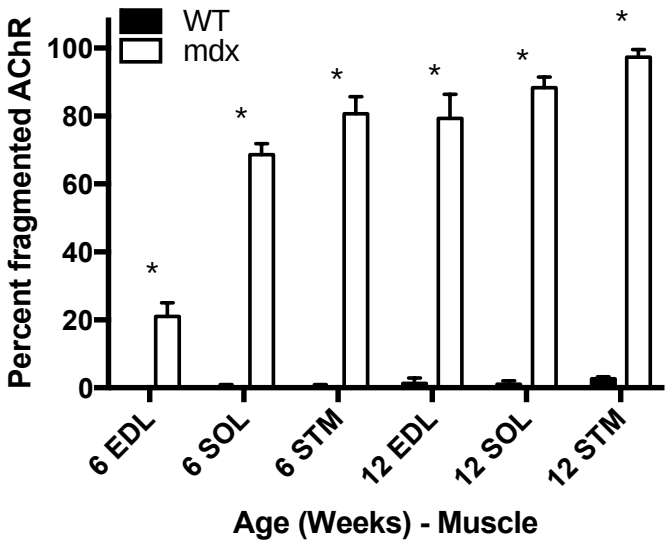

Figure 2.8 Rate of endplate fragmentation in different mdx and WT muscles.
Rate of endplate fragmentation in the EDL lags behind the SOL and STM at 6 weeks but is not significantly different from other muscles at 12 weeks. Fragmentation data from whole muscles is consistent with our observations in isolated myofibers. N = 3 mice and 300 NMJs per group. Analysis via two way ANOVA with Tukey *post hoc* test. * = $p < 0.05$.

2.4 Discussion

The results presented above demonstrate the progressive and persistent nature of the mdx pathology. By tracking pathological features through the lifespan of the mdx mouse, we were able to identify the degree to which these pathological features mimic the human disease in both severity and time course. It is unreasonable to expect that treatments will translate from the mouse to the human if the targets for treatment do not mimic the human disease.

The hypertrophied calf muscle of DMD boys is perhaps the signature feature of early pathology, however, in humans the hypertrophy gives way to atrophy and regenerative failure. In mdx mice, myofiber hypertrophy is progressive, such that in old age mdx myofibers are at their largest. It is clear from these results that at least a subset of mdx myofibers are resistant to age-related atrophy that is seen in DMD and aging WT mice. It seems that a large contributor to this hypertrophy is myofiber branching, which increases both the diameter and to a lesser degree, the length, of myofibers. The persistent hypertrophy of mdx myofibers was unexpected and does not replicate the human disease. Recently, inducing myofiber hypertrophy via manipulation of several different targets has been an area of intense research in the field. Inhibition of myostatin, a negative regulator of skeletal muscle size, is one such target to induce hypertrophy. Several treatments targeted at modulating this pathway have gone to clinical trials and been discontinued. While this target may show promise for treatment of the human disease, the mdx mouse would be an inappropriate model choice for inducing myofiber hypertrophy, as persistent hypertrophy is a feature of the pathology in mdx prior to any

therapeutic intervention. It is worth pointing out that despite hypertrophy on the level of single myofibers, these results do not indicate hypertrophy on the whole muscle level. Indeed, our own observations indicate that on a gross scale, the muscles of mdx mice are not larger than age-matched WT muscles, an observation that will be demonstrated in the subsequent section. The discrepancy between hypertrophy on the muscle fiber level but not on the whole-muscle level will be addressed in the subsequent section.

Muscle hypertrophy is thought to be supported by a preceding increase in myonuclei, presumed to be necessary to support the increased cell volume (Hall and Ralston, 1989). We observed a significant increase in myonuclei before the occurrence of hypertrophy, consistent with reports of hypertrophy induced in WT mice (Bruusgaard et al., 2010). In mdx, hypernucleation increases dramatically through the first year before decreasing in the second year of life. It is surprising that the myonuclear number decreases in the second year despite persistent hypertrophy at this time point. In order for the number of nuclei to decrease two possibilities present themselves. First, there may be a loss of myonuclei through apoptosis. Second, myonuclei may be lost in a myofiber damage event and are not adequately replaced upon repair, possibly as a result of satellite cell failure. There is some evidence that mice are less prone to SC exhaustion because they have longer telomeres than humans; however, it is still conceivable that SC exhaustion could occur in old age (Sacco et al., 2010). It is possible that SC failure occurs for reasons other than telomere shortening or that myonuclei loss in old age occurs for reasons other than SC failure.

We have found that the frequency of central nuclei in isolated myofibers of mdx mice is over 93% at 12 weeks of age. This is higher than previous reports that rely on analysis of transverse muscle fiber sections (Carnwath and Shotton, 1987), a discrepancy likely due to the fact that we analyzed isolated whole myofibers from tendon to tendon. Therefore, the result reported here is the frequency that central nuclei occur anywhere along the length of the myofiber, rather than within a given transverse section or series of sections. This is one disadvantage of analysis via transverse sections, a topic that will be covered in greater detail later. The number of central nuclei in mdx myofibers follows the same pattern as total myonuclear number, increasing for the first year of life and then decreasing thereafter. Between 1 and 2 years of age, we observed a 28% loss of myonuclei that corresponds with a 52% loss of central nuclei. This suggests that central nuclei are preferentially lost relative to peripheral nuclei in aged mdx muscle. Whether this indicates dysfunction in the population of central nuclei in old age, or a failure of regeneration in old age is open to interpretation and deserves further research. Regardless, it is clear that myonuclear loss occurs at a time when myofiber hypertrophy is persistent, causing the myonuclear domain of mdx mice to increase dramatically in old age.

Myonuclear domain is a reliable indicator of myofiber health, and dysregulation in myonuclear domain has been used as a marker for disease (Tews and Goebel, 1997; Tews et al., 1997; Allen et al., 1999). Indeed, we observed that the myonuclear domain of mdx mice remains at a constant depressed size throughout adulthood. It is possible that high rate of turnover in these diseased muscles requires a higher density of

myonuclei in order to attempt to repair muscle more effectively. As mdx mice enter old age, they undergo dramatic increase in myonuclear domain that is likely the result of continued myofiber hypertrophy coincident with myonuclear loss. It is easy to see how this could lead to myofiber damage and potentially loss as the decreased density of nuclei may not be able to support high demands of a cell in need of repeated repair. The activity and effectiveness of myonuclei in mdx is an area deserving of further investigation.

Myofiber branching has been shown to be a result of the repair process from many different types of muscle injury (Chan et al, 2007; Pichvant and Pavlath, 2014). The branch points are sites of mechanical weakness that are prone to contraction induced injury and may lead to repeated turnover and increased branching as a result. In isolated myofibers we observed a steady increase in myofiber branching throughout the lifespan. By old age, mdx fibers have an average of 3 branches per myofiber, compared to wild-type mice, which display negligible branching. These branches contribute to increased myofiber volume, primarily through increased diameter. We observed that myofiber branches do not feature synapses, and this may have negative consequences for the propagation of action potentials in muscle fibers. In our analysis of over 300 mdx myofiber branches, we found only a single instance of branching with an AChR aggregate (data not shown). In this instance, the branch occurred directly through the junctional area and the two aggregates lined up next to each other on their respective branches. We do not know if both aggregates were innervated because the fiber was isolated from the nerve.

We found that endplate fragmentation is dramatically elevated throughout the lifespan of mdx mice and increases in severity through the first year of life. In old age, mdx mice have slightly fewer AChR fragments per junction than at 1 year old. This result is unexpected. Although some evidence exists that NMJs can revert to less fragmented morphology in cases of exercise and caloric restriction (Valdez et al., 2010), there is no reason to anticipate that aged mdx mice would go through this process. There are several other possible explanations for this observation. First, aged mdx mice are undergoing partial/full denervation at their NMJs. As a result, some AChR fragments, no longer receiving axonal input, are lost. Indeed, some evidence exists that this is the case. When a partial block is put on a receptor aggregate using snake toxin, that area of the receptor is lost (Balice-Gordon et al., 1994). In addition, we observed some very faintly stained receptor fragments in old age mdx tissue that were excluded because they were under the intensity threshold required for analysis. These faint receptor fragments have been observed and reported previously (Valdez et al., 2010). Another possibility is that there is significant myofiber loss in aged mdx mice and that the loss preferentially occurs in a population of fibers that are more susceptible to damage. These same fibers, having undergone more cycles of degeneration and regeneration than their resistant counterparts, may also have a more severely fragmented endplate. This would leave behind a population of less severely fragmented endplates. We are aware of only one report that observed myofiber loss in mdx mice, but it was not quantified (Lefaucheur and Pastoret, 1995).

The results presented here extend the understanding of mdx pathology in relation to DMD. We demonstrate for the first time that mdx mice do not replicate the late stage muscle atrophy of DMD. Inducing muscle hypertrophy has been a popular therapeutic target over the last ten years; however, these results demonstrate that mdx myofibers are pathologically hypertrophic, making them a poor model for testing these therapies. On the other hand, mdx mice do replicate many of the pathological features of DMD such as central nuclei, myofiber branching, and potentially endplate fragmentation. Importantly, these features progressively increase in severity with age, making them valuable biomarkers for testing the efficacy of therapeutics. We conclude that the value of the mdx mouse model in testing therapeutic efficacy is target dependent, and the pathology of aged mdx mice deserves further examination.

3. MYOFIBER LOSS IN MDX MICE

3.1 Research Rationale

Mdx myofibers undergo progressive hypertrophy into old age (Section 2). However, we did not observe that these muscles were larger than age-matched WT muscles on a gross scale. Previous research supports this observation, indicating that if mdx and WT muscles are different in aged time points, mdx muscles are smaller (Lefaucheur and Pastoret, 1995). The observation that mdx myofibers are substantially hypertrophic, but mdx muscles are not initially seems contradictory. However, the loss of whole muscle fibers could explain these findings. In DMD, muscle fiber loss is a driver of pathology, leading to progressive muscle weakness. As a salient feature of DMD, myofiber loss has been assessed many times in the mdx mouse, but very little information is available regarding this effect in old age. Analysis of myofiber loss in aged mdx mice has important implications for the development of therapeutics. Prior to the advent of mechanical ventilation, respiratory failure due to diaphragm weakness was the primary cause of death in DMD patients. Therapeutics targeting prevention of myofiber loss in DMD stand to improve quality of life dramatically.

Previous research in the mdx mouse indicates that myofiber loss does not occur in mdx (Tanabe, 1986; Pagel and Partridge, 1999). On the contrary, increased myofiber number is reported in adult mdx mice. As discussed previously, only one report notes myofiber loss in aged mdx muscles, but does not quantify it (Lefaucheur and Pastoret, 1995). Complicating this matter, most reports on fiber number in mdx muscles have

relied on cross-sectional analysis for myofiber quantification. This preparation works well in WT mice, where there is minimal or no myofiber branching; however, there is significant branching in mdx muscles. When analyzing cross sections, there is no reliable method to distinguish a myofiber branch from an independent myofiber. As a result, cross-sectional analysis may lead to a substantial overestimation of myofiber number, skewing measurements of myofiber cross-sectional area and diameter for the same reason. This is demonstrated nicely in a report investigating myofiber number in the third compartment of the EDL muscle (Faber et al., 2014). By traditional methods, they find a 25% increase in myofiber number in the third compartment of the EDL in mdx mice but no corresponding increase in synapse number, indicating that there is no true hyperplasia in mdx, but rather dramatic myofiber branching. Here, we attempt to build on this work by extending these results into aged time points and using tissue clearing techniques to analyze three different whole muscles. The culmination of this work will determine if this hallmark feature of DMD is replicated in the mdx mouse, potentially identifying a new marker for testing the efficacy of therapeutics.

3.2 Materials and methods

3.2.1 Mouse strains

Mice were generated as in section 2.2.1. Three male mice per genotype and age were used for each experiment, totaling 56 mice in Sections 2 and 3. All experimental procedures were approved by the Texas A&M University Institutional Animal Care and

Use Committee (2016-0158 or 2019-0179) and in full compliance with the NIH Guidelines for the Humane Care and Use of Laboratory Animals.

3.2.2 Cross section analysis

Mice were sacrificed via intraperitoneal injection of 0.15 mL of Euthosol (Med-Pharmex). Following sacrifice, both sternomastoid, soleus, and extensor digitorum longus muscles were dissected, weighed, and pinned at resting length in a Sylgard-lined dish and fixed using 4% PFA for 30 minutes. After fixation, the muscles were washed 3 times in PBS. Muscles were placed into a 30% sucrose solution overnight in preparation for freezing. Muscles were frozen in optimal cutting temperature blocks by exposure isopentane cooled to -80 degrees C in liquid nitrogen. Muscles were sectioned through the belly of the muscle at a thickness of 15 μm. Sections were mounted on slides in preparation for staining.

Sections were labeled with wheat-germ agglutinin (1 mg/mL) conjugated to Alexa Fluor™ 488 (Thermo Fisher Scientific Cat# W11261) diluted 1:500, α-bungarotoxin (1 mg/ml) conjugated to Alexa Fluor™ 555 (Thermo Fisher Scientific Cat# B35451) diluted 1:500, and DAPI (1 mg/ml) (Thermo Fisher Scientific Cat# D3571) diluted 1:2000 in standard blocking solution. Sections were then washed 3 times with PBS and slides were cover slipped in anti-fade fluorescence mounting medium.

3.2.3 Muscle clearing

The following tissue clearing protocol was adapted from the MYOCLEAR protocol (Williams et al., 2019). Mice were sacrificed via intraperitoneal injection of 0.15 mL of Euthosol (Med-Pharmex). Following sacrifice, we performed transcardial perfusion with ice cold 4% PFA. STM, EDL, and SOL muscles were dissected, weighed, and pinned at resting length in a Sylgard-lined dish and fixed overnight in 4% PFA at 4 degrees C. Muscles were then washed in PBS overnight with 4 solution changes in preparation for the hydrogel/polymerization step.

Muscles were incubated in 12.5 mL of A4P0 (4% acrylamide, 0% paraformaldehyde) hydrogel solution in a 15 mL conical tube. Muscles were kept at 4 degrees C with gentle rocking overnight. The next day, samples were placed in a vacuum desiccator for 30 minutes. The chamber was then flooded with nitrogen gas and the tubes were capped and sealed. Muscles were incubated at 37 degrees C for 3 hours. Muscles were washed in PBS overnight with 4 solution changes in preparation for labeling.

Muscles were stained with α-bungarotoxin (1 mg/mL) conjugated to Alexa Fluor^{TM} 488 (Thermo Fisher Scientific Cat# B13422) diluted 1:500 and Draq5 (Thermo Fisher Scientific Cat# 62251) diluted 1:1000 in PBS with 0.01% sodium azide. Muscles were labeled at room temperature for 4 days, refreshing solution halfway though. Immediately after refreshing the staining solution, muscles were centrifuged for 2 hours at 600 g in order to increase the depth of antibody penetration (Lee et al., 2016). Subsequently, muscles were washed in PBS with 4 buffer changes over 24 hours. After

the third buffer change muscles were again centrifuged for 2 hours at 600g. Muscles were mounted in a column of agarose in a syringe with the tip removed. After allowing the agarose to solidify for 60 minutes, the syringes were placed in 15 mL conical vial containing 10 mL of refractive index matching solution (RIMS) made with 30g nycodenz (Alere Technologies Prod# 1002424) in 22.5 mL 0.02M phosphate buffer. The syringe was then partially depressed lowering the column of agarose and the sample into the RIMS. The samples were rocked for 2 days protected from light to create a uniform refractive index throughout the sample.

3.2.4 Image acquisition and analysis

Cross sections were analyzed using a Leica DMRX epifluorescence microscope with 20x (NA 0.6) or 10x (NA 0.3) objective. CSA was measured using the 20x images with wheat germ agglutinin to outline myofibers. BTX staining was used to ensure that the section was taken within the endplate band in the center of the muscle. CSA was measured in ImageJ by tracing the outline of the fiber with the freehand selection tool and measuring the area. 100-200 myofibers were analyzed per animal for a total of 350-550 CSA measurements per group. Myofiber number was counted by hand using wheat germ agglutinin labeling in 10x images of whole cross sections reconstructed from overlapping images.

Cleared muscles were imaged using a Zeiss Z.1 light sheet microscope using a 5x (0.16 NA) objective. Whole muscles were imaged in 3-8 overlapping stacks so that entire muscles could be reconstructed. The 488nm and 638nm lasers were used to image

the BTX and DRAQ5 staining respectively. Image stacks were imported in ImageJ and synapses were counted by hand through analysis of Z stacks.

3.2.5 Statistical analysis

For all experiments, muscles were grouped by age, adult (11-14 months) and aged (21-24 months) and genotype (WT and mdx). For analysis of muscle weight N=3 mice per group and 6 muscles per group were weighed. For analysis of CSA, N=3 mice per group and 100-200 myofibers were analyzed per animal for a total of 350-550 CSA measurements per group. For analysis of myofiber number in cross sections, N=3 mice per group were analyzed. For analysis of synapse number in cleared muscles, N=3 mice per group were analyzed. Two way ANOVA with Tukey *post hoc* analysis was used to assess significance between groups. All statistical analyses were performed using Prism GraphPad 7 software. Statistical significance was set at $P < 0.05$.

3.3 Results

3.3.1 Mdx muscle weights are not different from wild type

In the previous section we observed significant hypertrophy in mdx myofibers, but qualitatively observed that the muscles did not appear larger than their WT counterparts. Here we recorded wet weight of whole muscles (STM, SOL, EDL) from WT and mdx mice during adulthood (11-14 months) and old age (21-24 months) to determine if myofiber hypertrophy contributes to whole muscle hypertrophy. There were no

differences between age matched mdx and WT muscle weight in any of the three muscles (Figure 3.1). However, in the EDL we observed significant loss of muscle weight between adult and aged WT mice, and a trend towards the same loss in mdx (Figure 3.1 A). In the SOL there was a significant loss of muscle weight between adult and aged mdx mice, and a trend towards the same loss in WT (Figure 3.1B). This trend was not observed in the STM muscle (Figure 3.1C). This pattern of results fits well with previously published research (Sheard and Anderson, 2012) but appears to stand at odds with our previous findings that individual muscle fibers are hypertrophic.

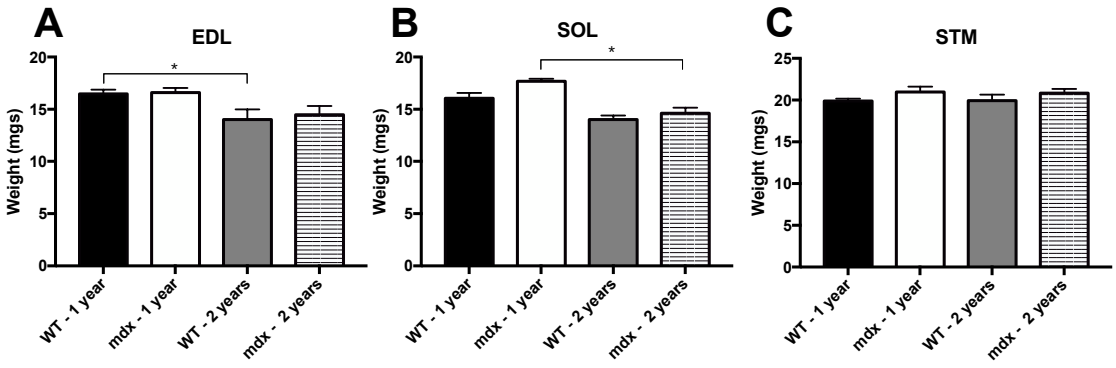

Figure 3.1 Muscle wet weights.
A) WT EDL muscle weight significantly decreases between 1 and 2 years of age. There is a trend towards the same finding in mdx. B) Mdx SOL muscle weight significantly decreases between 1 and 2 years of age. There is a trend towards the same in finding in WT. C) There is no difference in STM muscle weight between any group. Analysis via two way ANOVA with Tukey *post hoc* test. * = $p < 0.05$.

3.3.2 Muscle fiber cross-sectional area in mdx is characterized by increased variability but no mean difference from wild type

In the previous section, we demonstrated that isolated myofibers are hypertrophic, in part due to their increased diameter. From these results, it would be logical to expect that

cross-sectional area of mdx muscle fibers would also be larger. However, previous reports show no difference in mean cross-sectional area between mdx and WT, at least during adulthood. However, mdx myofibers have increased variability in their cross-sectional area due to what has been described as two distinct populations of fibers (Coulton et al., 1988). First are recently regenerated myofibers with small cross-sectional areas; second are large hypertrophic myofibers. Together these populations have the same mean as WT cross-sectional area but introduce increased variability. Certainly, there is a population of small caliber regenerating myofibers in mdx muscles. However, as we know from previous research there are an average of 3+ branches per myofiber in adult mdx tissue that bias this analysis (Chan et al., 2007). We posit that a portion of the population of small caliber myofibers are actually myofiber branches, indistinguishable from small caliber regenerating fibers. Here, we replicate the traditional analysis in order to demonstrate that our mdx mice are not different from those previously studied.

There is no difference in myofiber cross-sectional area between mdx and WT age matched groups. In all three muscles there is a trend towards reduced cross-sectional area in aged WT mice, but not in mdx. Mdx mice have greater variability in CSA in both adult and aged populations (Figure 3.2). These findings are in line with previous reports and demonstrate that the mdx mice in our colony are not different from populations previously studied.

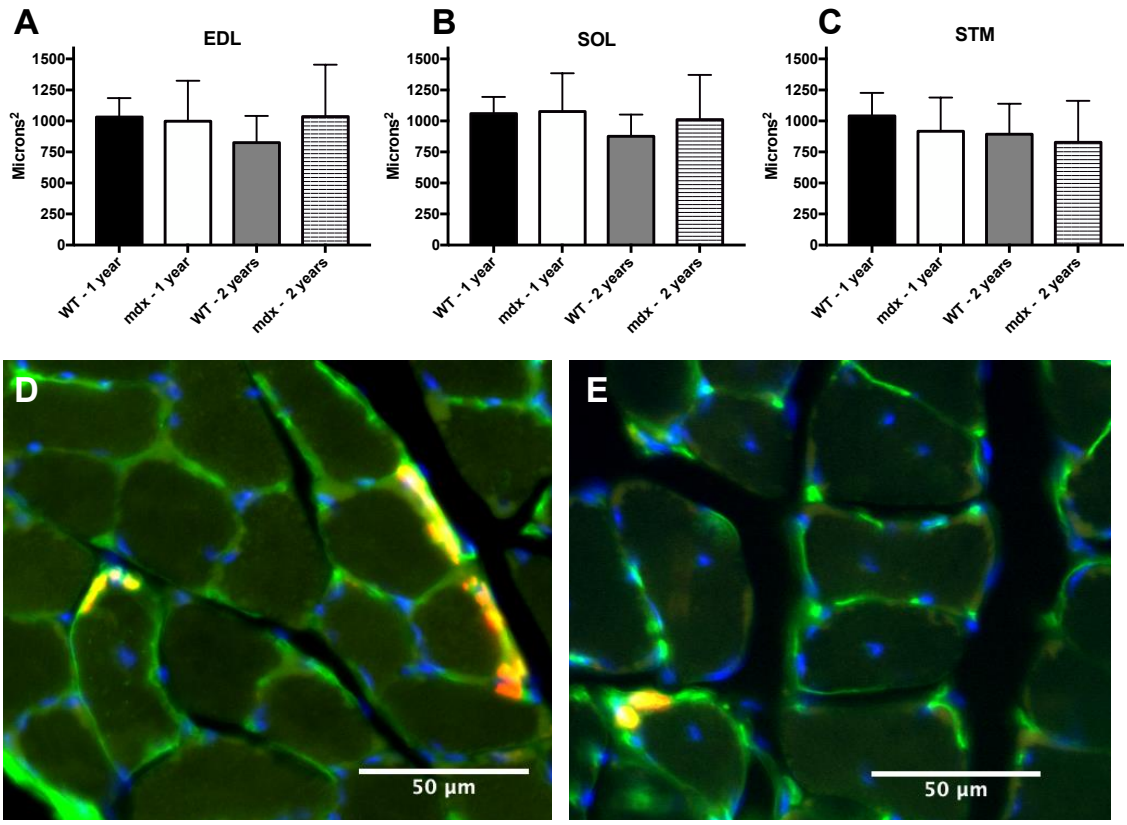

Figure 3.2 Cross-sectional area of adult and aged mdx and WT muscles.
There are no significant differences in age matched CSA between mdx and WT. However, there is greater variability in the CSA of mdx muscles relative to WT. A) CSA of adult and aged mdx and WT EDL muscles. B) CSA of adult and aged mdx and WT SOL muscles. C) CSA of adult and aged mdx and WT STM muscles. D) Transverse section of a WT adult mouse SOL muscle stained with wheat germ agglutinin to outline myofibers (green), DAPI to label nuclei (blue) and BTX to label AChRs (red). E) Transverse section of an mdx adult mouse SOL muscle stained with wheat germ agglutinin to outline myofibers (green), DAPI to label nuclei (blue) and BTX to label AChRs (red). Analysis via two way ANOVA with Tukey *post hoc* test.

3.3.3 Cross-sectional analysis shows no difference in myofiber number between age-matched mdx and WT muscles

In this section we replicate traditional myofiber number counts via cross section. Our findings align well with previous reports; we observed no significant difference in myofiber number between age-matched groups (Figure 3.3). Previous research indicates that the EDL and SOL muscles undergo significant myofiber loss between adult and aged time points but the STM is resistant to this change. Our results are generally in line with these reports. We observed a significant loss of muscle fibers in the EDL muscle of WT and mdx mice between adult and aged populations and a trend towards the same in the SOL. There was no significant myofiber loss in the STM (Figure 3.3A-C).

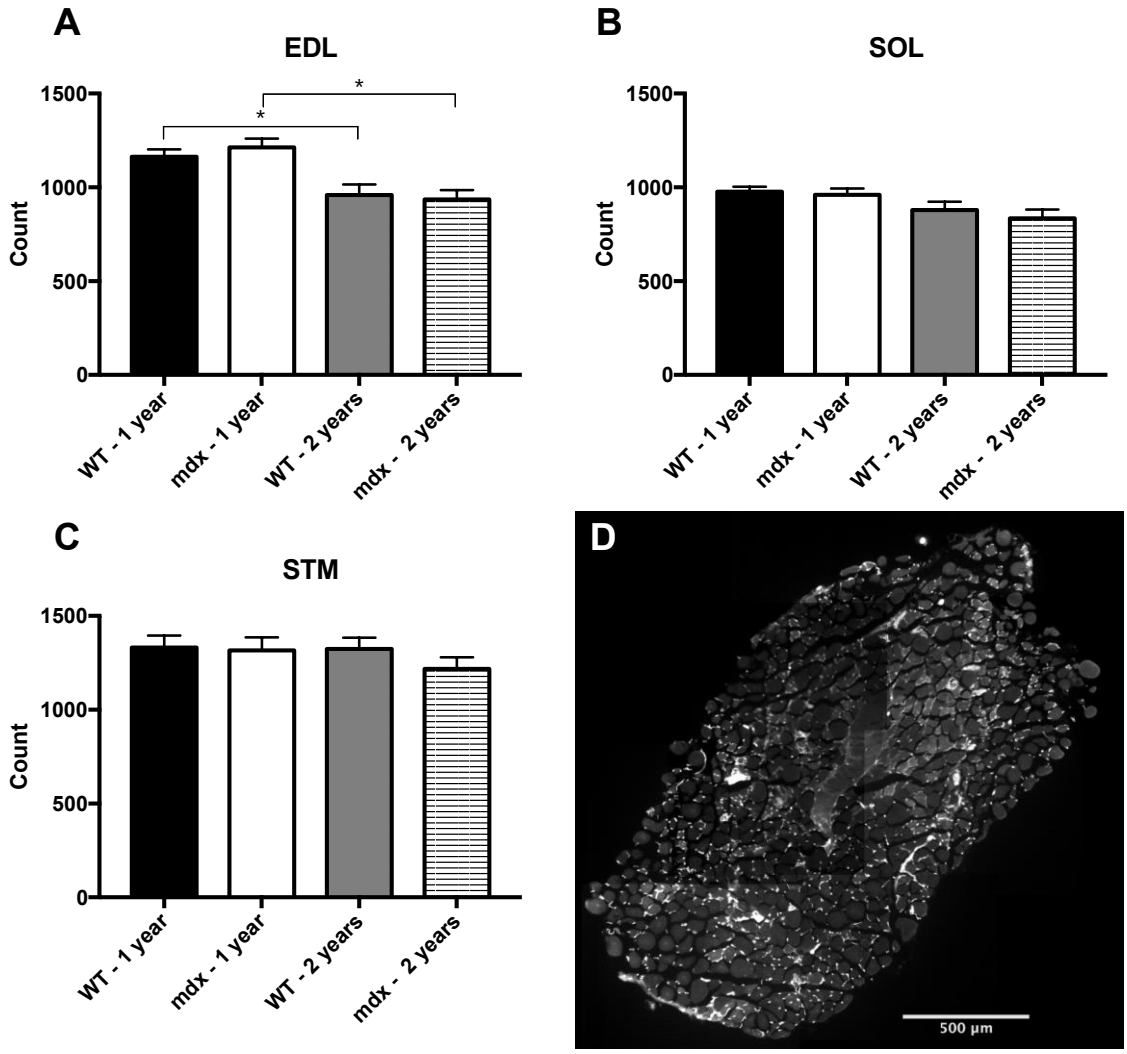

Figure 3.3 Myofiber number as counted by transverse sections.
A) Myofiber numbers in WT and mdx EDL muscles. There are no differences in myofiber number between mdx and WT age matched groups; however, both WT and mdx EDL muscles lose a significant number of myofibers as they age. B) Myofiber numbers in WT and mdx SOL muscles. There are no differences in myofiber number between mdx and WT age matched groups; however, there is a trend towards myofiber loss with age. C) Myofiber numbers in WT and mdx STM muscles. There are no differences in myofiber number between any groups in the STM muscle. (D) A cross section of an aged mdx SOL muscle reconstructed from overlapping images. Analysis via two way ANOVA with Tukey *post hoc* test. * = $p < 0.05$.

Previously, similar results have been interpreted to mean that mdx muscles do not undergo myofiber loss as seen in DMD. However, in cross section preparations it is very challenging to distinguish a myofiber branch from an independent myofiber. Given the significant degree of branching in adult and aged mdx muscles, there is evidence that substantial myofiber loss is being missed in this analysis due to counting myofiber branches as independent myofibers. In order to assess myofiber loss without bias by branching we counted synapses in cleared whole skeletal muscles.

3.3.4 Synapse counts in cleared tissue indicate significant myofiber loss in mdx mice

There is a robust one-to-one relationship between muscle fibers and innervating motor neurons after synapse elimination is complete. As noted in the previous section, this-one to-one relationship is preserved even in the instance of severe myofiber branching associated with the mdx pathology. Here, we utilize this information to count synapse number in cleared muscle tissue as a proxy for myofiber number. This strategy is employed in order to avoid the bias induced by counting myofiber branches in transverse sections.

WT mice undergo sarcopenia as a part of the normal aging process. This manifests itself both as a loss of muscle fibers, hypoplasia, and atrophy of existing myofibers. WT synapse counts followed the same pattern of results as WT myofiber counts. In WT EDL muscles, we observed a significant loss of synapses between adult and aged populations, and a trend towards the same in SOL and STM muscles. In mdx, all three muscles underwent significant synapse loss between adult and aged

populations, indicating that mdx mice are undergoing elevated rates of myofiber loss relative to WT (Figure 3.4).

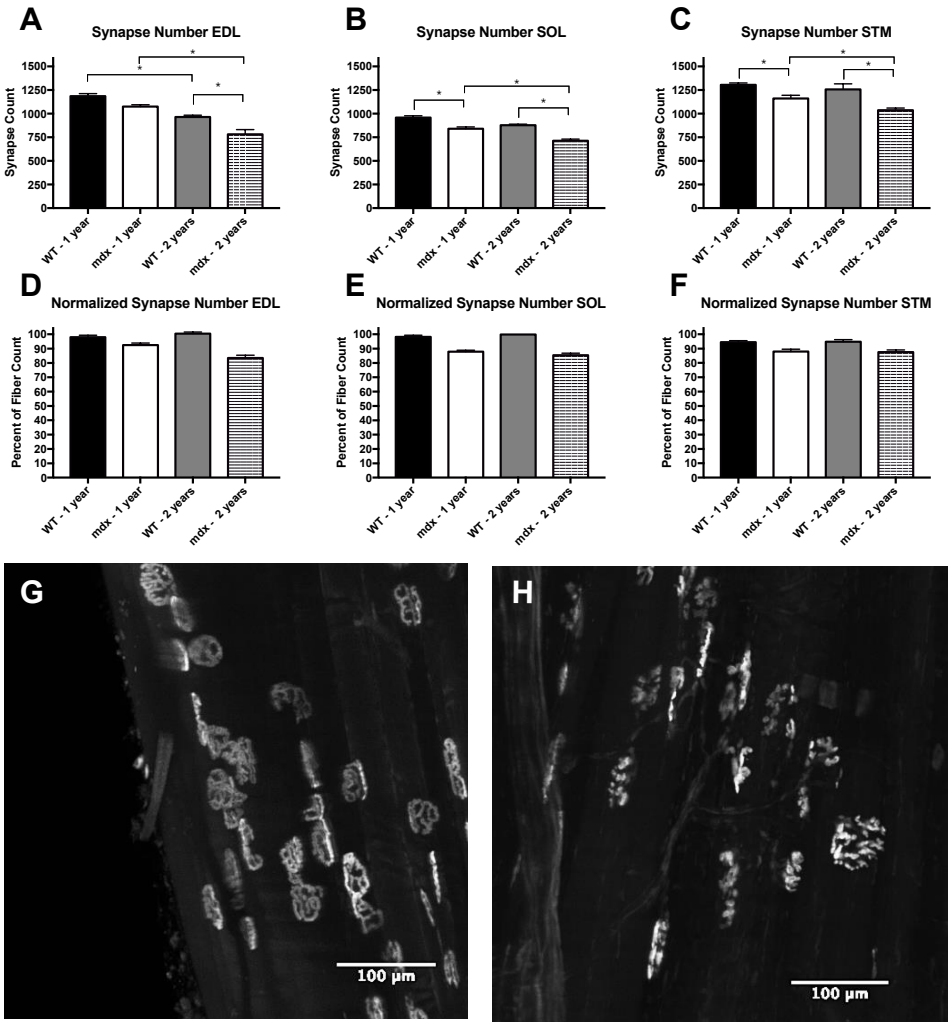

Figure 3.4 Raw and normalized synapse number in mdx and WT muscles.
A) Synapse loss occurs as a function of age in WT and mdx EDL muscles. At 2 years of age, mdx EDL muscles have significantly fewer synapses than age matched WT. B) Synapse loss occurs as a function of age in mdx SOL muscles and trends towards the same in WT. At 1 and 2 years of age mdx SOL muscles have significantly fewer synapses that age matched WT. C) Synapse loss occurs as a function of age in mdx STM muscles. At 1 and 2 years of age mdx STM muscles have significantly fewer synapses that age matched WT. D) Synapse number normalized against group matched myofiber number in the EDL muscle. E) Synapse number normalized against group matched myofiber number in the SOL muscle. F) Synapse number normalized against group matched myofiber number in the STM muscle. G) BTX labeled endplates from an adult WT EDL muscle. Most endplates display the normal continuous morphology. H) BTX labeled endplates from an adult mdx EDL muscle. Most endplates display the fragmented morphology. Analysis via two way ANOVA with Tukey *post hoc* test. * = $p < 0.05$.

At 1 year of age mdx SOL and STM muscles had significantly fewer synapses than age matched WT, indicating that myofiber loss had already taken hold. Synapse loss increased in severity with age; in every case aged mdx muscles had significantly fewer synapses than age matched WT muscles indicating significant myofiber loss in mdx beyond that associated with the sarcopenia (Figure 3.4A-C). WT synapse counts were on average 2.35% lower than their corresponding fiber count in transverse sections. The agreement of WT myofiber count via cross section and synapse count in cleared tissue indicates that counting synapses in cleared tissue is a reliable way to count myofibers. In comparison, synapse counts from adult and aged mdx muscles are on average 10.59% and 14.51% lower than their corresponding fiber counts respectively. By normalizing synapse count to age and genotype matched myofiber counts via cross section we demonstrate that mdx muscles have significantly fewer synapses than would be predicted by traditional myofiber counts (Figure 3.4 D-F). The uniformity of these results across three different muscles with different fiber type compositions indicates that this feature of the mdx pathology is widespread and preserved across muscles. Together these results indicate that mdx muscles undergo significant myofiber loss associated with disease pathology and replicate a hallmark feature of DMD.

3.4 Discussion

The results presented above indicate that mdx mice undergo substantial myofiber loss, potentially starting before 1 year of age and increasing in severity into old age. We performed whole muscle analysis to demonstrate that in three different muscles, aged

mdx mice have significantly fewer synapses than age matched WT. Synapse number was used as a proxy for myofiber number to avoid bias by including non-innervated myofiber branches. This builds on a previous report (Faber et al., 2014) and indicates that myofiber loss is a major feature of mdx pathology as it is in DMD (Emery, 2002).

In DMD, patients undergo transitory muscle hypertrophy that gives way to myofiber loss and a substantial decrease in muscle weight (Kornegay et al., 2012). The picture is less clear in mdx muscles. There is one report of extremely atrophied muscles in aged mdx mice (Lefaucheur and Pastoret, 1995), and many reports of hypertrophy in adult mdx mice (Pagel and Partridge, 1999). Here we find no difference in muscle weight between age-matched mdx and WT muscles, but a trend toward loss of muscle mass with age in the EDL and SOL but not the STM. It is possible that muscle weight is highly variable within mdx mice due to the degree of myofiber loss and fibrotic and adipose tissue deposition. Still, it is admittedly difficult to account for the dramatic difference in muscle weight between reports. We report that aged mdx muscles are not atrophied, despite significant myofiber loss. This indicates that myofiber branching and hypertrophy is responsible for the creation of enough new muscle volume to offset myofiber loss, but not enough to induce muscle hypertrophy.

Traditional analyses of cross-sectional area in mdx mice report no mean change but increased variability relative to WT, a finding we replicate here (Tanabe et al., 1986; Pastoret and Sebille, 1993a). These analyses, based on measurements from transverse sections, highlight two distinct populations of myofibers; the first population is comprised of small caliber regenerating myofibers and the second is comprised of large,

hypertrophic myofibers. These populations offset, resulting in no mean change in myofiber CSA, but a substantial increase in variability of CSA. While it is likely that a subset of the small caliber myofibers are regenerating, we propose that some are myofiber branches rather than distinct myofibers. If this is true, it would indicate that analysis excluding myofiber branches would trend towards increased CSA in mdx myofibers. This is an area requiring further research and could be tested by optical sectioning of whole muscles that would allow determination of each myofiber's status as independent (non-branched) or branched.

Myofiber loss is a driver of pathology in DMD. It contributes to the progressive weakness experienced by DMD patients that eventually leads to loss of ambulation and reliance on mechanical ventilation (Ciafaloni et al., 2016). It is an attractive target for therapeutics because it plays such a major role in loss of quality of life in patients. As such, myofiber loss has been assessed repeatedly in mdx mice. One of the first reports on mdx mice indicated that there is no change in myofiber number between mdx and WT (Tanabe et al., 1986). This finding was reinforced by several other reports indicating mdx mice had no change in myofiber number of adult EDL and SOL muscles (Coulton et al., 1988; Pagel and Partridge, 1999). However, others reported hyperplasia in adult mdx TA and EDL muscles (Pagel and Partridge, 1999, Faber et al., 2014). Clearly, myofiber number in mdx is influenced by age and muscle, but the consensus was that if there is change in myofiber number in mdx muscles, it is an increase rather than a decrease. This consensus was challenged by a report indicating that hyperplasia reported in mdx mice is likely the result of myofiber branching rather than actual hyperplasia

(Faber et al., 2014). In summary, analysis of muscles with substantial myofiber branching in cross section leads to overestimation of myofiber number. The results reported in this chapter extend the results of Faber et al. into multiple whole muscles and aged time points. These results indicate that the mdx mouse mimic myofiber loss in DMD and may be an excellent model for testing therapeutics targeting preventing muscle fiber loss.

4. SKELETAL MUSCLE TISSUE CLEARING AND COMPATIBILITY WITH COMMON NMJ MARKERS

4.1 Research rationale

Tissue clearing was introduced by the clear lipid-exchanged anatomically rigid imaging/immunostaining compatible tissue hydrogel (CLARITY) protocol. Skeletal muscle tissue clearing in combination with imaging the neuromuscular junction has great potential as a technique to assess pathology in neurodegenerative and muscle diseases. Tissue clearing allows for whole tissue analysis that is normally impossible in opaque skeletal muscle, and has potential to reveal large-scale changes in tissues that occur with development, aging, and disease pathology. NMJ morphology is an important marker for pathology in numerous disease states. Until recently, tissue clearing and NMJ staining had proven to be incompatible techniques (Milgroom and Ralston, 2016). A recently published tissue clearing protocol, MYOCLEAR, reported successful NMJ staining in partially cleared tissue (Williams et al., 2019). However, the primary drawback of this technique is that partial tissue clearing limits its utility to thinner muscles with a depth of 600 μm or less, and therefore is incompatible with analysis of thicker muscles such as those analyzed in previous chapters. Other tissue clearing techniques, like passive CLARITY technique (PACT), are available, which allow for excellent clearing through even thick skeletal muscles, an advantage over MYOCLEAR. However, these clearing protocols are not compatible with BTX staining, limiting applicability for analysis of the NMJ. In this chapter, we report the results of a study to optimize compatibility of

labeling for common NMJ-associated markers with PACT, in an effort to label the 3 components of the NMJ in whole cleared muscle tissue. In addition, we make substantial improvements to MYOCLEAR, demonstrating improved depth penetration and signal to noise ratio while cutting protocol time to 60% of the original.

4.2 Materials and methods

4.2.1 Mouse strains

C57BL/10ScSn-*Dmd*^{mdx}/J mice (mdx, RRID:IMSR_JAX:001801) and C57BL/10ScSnJ (BL/10J, RRID:IMSR_JAX:000476) mice were purchased from Jackson Laboratory and bred in house. Several lines of transgenic mice were utilized. Transgenic mice expressing green fluorescent protein in Schwann cells, (B6:D2-Tg(s100B-EGFP)1Wjt/J, RRID:IMSR_JAX:005621) and cyan fluorescent protein in motor axons (B6.Cg-Tg(Thy1-CFP)23Jrs/J, RRID:IMSR_JAX:003710) were utilized in these experiments. These mice have been previously described and all mice are available from Jackson Laboratory.

The red green (RG) mice were bred in house and named in accordance with the publishing paper (Shioi et al., 2009). RG mice were generated by crossing two transgenic lines. The first line expressed Cre recombinase driven by the human skeletal actin promoter (Tg(ACTA1-cre)79Jme, RRID:IMSR_JAX:006149). The second line expresses a Cre-inducible fluorescent reporter knocked into the Rosa26 locus and is available from Riken (R26R-RG, Accession # CDB0227K). In the presence of Cre, the

mice express mCherry-tagged histone 2B and enhanced green fluorescent protein fused to a glycosylphosphatidylinositol (GPI) signal sequence. The resulting RG mouse line expressed mCherry exclusively in myonuclei and eGFP in the muscle sarcolemma. A total of 15 mice were used for experiments reported in this chapter.

4.2.2 Tissue clearing protocols

The following clearing protocol was adapted from the MYOCLEAR protocol (Williams et al., 2019). Mice were sacrificed via intraperitoneal injection of 0.15 mL of Euthosol (Med-Pharmex). Following sacrifice, we performed transcardial perfusion with ice cold 4% paraformaldehyde (PFA). STM, EDL, and SOL muscles were dissected, and pinned at resting length in a Sylgard-lined dish and fixed overnight in 4% PFA at 4 degrees C. Muscles were then washed in 0.2 M boric acid buffer with 0.1% triton (BBT) overnight with 4 solution changes in preparation for the hydrogel/polymerization step.

Muscles were incubated in 12.5 mL of A4P0 (4% acrylamide, 0% paraformaldehyde) hydrogel solution in a 15 mL conical tube. Muscles were kept at 4 degrees C with gentle rocking overnight. The next day conical tubes were placed in a vacuum desiccator for 30 minutes. The chamber was then flooded with nitrogen and the tubes were capped and sealed. Muscles were incubated at 37 degrees C for 3 hours. Muscles were washed in BBT overnight with 4 solution changes in preparation for labeling.

Staining protocols differed depending on the label used. Staining with antibodies went as follows. Each sample was incubated in 1 mL of staining buffer with appropriate

concentration of primary antibody in a 1.5 mL tube. Muscles were incubated for 4 days with solutions exchanged every other day. After the first solution change muscles were centrifuged at 600g for 2 hours. After primary staining, muscles were washed in BBT for 24 hours with 4 solution changes. After the final solution change muscles were centrifuged at 600g for 2 hours. Muscles were incubated in 1 mL of staining buffer with secondary antibodies for 4 days, exchanging the solution every day. After the first solution change muscles were centrifuged at 600g for 2 hours. After secondary staining, muscles were washed in BBT for 24 hours with 4 solution changes. After the final solution change muscles were centrifuged at 600g for 2 hours.

For labeling with α-bungarotoxin and Draq5, BBT was replaced with PBS for all steps. Muscles were stained in PBS rather than staining buffer. Muscles were labeled at room temperature for 4 days, refreshing solution halfway through. Immediately after refreshing the staining solution, muscles were centrifuged for 2 hours at 600g (Lee et al., 2016). After staining was complete, muscles were washed in PBS with 4 buffer changes over 24 hours. After the final buffer change muscles were again centrifuged for 2 hours at 600g.

Muscles were mounted in a column of agarose within an insulin syringe with the tip removed. After allowing the agarose to solidify for 60 minutes, the syringes were placed in 15 mL conical vial containing 10 mL of RIMS made with 30g nycodenz (Alere Technologies Prod# 1002424) in 22.5 mL 0.02M phosphate buffer. The syringe was then partially depressed lowering the column of agarose and the sample into the RIMs. The

samples were rocked for 2 days protected from light to create a uniform refractive index throughout the sample.

Muscles cleared using the PACT protocol followed the modified MYOCLEAR protocol with the addition of a sodium dodecyl sulfate (SDS) based clearing step. After the hydrogel and polymerization step, muscles were placed in 14 mL of 8% SDS in 0.2 M boric acid buffer in a 15 mL tube. Tubes were rocked at 37 degrees C for 5 days, replacing the SDS solution every other day. Muscles were then moved on to the staining step outlined above.

For muscles that were cleared using the clear, unobstructed brain imaging cocktails and computational analysis (CUBIC) protocol, the following steps were taken. Mice were sacrificed via intraperitoneal injection of 0.15 mL of Euthosol (Med-Pharmex). Following sacrifice, we performed transcardial perfusion with ice cold 4% PFA. STM, EDL, and SOL muscles were dissected, and pinned at resting length in a Sylgard-lined dish and fixed overnight in 4% PFA at 4 degrees C for 24 hours. Muscles were then washed in PBS for 24 hours with 3 solution changes. Then muscles were moved into 50% CUBIC-delipidation solution for 12 hours and then 100% CUBIC-delipidataion solution for 4 days. CUBIC-L was replaced after the first and second day. After delipidation, muscles were washed in PBS for 24 hours with 3 solution changes. After washing, muscles went through the normal staining procedure outlined above. After staining, muscles were incubated in 50% CUBIC refractive index matching solution for 1 day and 100% for 2 days.

4.2.3 Tissue staining

The fluorescent markers used in this chapter are listed below along with their concentrations and sources. To stain AChRs, we used α-bungarotoxin (1 mg/mL) conjugated to Alexa Fluor™ 488 (Thermo Fisher Scientific Cat# B13422) diluted 1:500 and mAb35 diluted 1:400 (Developmental Studies Hybridoma Bank RRID:AB_528405). We also used α-bungarotoxin (1 mg/mL) conjugated to biotin (Thermo Fisher Scientific Cat# B1196) diluted 1:500 and streptavidin (1mg/mL) conjugated to Alexa Fluor™ 546 (Thermo Fisher Scientific Cat# S11225) diluted 1:500. We used anti-choline acetyltransferase to label motor neurons (Millipore Sigma Cat# AB144P-1ML). We used Draq5 (Thermo Fisher Scientific Cat# 62251) diluted 1:1000 to label nuclei. We used the Rap2 antibody (a gift from Dr. Michael Ferns) diluted 1:500 to label rapsyn. Finally, we used Fasciculin-II conjugated to Alexa Fluor™ 647 (Sigma Product# F4293) diluted 1:500 to label acetylcholinesterase. We used an antibody against laminin beta-2 (a gift from Dr. Sasako Takaki) diluted 1:400 (Sasaki et al., 2002).

4.2.4 Image acquisition and analysis

Cleared muscles were imaged using a Zeiss Z.1 lightsheet microscope using a 5x (0.16 NA) objective. Whole muscles were imaged in 3-5 overlapping stacks so that entire muscles could be reconstructed. The 488nm and 638nm lasers were used to image markers of interest. Signal to noise ratio was measured in ImageJ by outlining endplates with the freehand tool and taking the average intensity. The outline shape was preserved and shifted to adjacent background. The average intensity of the background was

subtracted from the average intensity of the endplate to get average signal intensity. Average signal intensity was divided by the standard deviation of the background in accordance with the following formula, SNR = signal mean/standard deviation of noise.

4.3 Results

4.3.1 PACT and CUBIC protocols are incompatible with BTX staining in mouse skeletal muscle

Tissue clearing techniques have immense potential for large-scale analysis of tissue pathology in numerous disease states. There are multiple published protocols available for whole-tissue clearing, which vary in their compatibility with fluorescent labeling and immunostaining. We first compared the efficacy of two tissue clearing techniques, PACT and MYOCLEAR, on clearing of whole muscle tissue (Figure 4.1). The MYOCLEAR protocol results in partial clearing that is acceptable for thinner tissues. The PACT protocol results in excellent clearing, even through thick tissue.

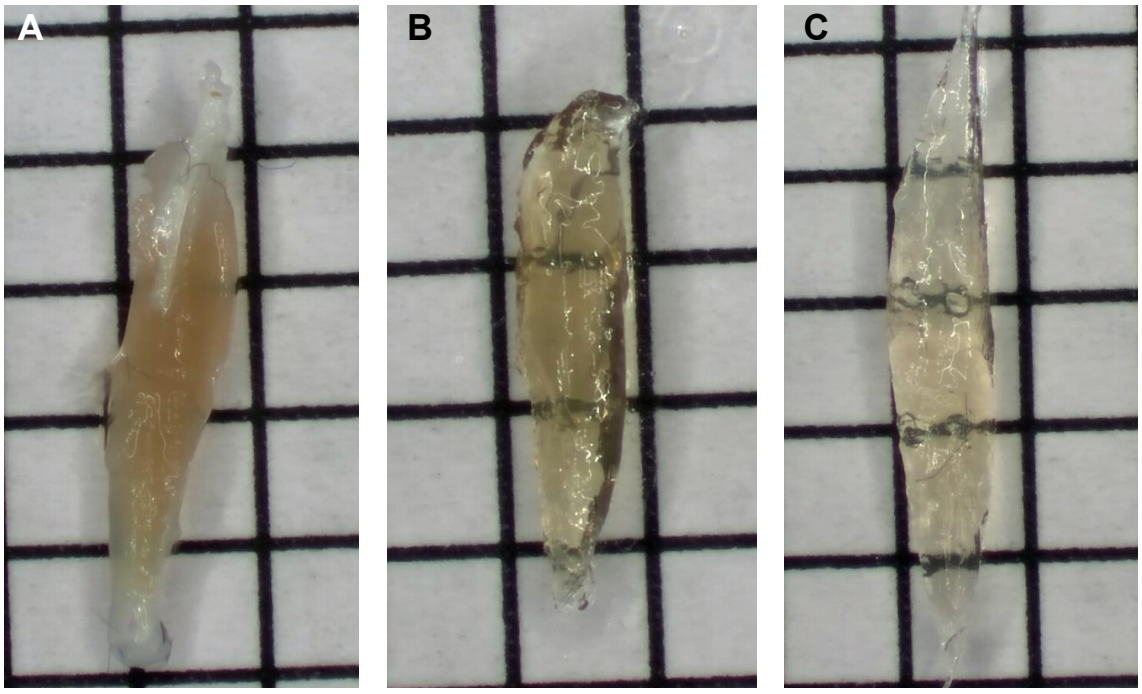

Figure 4.1 Muscle clarity after MYOCLEAR and PACT protocols.
A) SOL muscle without tissue clearing, the muscle obstructs view of black lines on the graph paper. B) SOL muscle cleared with MYOCLEAR results in partial clearing, black lines are partially visible through the tissue. C) SOL muscle cleared with PACT results in excellent clearing, black lines are easily visible through the tissue.

For neurodegenerative and muscle diseases, one of the most widely used markers is BTX, a reliable marker of nicotinic acetylcholine receptors on the postsynaptic side of the NMJ. Unfortunately, reports to date have been unable to successfully use BTX in combination with numerous clearing protocols. Although MYOCLEAR recently reported successful BTX labeling (Williams et al., 2019), we were only able to achieve partial tissue clearing using this technique (Figure 4.1B). We therefore sought to examine the compatibility of BTX staining in combination with alternative tissue

clearing protocols in order to achieve improved labeling of NMJ components in optimally cleared tissue.

The usefulness of tissue clearing partially relies on compatibility with tissue labeling and staining techniques, which varies with different protocols. We therefore asked whether we could identify discrete steps in tissue clearing protocols that resulted in failure of BTX labeling. A common cause of staining failure results from exposure to chemicals that quench fluorescent reporters. We hypothesized that the previously reported failure of BTX staining was the result of quenching the fluorescent reporter during SDS clearing, a step common to clearing techniques, but not used in MYOCLEAR. Therefore, we assessed whether BTX staining was dependent on timing relative to the SDS clearing step. If staining after SDS clearing was successful but staining prior to SDS clearing was not, it seemed likely that fluorescence quenching was the cause of staining failure. In order to test this in another way, we used biotinylated BTX to label AChRs prior to SDS clearing and then streptavidin conjugated to Alexa Fluor^{TM} 546 after SDS clearing to protect the fluorescence. In all cases we observed no BTX staining in muscles, indicating that fluorophore stability was unlikely to be the cause of BTX staining failure.

SDS-based clearing approaches extract lipids to reduce the opacity of tissue. While most proteins survive this process, a subset are extracted from the tissue, especially those bound to membranes (Chung et al., 2013). Therefore, we hypothesized that AChRs were being extracted from the tissue during SDS clearing, leaving nothing for BTX to bind to. We tested the length of SDS exposure and concentration of SDS to

determine if BTX staining failed even when minimal delipidation occurred. We tested 4 different lengths of SDS exposure (12 hours, 2 days, 4 days and 5 days) and 6 different concentrations of SDS (0.1%, 0.5%, 1%, 2%, 4% and 8%). These variables were chosen to produce a full range of tissue clearing. For example, a 12-hour exposure to 0.1% SDS results in no discernable tissue clearing and therefore little to no lipid/AChR extraction; a 5-day exposure to 8% SDS, the standard PACT procedure, results in excellent tissue clearing. Once again, in all cases we observed no BTX staining in our samples. While this does not necessarily mean that AChRs are not being extracted during the normal PACT protocol, it does indirectly indicate that receptor extraction is not the only cause of BTX staining failure. Instead a more likely scenario is that SDS exposure, even at low concentrations and low exposure times, denatures the epitope that BTX binds to and prevents binding all together.

Because we observed that any concentration of SDS examined was incompatible with BTX staining, we decided to try another clearing protocol that does not rely on SDS-based clearing. We chose the CUBIC protocol because it uses a completely unique chemical set relative to PACT (Susaki et al., 2015). After following the standard CUBIC protocol, we again observed no BTX staining in our samples. Like PACT, CUBIC relies heavily on detergents to extract lipids, and may also denature the epitope BTX binds. In lieu of repeating the above experiments in the CUBIC protocol, we decided a better course of action would be to test alternative AChR and post-synaptic NMJ markers in the PACT protocol.

4.3.2 PACT is compatible with alternative markers for neuromuscular analysis

The passive CLARITY technique results in excellent muscle clearing through even deep muscle tissue, making it compatible with a wide range of mouse muscles (Figure 4.1C). However, like all SDS based clearing techniques, PACT is only compatible with a subset of tissue labels. We therefore tested alternative markers for AChRs and other markers that may prove valuable in analysis of NMJs in cleared tissue. Our first choice was mAb35, which binds selectively to the alpha subunit of nicotinic acetylcholine receptors (Tzartos et al., 1981). This antibody produces robust staining in skeletal muscle, but failed to stain in PACT cleared muscles (Table 4.1). As we were unable to label AChRs directly, we began to look for proteins enriched at the NMJ.

Marker compatibility with PACT	Success	Failure
mAB35		X
Rap2	X	
RG transgenic mouse – mCherry		X
Draq5	X	
Fas2		X
Laminin beta-2		X
ChAT	X	
Kosmos transgenic mouse - eGFP	X	

Table 4.1 Compatibility of NMJ associated markers with the PACT protocol.

Rapsyn is enriched the NMJ and binds to AChRs. It shows the same pattern of staining in immunostained tissue as AChRs and is required to induce AChR clustering (Apel et al., 1997). For these reasons we chose to stain for rapsyn as a potential proxy for AChRs. We found that the Rap2 antibody showed staining in PACT cleared skeletal muscle (Figure 4.2A). However, we also observed a high level of background staining, low signal to noise ratio and it appears to also stain some presynaptic components. As a result, Rap2 is not a good option to replace BTX staining.

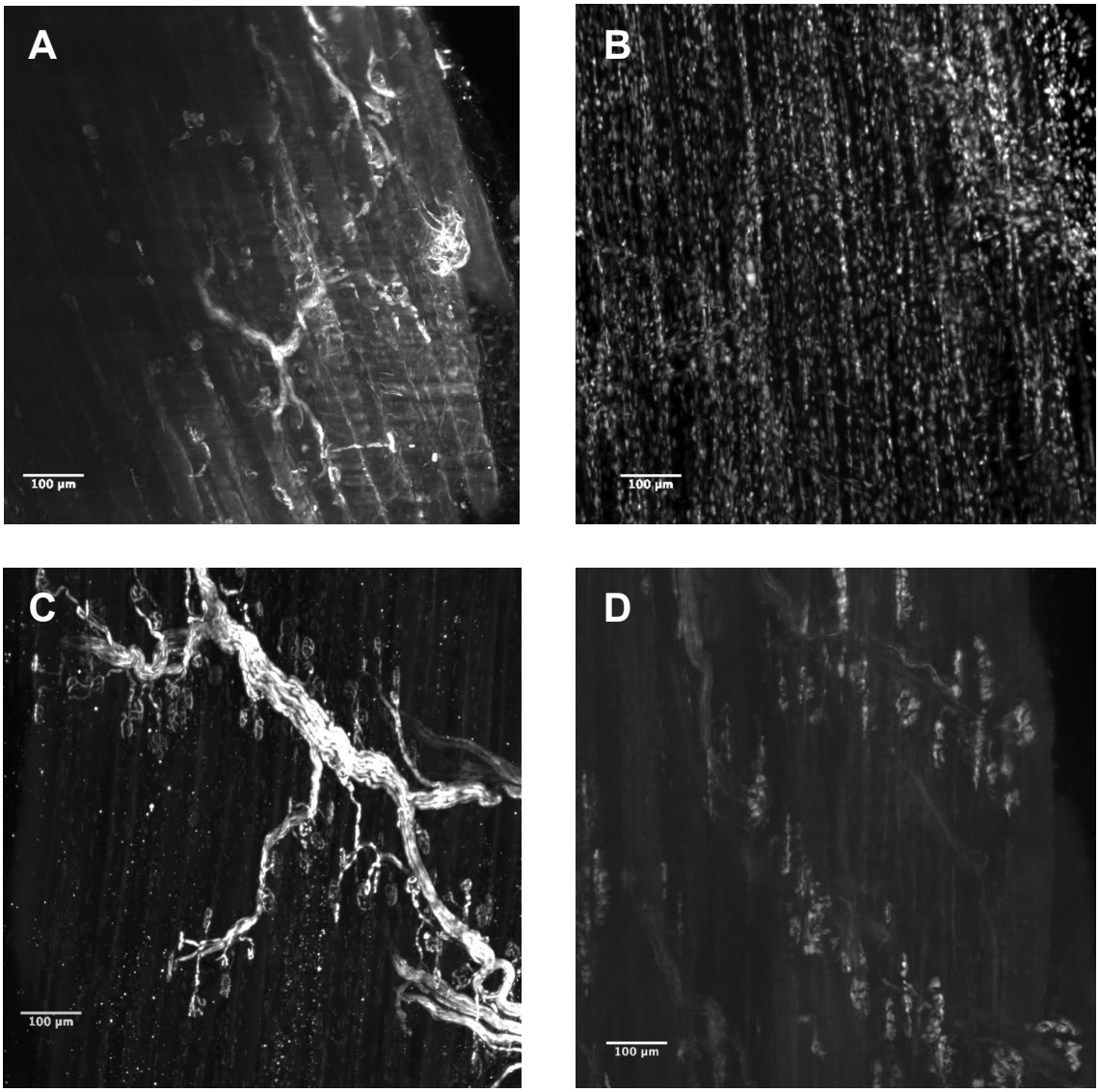

Figure 4.2 PACT compatible NMJ labels.
A) Antibody against rapsyn stains NMJs but the signal to noise ratio is poor. B) Draq5 is an excellent marker for nuclei. C) Antibody against choline acetyltransferase labels motor axons and nerve terminals well. D) Transgenic S100 driven eGFP labels tSCs and myelinating Schwann cells. Scale bar = 100 µm.

Synaptic myonuclei aggregate beneath the NMJ and provide transcripts to maintain the AChR aggregate (Grady et al., 2005). We utilized the RG transgenic line of mice that express mCherry specifically in myonuclei in order to image this population of

nuclei. We tested this transgenic marker in PACT cleared skeletal muscle tissue and observed no fluorescence after clearing (Table 4.1). In order to image nuclei, we stained with the nuclear marker Draq5, and found that this label produced robust staining in PACT cleared skeletal muscle tissue (Figure 4.2B).

Another protein of interest at the NMJ is acetylcholinesterase (AChE). AChE breaks down acetylcholine in the synaptic cleft and mirrors AChR staining. Fasciculin-II (Fas2), a component of the venom of the green mamba snake, binds selectively to AChE and stains well in skeletal muscle. We attempted to stain AChE with Fas2 bound to Alexa Fluor^{TM} 488 in PACT cleared tissue but found no observable staining in any case Table 4.1). We also tried an antibody against the laminin beta-2 subunit which stains well in whole mounted skeletal muscles but found little to no staining in PACT cleared tissue (Table 4.1).

In order to image the presynaptic components of the NMJ, we tested an antibody against choline acetyltransferase (ChAT). ChAT is responsible for the synthesis of acetylcholine and is present at high levels in the motor nerve terminals. We found that immunostaining against ChAT resulted in robust staining in PACT cleared muscles (Figure 4.2C), allowing excellent visualization of motor axons and nerve terminals.

Finally, we tested the compatibility of another transgenic reporter mouse with PACT. The Kosmos mouse expresses eGFP driven by the S100B promoter, resulting in fluorescence in terminal Schwann cells, which cap the presynaptic side of the NMJ and provide trophic support, among other functions, to the NMJ (Zuo et al., 2004). The number and proliferation of terminal Schwann cells has been shown to be affected in

disease states (Haddix et al., 2018). We found that muscle tissue from kosmos mice is compatible with PACT clearing and allows for clear visualization of terminal Schwann cells and myelinating Schwann cells around the motor axons (Figure 4.2D).

Here we demonstrated compatibility of PACT with reliable markers for numerous NMJ associated components. We successfully imaged fluorescently labeled Schwann cells, motor neurons, nerve terminals, and myonuclei in PACT cleared muscle tissue. However, we were unable to achieve high quality visualization of the AChR aggregate. In order to obtain quality NMJ staining we next sought to optimize the MYOCLEAR protocol.

4.3.3 Modified MYOCLEAR improves depth of tissue labeling and reduces protocol time

As stated above, the MYOCLEAR protocol is compatible with BTX staining while achieving partial tissue clearing (Williams et al., 2019). The primary drawback of this approach is that successful clearing is possible only in muscles less than 600 μm in thickness. This is a major limitation preventing its utilization for the analysis of whole muscles thicker than the diaphragm. We therefore sought to address this limitation in order to extend the utility of MYOCLEAR.

The tissue thickness limitation in MYOCLEAR is likely in large part due to incomplete tissue clearing (Figure 4.1B). Using confocal microscopy, the emitted laser light must travel through the tissue to reach the excitable fluorescent molecules within. The emitted fluorescence then travels back up through the tissue toward the detector.

Because confocal microscopy depends heavily on the use of a pinhole aperture to remove out of focus light, any scattering caused by partially cleared tissue will result in loss of signal due to rejection from the aperture (Figure 4.3A). Use of light sheet microscopy can improve signal to noise ratio in tissues greater than 600 μm. Light sheet microscopes use emitted light sheets from both sides of the sample, which depending on sample orientation can dramatically reduce the needed penetrance of the excitatory light (Figure 4.3B).

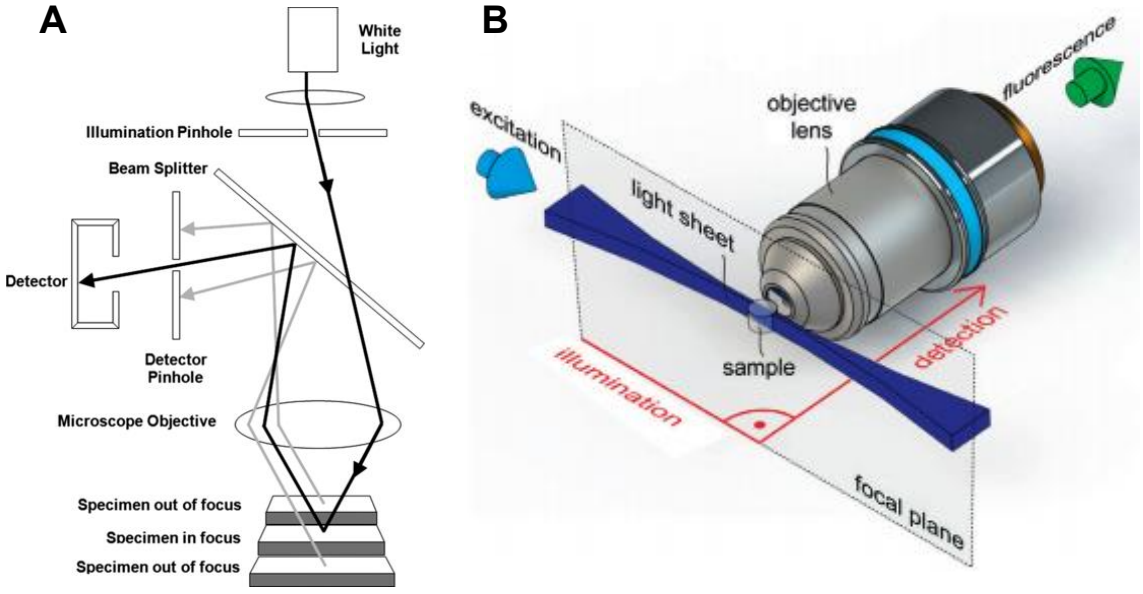

Figure 4.3 Schematics of confocal and light sheet microscopy techniques.
A) Schematic of confocal microscopy demonstrating how in focus light (black lines) reaches the detector by passing through a pinhole and out of focus light (grey lines) is rejected by the pinhole. Reprinted from (Weller et al., 2012). B) Reprinted from Schematic of light sheet microscopy demonstrating light sheets coming from each side of the sample, illuminating only the focal plane. (Selchow and Huisken, 2013).

In order to improve BTX signal in tissues deeper than 600 μm we attempted to improve the signal to noise ratio (SNR) of our samples. We first used biotinylated BTX and streptavidin conjugated to Alexa Fluor™ 546 to boost signal. This resulted in no noticeable improvement in signal and therefore SNR. Next, we attempted to combine MYOCLEAR with tyramide signal amplification (Adams, 1992). Tyramide signal amplification works by dramatically increasing binding sites for fluorescent reporters and boasts 10-200 times signal amplification. Unfortunately, in cleared skeletal muscle the boost in signal was accompanied by a boost in background that resulted in a worse signal to noise ratio on average (data not shown). Finally, we employed centrifuge staining in an effort to improve the depth penetration of our stains and wash steps (Lee et al., 2016). We saw a modest but consistent improvement in average signal to noise ratio of EDL muscles throughout their depth using centrifuge staining. Our modified MYOCLEAR protocol substantially outperformed the original in both SNR and depth of penetration (Figure 4.4). We demonstrate acceptable SNR to recognize NMJs in tissue at depths of 1000+ μm.

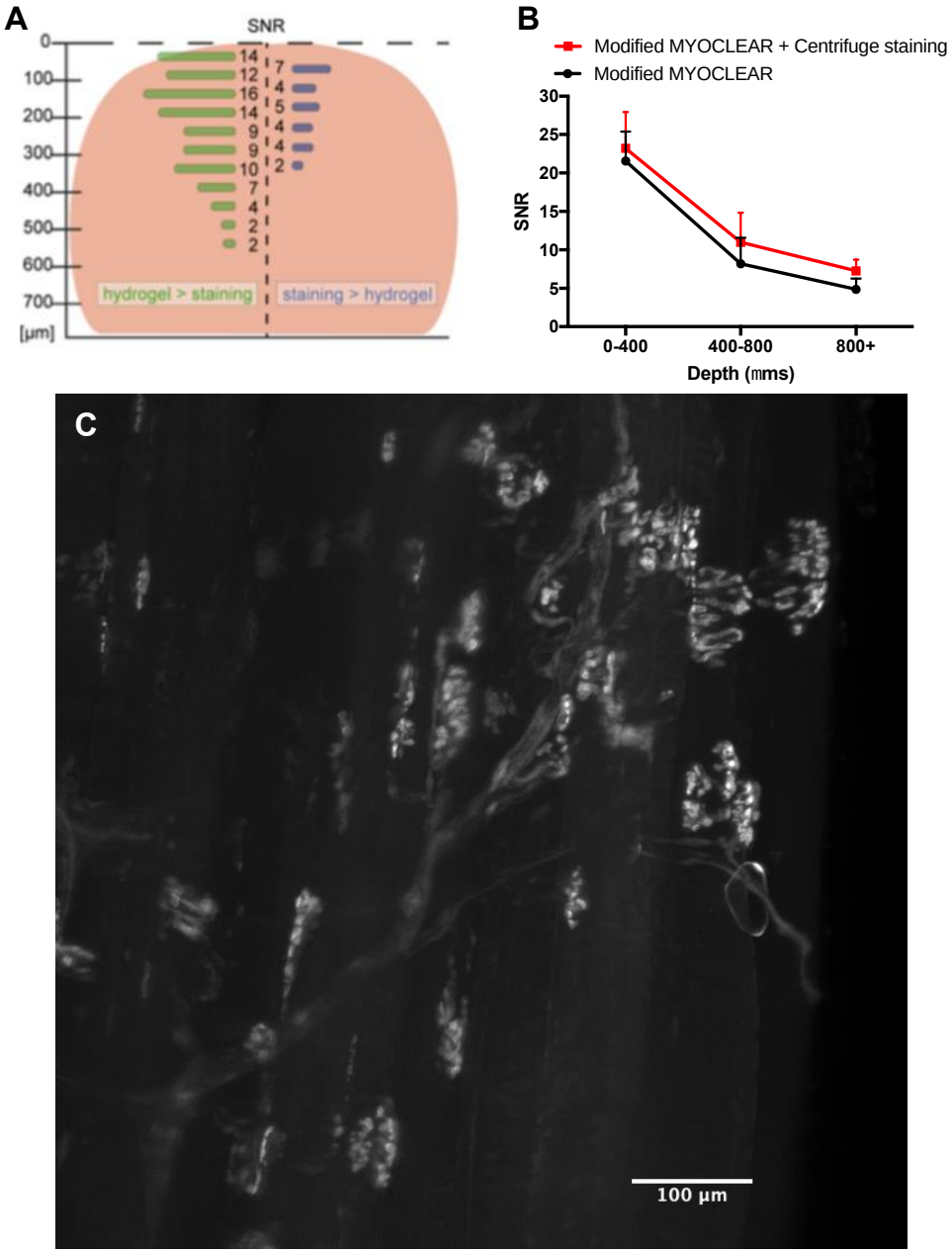

Figure 4.4 Signal to noise ratio as a function of tissue depth and protocol.
A) SNRs from BTX stained endplates of EDL muscles in the original MYOCLEAR protocol (green). SNR drops rapidly with tissue depth, demonstrating discernable stain up to 600 µm. Reprinted from (Williams et al., 2019). B) SNRs from BTX stained endplates of EDL muscles in our modified MYOCLEAR protocol demonstrate improved SNR and depth compatibility. Centrifuge staining shows a modest improvement in SNR. C) An example of BTX staining in an mdx EDL muscle cleared with our modified MYOCLEAR protocol. NMJ morphology is easily apparent and SNR is improved relative to published data.

The original MYOCLEAR protocol takes 18 days to complete with BTX staining, largely as a result of lengthy hydrogel embedding and staining steps, and we questioned whether these lengthy steps were necessary. In order to reduce protocol time, we performed the hydrogel embedding overnight instead of for 6 days. We also used centrifuge staining to shorten the staining and wash steps (Lee et al., 2016). Centrifugation causes muscles to temporarily deform, allowing improved depth penetration of the stains. We ultimately reduced protocol time to 11 days, about 60% of the length of the original protocol (Figure 4.5).

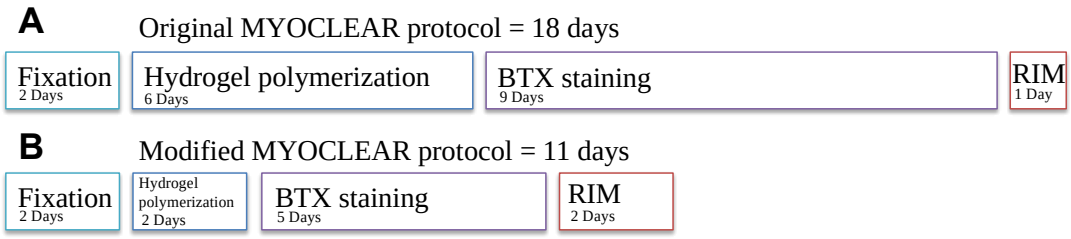

Figure 4.5 Time to complete MYOCLEAR protocols
A) The time to complete the original MYOCLEAR protocol broken down by steps. The protocol takes 18 days. B) The time to complete our modified MYOCLEAR protocol broken down by steps. The protocol takes 11 days, a nearly 40% reduction.

4.4 Discussion

The results presented in this chapter have advanced the utility of skeletal muscle tissue clearing and staining with three different clearing protocols. We identified SDS exposure as the incompatible step with BTX staining in skeletal muscle and present evidence that failed BTX stain is not caused by fluorescence quenching or by AChR extraction from the sarcolemma. In light of this information, we suggest SDS exposure,

even at low concentration and time of exposure, denatures the epitope that BTX binds to. However, our results with the CUBIC protocol demonstrate that this incompatibility is not specific to SDS but likely shared by detergents used in tissue clearing. Despite incompatibility with BTX stain, we have identified several useful NMJ markers that are compatible with PACT. On the presynaptic side, ChAT labels motor neurons and nerve terminals and transgenic S100 driven eGFP labels terminal Schwann cells. On the postsynaptic side Rap2 labels rapsyn at the NMJ but with poor signal and Draq5 labels nuclei with a high degree of clarity. To get higher quality imaging of AChRs we turned to the recently published MYOCLEAR protocol. We improved this protocol by reducing time to completion from 18 days to 11 days while improving staining quality.

If the PACT or CUBIC protocols were compatible with BTX staining, they would be preferable to MYOCLEAR. PACT and CUBIC demonstrate superior clearing and allow for use of thicker muscles that are commonly studied, such as the tibialis anterior. Because of this value, attempting to accomplish BTX staining using a full clearing technique is an area deserving of more research. There are numerous clearing protocols we did not try, 3DISCO for example, that rely on unique chemical sets to achieve clearing. It is possible that one of these chemical sets is compatible with BTX staining and would expand the utility of this technique to larger muscles. On the other hand, it is possible that AChR staining via BTX is incompatible with all clearing techniques. In this case there may be other ways to visualize AChRs. For example, fluorescent fusion constructs targeted to γ and ε subunits of nicotinic AChRs exist, and when injected into muscles the AChR subunits fluoresce (Gensler et al., 2001). While

we are unaware of any transgenic mouse line causing fluorescence in AChRs, that could be another successful strategy to attempt in cleared tissue. Barring direct reporting from AChRs, there may be other proteins that would serve as a satisfactory proxy. In this work we attempted to stain rapsyn, AChE, and LamB2 as potential AChR proxies. Rapsyn staining worked, but with poor signal to noise ratio, demonstrating that some proteins at the NMJ can be labeled in cleared tissue. There are many other candidates that might make excellent proxies that we did not try in this work, such as proteins of the dystroglycan complex. Obtaining fluorescent signal from AChRs is essential for this technique to be utilized for studies of neuromuscular and neurodegenerative pathologies, but it is not the only target of interest.

In the preceding chapter we attempt to identify NMJ labels that can be used as reliable presynaptic, synaptic, and postsynaptic markers that may be useful for assessing disease pathology. We demonstrate that ChAT is an excellent marker for presynaptic staining that labels the nerve terminals and axons as they extend away from the junctional area. This marker has immense utility in tracking pathology in both neurodegenerative and muscle diseases such as Amyotrophic Lateral Sclerosis (ALS) and Duchenne muscular dystrophy respectively. In addition, we showed that transgenic eGFP driven by S100 reports robust fluorescence in both myelinating and non-myelinating Schwann cells. Glial cells are known to modulate synaptic neurotransmission and respond to neuronal activity (Araque et al., 1999) and specifically modulate synaptic efficacy at the NMJ (Robitaille, 1998). Schwann cells also play important roles in axonal protection (Griffin and Thompson, 2008) and synapse

elimination (Smith et al., 2013). The number and proliferation of tSCs are known to be affected in the mdx mouse as well (Haddix et al., 2018). The compatibility of this kosmos mouse with PACT gives researchers another tool to assess pathology on a large scale using tissue clearing techniques. Draq5 robustly labels nuclei in PACT cleared tissue. The NMJ is a tripartite synapse; here we have demonstrated the efficacy of markers for two of the three parts, tSCs and motor axon nerve terminals.

Despite incompatibility with PACT and CUBIC, BTX staining works well with MYOCLEAR (Williams et al., 2019). MYOCLEAR is a partial clearing technique that relies heavily on refractive index matching and avoids heavy use of detergents as in full clearing protocols. This presents limitations in sample thickness that full clearing techniques do not have. The primary advantage of MYOCLEAR is its compatibility with BTX staining. The primary drawback to MYOCLEAR is the loss of efficacy in samples thicker than 600 μm, which significantly limits the scope of application of the technique. In this work we demonstrate acceptable signal to noise ratio of BTX staining at depths over 1000 μm, dramatically increasing the number of muscles compatible with MYOCLEAR.

In this application, light sheet microscopy has several advantages over confocal microscopy. First, illumination of the sample occurs from both sides, reducing concerns about penetration of the excitation light into the sample. Second, confocal microscopes make use of a pinhole aperture to reject out of focus fluorescence. Some of the emitted light form the sample may be scattered by the incompletely cleared tissue resulting in

loss of signal. By using light sheet microscopy, we were able dramatically increase the imaging depth relative to confocal.

In the original MYOCLEAR paper, the signal to noise ratio of BTX staining drops from 12-16 at tissue depths of 0-200 μm, to 2 at 500+ μm (Williams et al., 2019). In an effort to improve the SNR at greater depths we tried to increase the signal utilizing a biotin streptavidin reaction, tyramide signal amplification, and centrifuge staining. The biotin streptavidin technique makes use of the strong binding affinity between the two reagents. The reaction often improves signal by tagging a poorly detectable molecule with biotin for strong binding by a fluorescently conjugated streptavidin later on. In our experiments we observed no discernable improvement in BTX signal, indicating that binding affinity is already very high between BTX and AChRs. Next, we tried tyramide signal amplification, which works by dramatically increasing the number of binding sites for the fluorescently labeled streptavidin to bind to. This resulted in a dramatic boost in signal, but also in background. The resulting staining had worse SNR than simple BTX staining. Finally, we attempted to use centrifuge staining to improve stain penetration in the muscle (Lee et al., 2016). We saw a modest but consistent improvement in the SNR of centrifuge stained tissue. This is likely the combination of slight signal improvement from centrifuge staining and a slight decrease in background as a result of centrifuge washing. Together, these led to better SNR than muscles that did not receive centrifuge staining and washing.

Another limitation of MYOCLEAR is the long protocol time. Here we demonstrate reduction in protocol time to 60% of its original length. This was

accomplished primarily by shortening the hydrogel embedding and staining steps. In addition, we address the limitation of single channel staining by using BTX conjugated to Alexa Fluor™ 488 in our samples and achieving an acceptable SNR. Williams et al. (2019) report massive PFA induced autofluorescence in both green and red channels that we did not observe. There is some autofluorescence but not enough to cause poor SNR in those channels. This difference may be the result of different chemicals used during staining and washing steps. It is also possible that the reduced protocol time in combination with use of sodium azide to prevent bacterial growth also decreases background. These improvements to the standard MYOCLEAR dramatically increase the potential applications of this technique while reducing total protocol time to approximately 60% of the original.

In this study we have shown the compatibility of some important NMJ markers with PACT, and demonstrated significant improvements to the MYOCLEAR protocol while extending knowledge of tissue clearing in skeletal muscle. The importance of this work lies in the potential of the technique to provide large-scale analysis of NMJ pathology. Many diseases manifest in part at the NMJ, and muscle opacity prevents analysis of all but the most surface level NMJs. Tissue clearing represents substantial increase in the number of NMJs that can be assessed per muscle and has the added benefit of keeping the tissue intact.

5. CONCLUSIONS

5.1 Pathology of the mdx mouse through the lifespan

The results presented above characterize the pathology of the mdx mouse throughout the lifespan by tracking hallmark features of pathology in isolated myofibers. We conclude that that the mdx mouse mimics DMD in the pathological progression of some of these features, but not in others. Muscle hypertrophy has consistently been reported in DMD as well as in the GRMD and mdx models, however in DMD and GRMD that hypertrophy gives way to myofiber loss and atrophy (Kornegay et al., 2012). An important distinction here is the difference between myofiber hypertrophy and muscle hypertrophy. Myofiber hypertrophy is the primary cause of muscle hypertrophy but in some cases hyperplasia, an increase in myofiber number, can also cause hypertrophy (Bruusgaard et al., 2010; Duddy et al., 2015). In the mdx mouse we observed persistent and progressive myofiber hypertrophy that continues throughout the lifespan; myofibers of mdx mice increased in volume by 18% between 1 and 2 years of age. During this same time period WT myofibers lost about 27% of their volume due to age related sarcopenia. Previous reports indicate that myofibers of mdx mice are hypertrophic at adult time points (Duddy et al., 2015), but this is the first report in aged mdx mice. This finding demonstrates that the mdx mouse does not replicate the pattern of myofiber growth and atrophy that is seen in DMD and other models such as GRMD. It is possible that this difference is linked to differences in SC exhaustion. Mdx mice with transgenically shortened telomeres display a more severe pathology that results from

failures in regeneration (Sacco et al., 2010). It is possible that this more accurately mimics the human disease, however; we demonstrated above that at least a subset of myofibers suffer from regenerative failure.

A previous report demonstrates that myofiber hypertrophy induced by overload exercise is supported by a preceding increase in myonuclei in WT mice (Bruusgaard et al., 2010). Our results indicate that this temporal relationship holds true in mdx mice where hypertrophy is caused by disease induced muscle damage. Mdx myofibers became hypernucleated between 6 and 12 weeks of age however, we did not observe significant hypertrophy until 24 weeks of age. It should be noted that at 12 weeks of age, mdx myofibers trended towards hypertrophy but there was high variability in the data. This makes sense in the context of pathology; at 12 weeks of age mdx muscle fibers are in the midst of the first few cycles of myofiber damage and repair. Our results indicate that in the first 24 weeks of life every single muscle fiber undergoes damage and repair to some extent. The variability at this time point likely reflects many regenerating myofibers and many recently regenerated myofibers that are recruiting new myonuclei but have not yet had the necessary time to grow to hypertrophy. The preservation of the finding that increased myonuclear number proceeds hypertrophy across vastly different circumstances indicates that it might be a requirement for novel myofiber hypertrophy. This makes sense from a protein synthesis perspective (Gunderson, 2016). The rate-limiting factor in myofiber size is likely net protein increase. The mdx mouse must have a massive capacity for protein production in order to not only induce hypertrophy but also overcome the massive protein degradation associated with cycles of myofiber

degeneration. Indeed, our finding that the myonuclear domain is depressed in mdx mice is consistent with this idea.

The myonuclear domain of mdx mice increases between 2 and 6 weeks of age, just as in WT, but is then held constant through the first year of life. In comparison, the WT myonuclear domain grows slowly over the first year of life due to slow myofiber growth without myonuclear addition. The myonuclear domain of mdx myofibers is depressed relative to WT at 12, 24, and 52 weeks of age. A smaller myonuclear domain indicates increased nuclear density and this increased density is occurring in myofibers that are massively hypertrophic. The result is that mdx myofibers contain nearly 1000 myonuclei at 1 year of age compared to about 320 in WT. In other words, the increase in the number of myonuclei is more significant than the increase in volume. Preservation of the myonuclear domain at the level of 6-week-old WT myofibers may reflect the myonuclear domain of growing myofibers. In order to achieve hypertrophy, myofibers must contain a higher density of myonuclei than needed to support the current cell volume. In mdx mice, muscle fibers are becoming progressively hypertrophic and having to repair myofiber damage regularly. It seems likely that the depressed myonuclear domain is a mechanism to deal with these high demands for protein synthesis. It is interesting then that the number of central nuclei accounts for the hypernucleation in mdx. It would follow logically that these myonuclei are absolutely necessary to deal with the protein demands of the cell and it is possible that their central location helps deal with increased cell diameter in regards to diffusion of transcripts. However, no investigation of this type has been made. In order for hypernucleation to

lead to increased protein synthesis, a corresponding increase in ribosomes would be necessary to handle translation. An analysis of ribosome abundance in mdx mice would extend this work and provide us with insight about the protein synthesis capacity of mdx myofibers.

Fragmentation of endplates increases in severity throughout the first year of life in mdx. Central nuclei numbers increase over the same time period. These findings indicate continued myofiber turnover in the EDL muscle of mdx mice. This finding fits well with recently published results indicating increased AChR turnover in the STM muscle throughout most of the lifespan (Haddix et al., 2018). While it must be considered that other causes can induce fragmentation of motor endplates, observations in the mdx mouse are consistent with the idea that damage in area of the NMJ induces endplate fragmentation. This has been demonstrated in both WT and mdx mice by direct muscle damage (Li and Thompson, 2011; Haddix et al., 2018). In addition, observations reported here show increasing number of central nuclei are correlated with endplate fragmentation. While no thorough report has investigated fragmentation in DMD, it has also been reported in the GRMD model and persistence of this feature across mammalian models suggests that it is preserved. We are only aware of one study on fragmentation in DMD and junctions were assessed in transverse sections (Theroux, 2018). Complicating the matter, human NMJs are configured in a more fragmented morphology to start as compared to mice and dogs.

Finally, the progressive increase in myofiber branching is not a novel finding in mdx, but adds to the evidence that myofiber turnover is continuing in this model. In aged

mdx, myofiber architecture no longer resembles simple cylindrical syncitia, often branching many times in quick succession before fusing back together. Similarly, inside muscle fibers there are often numerous parallel chains of central nuclei, which may result from fusion of myotubes that form within the same basal lamina sheath during the repair process.

Together the results in this section demonstrate that the pathology of the mdx mouse is progressive and severe in the EDL muscle. Morphological features of pathology such as hypertrophy, central nucleation, endplate fragmentation, and branching are all associated with the process of myofiber repair. The severity of these pathological features increases throughout the first year of life, indicating that myofiber damage and repair is ongoing. Additionally, we have characterized these features of pathology throughout the lifespan, demonstrating that some features such as, central nucleation, branching, and potentially endplate fragmentation mimic DMD, while other features such as myofiber hypertrophy do not. These results will inform preclinical trials that utilize the mdx mouse going forward.

5.2 Myofiber loss in mdx mice

In DMD, myofiber loss results in progressive weakness, loss of ambulation and respiratory failure. It is an excellent biomarker for testing the efficacy of therapeutics because prevention of myofiber loss would dramatically improve and extend the quality of life in patients. Studies indicate that myofiber loss is not replicated in the mdx mouse (Tanabe et al., 1986; Carnwath et al., 1987). In fact, some reports indicate hyperplasia in

mdx muscles (Pagel and Partridge, 1999). This assertion was challenged by a report demonstrating a high correlation between myofiber branching and myofiber hyperplasia in adult mdx mice, indicating that hypertrophy of mdx muscles is caused by branching rather than hyperplasia. This is elegantly demonstrated by comparing synapse number to cross section myofiber counts in the third digit of the mdx EDL. The results show a 25% increase in fiber number with no corresponding change in synapse number (Faber et al., 2014).

Here we used a similar technique to demonstrate that myofiber loss has been masked by myofiber branching in previous analyses utilizing transverse sections to count myofibers. We employed tissue clearing to analyze whole EDL, SOL, and STM muscles. Taking advantage of the 1 to 1 ratio of NMJs to myofibers, we analyzed synapse number in whole cleared skeletal muscles as a proxy for myofiber number in order to avoid bias by myofiber branches.

We observed hypertrophy in mdx muscles on the cellular level (myofibers), but not on the level of whole muscles. In light of our other findings, it seems likely that myofiber loss is offset by myofiber hypertrophy resulting in no net change in muscle weight. Using traditional transverse sections, we replicated published reports on CSA and myofiber number in adult mdx and WT mice and used these values to normalize our synapse counts (Tanabe et al., 1986; Terada et al., 2012).

Our results indicate myofiber loss is occurring in mdx even before 1 year of age in the SOL and STM muscles. By 2 years of age all three muscles had significantly fewer synapses, and thus myofibers, in mdx as compared to age matched WT. This is

strong evidence that mdx mice are losing myofibers beyond what is expected from age related sarcopenia. In aged mdx tissue we observed 14% - 17.5% fewer synapses in cleared tissue than myofibers in transverse sections across three different muscles. This indicates that myofiber branching in the mdx mouse significantly biases analyses via transverse sections. This applies to myofiber counts as well as measurements of cross-sectional area. Previous reports in the mdx mouse demonstrate no change in CSA compared to WT, a finding we replicate here using transverse sections. However, this stands at odds with our findings in isolated myofibers that demonstrate significant myofiber hypertrophy caused primarily by increased diameter. Bias by myofiber branches may at least partially explain the difference in these findings as myofiber branches significantly smaller in diameter than independent myofibers. This is biasing the CSA measurements towards a smaller mean and may be masking true hypertrophy of myofibers. In addition, this work is important because it demonstrates that the mdx mouse is replicating a severe and important feature of DMD pathology that can be utilized as a biomarker to test efficacy of therapeutics.

5.3 Skeletal muscle tissue clearing

Tissue clearing techniques were originally designed as a tool to help elucidate neural circuitry in the central nervous system (Chung and Deisseroth, 2013). However, the technique holds great potential for assessing neuromuscular disease in whole skeletal muscles. The depth and opacity of skeletal muscle prevents whole muscle analysis that can be accomplished with clearing. In order to analyze neuromuscular disease states in

cleared tissue, we need fluorescent reporters for the 3 main components of the NMJ, tSCs, motor axons terminals, and the motor endplate. Our results characterize compatibility of NMJ stains with the PACT protocol and extend the utility of the MYOCLEAR protocol in several key ways.

Compatibility of BTX staining with clearing protocols has been a continual issue for skeletal muscle clearing. We report that BTX staining is incompatible with SDS exposure even at very low concentrations. In our experiments, BTX staining failed with exposure to 0.1% SDS for 12 hours. Interestingly, no discernable tissue clearing occurred with this exposure and therefore extraction of lipids was very limited or did not occur. This indicates that extraction of AChRs is not the cause of BTX staining failure, or at least the only cause. It seems more likely that SDS exposure damages the epitope of the AChR that BTX binds to. However, this property is not unique to SDS. We also tested BTX compatibility with the CUBIC protocol because it does not use SDS based clearing and again found no staining. CUBIC uses a high concentration of Triton X-101 to extract lipids, which may also prevent BTX binding. Several tissue-clearing techniques, such as SeeDB and ClearT2, do not use detergents in order to achieve clearing but their compatibility with skeletal muscle is not known (Ke et al., 2013; Kuwajima et al., 2013). Testing BTX binding compatibility with these protocols would be a logical next step. Despite incompatibility with BTX, PACT demonstrates excellent staining for tSCs and motor axons using transgenic eGFP expression and antibody against ChAT.

The MYOCLEAR protocol results in inferior tissue clearing relative to other protocols but is compatible with BTX staining. We improved this protocol by reducing protocol time to 60% of the original while improving depth penetration and SNR. Despite our improvements, MYOCLEAR is still limited by tissue thickness. Therefore, it is still preferable to find a clearing technique that not only results in complete clearing but also is compatible with BTX. Another possibility is that MYOCLEAR may work in conjunction with another clearing technique.

Using MYOCLEAR to image BTX at the NMJ could be paired with PACT in order achieve full NMJ labeling in skeletal muscles. The muscle would be put through the MYOCLEAR protocol, imaged for BTX, and then put through the PACT protocol and imaged for ChAT and tSCs. The images would then be aligned allowing for full NMJ staining in whole skeletal muscles. This could be a powerful technique to assess pathology at the NMJ in neuromuscular disease states allowing at least 1000 μm depth penetration, far better than what is available in opaque tissue.

5.4 Summary

In total, our results extend understanding of pathological features of the mdx mouse as they relate to DMD by characterizing their onset, progression and severity. We identify a previously underappreciated feature of the mdx mouse that mimics DMD and extend the utility of methods used to analyze neuromuscular diseases. In summary we found:

1) Pathological features associated with cycles of myofiber damage and repair such as endplate fragmentation, deposition of central nuclei and myofiber

branching all increase progressively through the first year of life. This is a strong indication that myofiber degeneration and regeneration is ongoing in the mdx EDL muscle.

2) Myofiber hypertrophy in the mdx EDL continues progressively throughout the lifespan rather than becoming atrophied with age as in DMD, and does not correlate with whole muscle hypertrophy.
3) Muscle weight in the mdx mouse is not different from age matched WT muscles. This finding was observed in three different muscles (EDL, SOL, and STM) that vary in body position and fiber type makeup.
4) Analysis of myofiber number via transverse sections is biased by myofiber branching in the mdx mouse, leading to a 14.5% overestimation of myofiber number across 3 muscles.
5) At 1 year of age mdx SOL and STM muscles contain significantly fewer synapses than age matched WT muscles, indicating that significant myofiber loss has already occurred at 1 year of age in some mdx muscles.
6) At 2 years of age mdx muscles contain significantly fewer synapses than age matched WT muscles, indicating significant myofiber loss beyond what is expected from normal aging.
7) Myofiber loss in the mdx mouse is preserved across three muscles of different body positions and fiber type makeups.
8) Morphological changes in myofibers and at the NMJ of aged mdx mice are excellent biomarkers for measuring disease progression.

9) Skeletal muscle tissue clearing via PACT is compatible with numerous valuable NMJ associated labels, but is incompatible with BTX staining due to SDS exposure.
10) We have improved the MYOCLEAR protocol by shortening the protocol time to 60% of its original length, increasing its compatibility with thicker tissue and improving the signal to noise ratio of BTX staining.

REFERENCES

Adams, J. C. (1992). "Biotin amplification of biotin and horseradish peroxidase signals in histochemical stains." J Histochem Cytochem 40(10): 1457-1463.

Allen, D. L., R. R. Roy and V. R. Edgerton (1999). "Myonuclear domains in muscle adaptation and disease." Muscle Nerve **22**(10): 1350-1360.

Andersen, J. L., Terzis, G., and Kryger, A. (1999). Increase in the degree of coexpression of myosin heavy chain isoforms in skeletal muscle fibers of the very old. *Muscle Nerve* 22, 449–454.

Andersen, J. L. (2003). "Muscle fibre type adaptation in the elderly human muscle." Scand J Med Sci Sports 13(1): 40-47.

Apel, E. D., D. J. Glass, L. M. Moscoso, G. D. Yancopoulos and J. R. Sanes (1997). "Rapsyn is required for MuSK signaling and recruits synaptic components to a MuSK-containing scaffold." Neuron 18(4): 623-635.

Araque, A., V. Parpura, R. P. Sanzgiri and P. G. Haydon (1999). "Tripartite synapses: glia, the unacknowledged partner." Trends Neurosci 22(5): 208-215.

Au, Y. (2004). "The muscle ultrastructure: a structural perspective of the sarcomere." Cell Mol Life Sci 61(24): 3016-3033.

Bachrach, E., S. Li, A. L. Perez, J. Schienda, K. Liadaki, J. Volinski, A. Flint, J. Chamberlain and L. M. Kunkel (2004). "Systemic delivery of human microdystrophin to regenerating mouse dystrophic muscle by muscle progenitor cells." Proc Natl Acad Sci U S A 101(10): 3581-3586.

Balice-Gordon, R. J. and J. W. Lichtman (1994). "Long-term synapse loss induced by focal blockade of postsynaptic receptors." Nature 372(6506): 519-524.

Belanto, J. J., T. L. Mader, M. D. Eckhoff, D. M. Strandjord, G. B. Banks, M. K. Gardner, D. A. Lowe and J. M. Ervasti (2014). "Microtubule binding distinguishes dystrophin from utrophin." Proc Natl Acad Sci U S A 111(15): 5723-5728.

Bengtsson, N. E., J. K. Hall, G. L. Odom, M. P. Phelps, C. R. Andrus, R. D. Hawkins, S. D. Hauschka, J. R. Chamberlain and J. S. Chamberlain (2017). "Muscle-specific CRISPR/Cas9 dystrophin gene editing ameliorates pathophysiology in a mouse model for Duchenne muscular dystrophy." Nat Commun 8: 14454.

Blake, D. J., A. Weir, S. E. Newey and K. E. Davies (2002). "Function and genetics of dystrophin and dystrophin-related proteins in muscle." Physiol Rev 82(2): 291-329.

Blaveri, K., L. Heslop, D. S. Yu, J. D. Rosenblatt, J. G. Gross, T. A. Partridge and J. E. Morgan (1999). "Patterns of repair of dystrophic mouse muscle: studies on isolated fibers." Dev Dyn 216(3): 244-256.

Bonilla, E., C. E. Samitt, A. F. Miranda, A. P. Hays, G. Salviati, S. DiMauro, L. M. Kunkel, E. P. Hoffman and L. P. Rowland (1988). "Duchenne muscular dystrophy: deficiency of dystrophin at the muscle cell surface." Cell 54(4): 447-452.

Bruusgaard, J. C., I. B. Johansen, I. M. Egner, Z. A. Rana and K. Gundersen (2010). "Myonuclei acquired by overload exercise precede hypertrophy and are not lost on detraining." Proc Natl Acad Sci U S A 107(34): 15111-15116.

Bruusgaard, J. C., K. Liestol, M. Ekmark, K. Kollstad and K. Gundersen (2003). "Number and spatial distribution of nuclei in the muscle fibres of normal mice studied in vivo." J Physiol 551(Pt 2): 467-478.

Bulfield, G., W. G. Siller, P. A. Wight and K. J. Moore (1984). "X chromosome-linked muscular dystrophy (mdx) in the mouse." Proc Natl Acad Sci U S A 81(4): 1189-1192.

Burden, S. J., M. G. Huijbers and L. Remedio (2018). "Fundamental Molecules and Mechanisms for Forming and Maintaining Neuromuscular Synapses." Int J Mol Sci 19(2).

Burden, S. J., P. B. Sargent and U. J. McMahan (1979). "Acetylcholine receptors in regenerating muscle accumulate at original synaptic sites in the absence of the nerve." J Cell Biol 82(2): 412-425.

Capers, C. R. (1960). "Multinucleation of skeletal muscle in vitro." J Biophys Biochem Cytol 7: 559-566.

Carnwath, J. W. and D. M. Shotton (1987). "Muscular dystrophy in the mdx mouse: histopathology of the soleus and extensor digitorum longus muscles." J Neurol Sci 80(1): 39-54.

Chamberlain, J. S., J. Metzger, M. Reyes, D. Townsend and J. A. Faulkner (2007). "Dystrophin-deficient mdx mice display a reduced life span and are susceptible to spontaneous rhabdomyosarcoma." FASEB J 21(9): 2195-2204.

Chan, S., S. I. Head and J. W. Morley (2007). "Branched fibers in dystrophic mdx muscle are associated with a loss of force following lengthening contractions." Am J Physiol Cell Physiol 293(3): C985-992.

Chung, K. and K. Deisseroth (2013). "CLARITY for mapping the nervous system." Nat Methods 10(6): 508-513.

Chung, K., J. Wallace, S. Y. Kim, S. Kalyanasundaram, A. S. Andalman, T. J. Davidson, J. J. Mirzabekov, K. A. Zalocusky, J. Mattis, A. K. Denisin, S. Pak, H. Bernstein, C. Ramakrishnan, L. Grosenick, V. Gradinaru and K. Deisseroth (2013). "Structural and molecular interrogation of intact biological systems." Nature 497(7449): 332-337.

Ciafaloni, E., A. Kumar, K. Liu, S. Pandya, C. Westfield, D. J. Fox, K. M. Caspers Conway, C. Cunniff, K. Mathews, N. West, P. A. Romitti and M. P. McDermott (2016). "Age at onset of first signs or symptoms predicts age at loss of ambulation in Duchenne and Becker Muscular Dystrophy: Data from the MD STARnet." J Pediatr Rehabil Med 9(1): 5-11.

Ciruna, B. and J. Rossant (2001). "FGF signaling regulates mesoderm cell fate specification and morphogenetic movement at the primitive streak." Dev Cell 1(1): 37-49.

Condon, K., L. Silberstein, H. M. Blau and W. J. Thompson (1990). "Differentiation of fiber types in aneural musculature of the prenatal rat hindlimb." Dev Biol 138(2): 275-295.

Coulton, G. R., J. E. Morgan, T. A. Partridge and J. C. Sloper (1988). "The mdx mouse skeletal muscle myopathy: I. A histological, morphometric and biochemical investigation." Neuropathol Appl Neurobiol 14(1): 53-70.

Dangain, J. and G. Vrbova (1984). "Muscle development in mdx mutant mice." Muscle Nerve 7(9): 700-704.

Darras, B. T., P. Blattner, J. F. Harper, A. J. Spiro, S. Alter and U. Francke (1988). "Intragenic deletions in 21 Duchenne muscular dystrophy (DMD)/Becker muscular dystrophy (BMD) families studied with the dystrophin cDNA: location of breakpoints on HindIII and BglII exon-containing fragment maps, meiotic and mitotic origin of the mutations." Am J Hum Genet 43(5): 620-629.

DelloRusso, C., J. M. Scott, D. Hartigan-O'Connor, G. Salvatori, C. Barjot, A. S. Robinson, R. W. Crawford, S. V. Brooks and J. S. Chamberlain (2002). "Functional correction of adult mdx mouse muscle using gutted adenoviral vectors expressing full-length dystrophin." Proc Natl Acad Sci U S A 99(20): 12979-12984.

Doherty, K. R. and E. M. McNally (2003). "Repairing the tears: dysferlin in muscle membrane repair." Trends Mol Med 9(8): 327-330.

Du, L. and R. A. Gatti (2009). "Progress toward therapy with antisense-mediated splicing modulation." Curr Opin Mol Ther 11(2): 116-123.

Duddy, W., S. Duguez, H. Johnston, T. V. Cohen, A. Phadke, H. Gordish-Dressman, K. Nagaraju, V. Gnocchi, S. Low and T. Partridge (2015). "Muscular dystrophy in the mdx mouse is a severe myopathy compounded by hypotrophy, hypertrophy and hyperplasia." Skelet Muscle 5: 16.

Dudley, R. W., Y. Lu, R. Gilbert, S. Matecki, J. Nalbantoglu, B. J. Petrof and G. Karpati (2004). "Sustained improvement of muscle function one year after full-length dystrophin gene transfer into mdx mice by a gutted helper-dependent adenoviral vector." Hum Gene Ther 15(2): 145-156.

Echevarria, L., P. Aupy and A. Goyenvalle (2018). "Exon-skipping advances for Duchenne muscular dystrophy." Hum Mol Genet 27(R2): R163-R172.

Emery, A. E. (2002). "The muscular dystrophies." Lancet 359(9307): 687-695.

Engel, A. G., and Ozawa, E. (2004). “Dystrophinopathies,” in Myology, Vol. 2, eds A. G. Engel and C. Franzini-Armstrong (New-York, NY: McGraw-Hill), 961–1026.

Englander, L. L. and L. L. Rubin (1987). "Acetylcholine receptor clustering and nuclear movement in muscle fibers in culture." J Cell Biol 104(1): 87-95.

Faber, R. M., J. K. Hall, J. S. Chamberlain and G. B. Banks (2014). "Myofiber branching rather than myofiber hyperplasia contributes to muscle hypertrophy in mdx mice." Skelet Muscle 4: 10.

Fall, A. M., R. Johnsen, K. Honeyman, P. Iversen, S. Fletcher and S. D. Wilton (2006). "Induction of revertant fibres in the mdx mouse using antisense oligonucleotides." Genet Vaccines Ther 4: 3.

Faulkner, J. A., L. M. Larkin, D. R. Claflin and S. V. Brooks (2007). "Age-related changes in the structure and function of skeletal muscles." Clin Exp Pharmacol Physiol 34(11): 1091-1096.

Ferns, M. J., J. T. Campanelli, W. Hoch, R. H. Scheller and Z. Hall (1993). "The ability of agrin to cluster AChRs depends on alternative splicing and on cell surface proteoglycans." Neuron 11(3): 491-502.

Fisher, A. L. (2004). "Of worms and women: sarcopenia and its role in disability and mortality." J Am Geriatr Soc 52(7): 1185-1190.

Folker, E. S. and M. K. Baylies (2013). "Nuclear positioning in muscle development and disease." Front Physiol 4: 363.

Gautam, M., P. G. Noakes, J. Mudd, M. Nichol, G. C. Chu, J. R. Sanes and J. P. Merlie (1995). "Failure of postsynaptic specialization to develop at neuromuscular junctions of rapsyn-deficient mice." Nature 377(6546): 232-236.

Gensler, S., A. Sander, A. Korngreen, G. Traina, G. Giese and V. Witzemann (2001). "Assembly and clustering of acetylcholine receptors containing GFP-tagged epsilon or gamma subunits: selective targeting to the neuromuscular junction in vivo." Eur J Biochem 268(8): 2209-2217.

Gillies, A. R. and R. L. Lieber (2011). "Structure and function of the skeletal muscle extracellular matrix." Muscle Nerve 44(3): 318-331.

Grady, R. M., D. A. Starr, G. L. Ackerman, J. R. Sanes and M. Han (2005). "Syne proteins anchor muscle nuclei at the neuromuscular junction." Proc Natl Acad Sci U S A 102(12): 4359-4364.

Griffin, J. W. and W. J. Thompson (2008). "Biology and pathology of nonmyelinating Schwann cells." Glia 56(14): 1518-1531.

Gros, J., M. Scaal and C. Marcelle (2004). "A two-step mechanism for myotome formation in chick." Dev Cell 6(6): 875-882.

Gundersen, K. (2016). "Muscle memory and a new cellular model for muscle atrophy and hypertrophy." J Exp Biol 219(Pt 2): 235-242.

Haddix, S. G., Y. I. Lee, J. N. Kornegay and W. J. Thompson (2018). "Cycles of myofiber degeneration and regeneration lead to remodeling of the neuromuscular junction in two mammalian models of Duchenne muscular dystrophy." PLoS One 13(10): e0205926.

Hall, Z. W. and E. Ralston (1989). "Nuclear domains in muscle cells." Cell 59(5): 771-772.

Hall, Z. W. and J. R. Sanes (1993). "Synaptic structure and development: the neuromuscular junction." Cell 72 Suppl: 99-121.

Han, H., S. H. Yang and W. D. Phillips (2000). "Overexpression of rapsyn modifies the intracellular trafficking of acetylcholine receptors." J Neurosci Res 60(2): 155-163.

Han, R. and K. P. Campbell (2007). "Dysferlin and muscle membrane repair." Curr Opin Cell Biol 19(4): 409-416.

Hepple, R. T. (2012). "Muscle atrophy is not always sarcopenia." J Appl Physiol (1985) 113(4): 677-679.

Hernandez-Deviez, D. J., M. T. Howes, S. H. Laval, K. Bushby, J. F. Hancock and R. G. Parton (2008). "Caveolin regulates endocytosis of the muscle repair protein, dysferlin." J Biol Chem 283(10): 6476-6488.

Hoffman, E. P., R. H. Brown, Jr. and L. M. Kunkel (1987). "Dystrophin: the protein product of the Duchenne muscular dystrophy locus." Cell 51(6): 919-928.

Horst, D., S. Ustanina, C. Sergi, G. Mikuz, H. Juergens, T. Braun and E. Vorobyov (2006). "Comparative expression analysis of Pax3 and Pax7 during mouse myogenesis." Int J Dev Biol 50(1): 47-54.

Hubaud, A. and O. Pourquie (2014). "Signalling dynamics in vertebrate segmentation." Nat Rev Mol Cell Biol 15(11): 709-721.

Hutcheson, D. A., J. Zhao, A. Merrell, M. Haldar and G. Kardon (2009). "Embryonic and fetal limb myogenic cells are derived from developmentally distinct progenitors and have different requirements for beta-catenin." Genes Dev 23(8): 997-1013.

Janssen, I., D. S. Shepard, P. T. Katzmarzyk and R. Roubenoff (2004). "The healthcare costs of sarcopenia in the United States." J Am Geriatr Soc 52(1): 80-85.

Jevsek, M. and S. J. Burden (2006). "Microarray screen for synaptic genes in the neuromuscular junction." J Mol Neurosci 30(1-2): 29-30.

Jevsek, M., A. Jaworski, L. Polo-Parada, N. Kim, J. Fan, L. T. Landmesser and S. J. Burden (2006a). "CD24 is expressed by myofiber synaptic nuclei and regulates synaptic transmission." Proc Natl Acad Sci U S A 103(16): 6374-6379.

Jevsek, M., A. Jaworski, L. Polo-Parada, N. Kim, J. Fan, L. T. Landmesser and S. J. Burden (2006b). "CD24 is expressed by myofiber synaptic nuclei and regulates synaptic transmission." Proc Natl Acad Sci U S A 103(16): 6374-6379.

Jirmanova, I. and S. Thesleff (1972). "Ultrastructural study of experimental muscle degeneration and regeneration in the adult rat." Z Zellforsch Mikrosk Anat 131(1): 77-97.

Jung, D., B. Yang, J. Meyer, J. S. Chamberlain and K. P. Campbell (1995). "Identification and characterization of the dystrophin anchoring site on beta-dystroglycan." J Biol Chem 270(45): 27305-27310.

Kang, H. and J. W. Lichtman (2013). "Motor axon regeneration and muscle reinnervation in young adult and aged animals." J Neurosci 33(50): 19480-19491.

Kang, H., L. Tian, M. Mikesh, J. W. Lichtman and W. J. Thompson (2014). "Terminal Schwann cells participate in neuromuscular synapse remodeling during reinnervation following nerve injury." J Neurosci 34(18): 6323-6333.

Kang, H., L. Tian and W. Thompson (2003). "Terminal Schwann cells guide the reinnervation of muscle after nerve injury." J Neurocytol 32(5-8): 975-985.

Kassar-Duchossoy, L., E. Giacone, B. Gayraud-Morel, A. Jory, D. Gomes and S. Tajbakhsh (2005). "Pax3/Pax7 mark a novel population of primitive myogenic cells during development." Genes Dev 19(12): 1426-1431.

Kawamura, Y., P. O'Brien, H. Okazaki and P. J. Dyck (1977). "Lumbar motoneurons of man II: the number and diameter distribution of large- and intermediate-diameter cytons in "motoneuron columns" of spinal cord of man." J Neuropathol Exp Neurol 36(5): 861-870.

Ke, M. T., S. Fujimoto and T. Imai (2013). "SeeDB: a simple and morphology-preserving optical clearing agent for neuronal circuit reconstruction." Nat Neurosci 16(8): 1154-1161.

Kelly, A. M. and S. I. Zacks (1969). "The fine structure of motor endplate morphogenesis." J Cell Biol 42(1): 154-169.

Kim, N. and S. J. Burden (2008). "MuSK controls where motor axons grow and form synapses." Nat Neurosci 11(1): 19-27.

Kim, N., A. L. Stiegler, T. O. Cameron, P. T. Hallock, A. M. Gomez, J. H. Huang, S. R. Hubbard, M. L. Dustin and S. J. Burden (2008). "Lrp4 is a receptor for Agrin and forms a complex with MuSK." Cell 135(2): 334-342.

Ko, C. P. and R. Robitaille (2015). "Perisynaptic Schwann Cells at the Neuromuscular Synapse: Adaptable, Multitasking Glial Cells." Cold Spring Harb Perspect Biol 7(10): a020503.

Kornegay, J. N., M. K. Childers, D. J. Bogan, J. R. Bogan, P. Nghiem, J. Wang, Z. Fan, J. F. Howard, Jr., S. J. Schatzberg, J. L. Dow, R. W. Grange, M. A. Styner, E. P. Hoffman and K. R. Wagner (2012). "The paradox of muscle hypertrophy in muscular dystrophy." Phys Med Rehabil Clin N Am 23(1): 149-172, xii.

Kuwajima, T., A. A. Sitko, P. Bhansali, C. Jurgens, W. Guido and C. Mason (2013). "ClearT: a detergent- and solvent-free clearing method for neuronal and non-neuronal tissue." Development 140(6): 1364-1368.

Lee, E., J. Choi, Y. Jo, J. Y. Kim, Y. J. Jang, H. M. Lee, S. Y. Kim, H. J. Lee, K. Cho, N. Jung, E. M. Hur, S. J. Jeong, C. Moon, Y. Choe, I. J. Rhyu, H. Kim and W. Sun (2016). "ACT-PRESTO: Rapid and consistent tissue clearing and labeling method for 3-dimensional (3D) imaging." Sci Rep 6: 18631.

Lee, Y. I., Y. Li, M. Mikesh, I. Smith, K. A. Nave, M. H. Schwab and W. J. Thompson (2016). "Neuregulin1 displayed on motor axons regulates terminal Schwann cell-mediated synapse elimination at developing neuromuscular junctions." Proc Natl Acad Sci U S A 113(4): E479-487.

Lefaucheur, J. P., C. Pastoret and A. Sebille (1995). "Phenotype of dystrophinopathy in old mdx mice." Anat Rec 242(1): 70-76.

Lehman, W., P. Vibert, P. Uman and R. Craig (1995). "Steric-blocking by tropomyosin visualized in relaxed vertebrate muscle thin filaments." J Mol Biol 251(2): 191-196.

Lepper, C., T. A. Partridge and C. M. Fan (2011). "An absolute requirement for Pax7-positive satellite cells in acute injury-induced skeletal muscle regeneration." Development 138(17): 3639-3646.

Lexell, J., D. Downham and M. Sjostrom (1986). "Distribution of different fibre types in human skeletal muscles. Fibre type arrangement in m. vastus lateralis from three groups of healthy men between 15 and 83 years." J Neurol Sci 72(2-3): 211-222.

Lexell, J., C. C. Taylor and M. Sjostrom (1988). "What is the cause of the ageing atrophy? Total number, size and proportion of different fiber types studied in whole vastus lateralis muscle from 15- to 83-year-old men." J Neurol Sci 84(2-3): 275-294.

Li, L., W. C. Xiong and L. Mei (2018). "Neuromuscular Junction Formation, Aging, and Disorders." Annu Rev Physiol 80: 159-188.

Li, Y., Y. Lee and W. J. Thompson (2011). "Changes in aging mouse neuromuscular junctions are explained by degeneration and regeneration of muscle fiber segments at the synapse." J Neurosci 31(42): 14910-14919.

Li, Y. and W. J. Thompson (2011). "Nerve terminal growth remodels neuromuscular synapses in mice following regeneration of the postsynaptic muscle fiber." J Neurosci 31(37): 13191-13203.

Lyons, G. E., M. Ontell, R. Cox, D. Sassoon and M. Buckingham (1990). "The expression of myosin genes in developing skeletal muscle in the mouse embryo." J Cell Biol 111(4): 1465-1476.

Lyons, P. R. and C. R. Slater (1991). "Structure and function of the neuromuscular junction in young adult mdx mice." J Neurocytol 20(12): 969-981.

Manzur, A. Y., T. Kuntzer, M. Pike and A. Swan (2008). "Glucocorticoid corticosteroids for Duchenne muscular dystrophy." Cochrane Database Syst Rev(1): CD003725.

Marini, J. F., F. Pons, J. Leger, N. Loffreda, M. Anoal, M. Chevallay, M. Fardeau and J. J. Leger (1991). "Expression of myosin heavy chain isoforms in Duchenne muscular dystrophy patients and carriers." Neuromuscul Disord 1(6): 397-409.

Marques, M. J., J. A. Conchello and J. W. Lichtman (2000). "From plaque to pretzel: fold formation and acetylcholine receptor loss at the developing neuromuscular junction." J Neurosci 20(10): 3663-3675.

Marshall, L. M., J. R. Sanes and U. J. McMahan (1977). "Reinnervation of original synaptic sites on muscle fiber basement membrane after disruption of the muscle cells." Proc Natl Acad Sci U S A 74(7): 3073-3077.

McClung, J. M., J. M. Davis and J. A. Carson (2007). "Ovarian hormone status and skeletal muscle inflammation during recovery from disuse in rats." Exp Physiol 92(1): 219-232.

McDade, J. R., A. Archambeau and D. E. Michele (2014). "Rapid actin-cytoskeleton-dependent recruitment of plasma membrane-derived dysferlin at wounds is critical for muscle membrane repair." FASEB J 28(8): 3660-3670.

McMahan, U. J. (1990). "The agrin hypothesis." Cold Spring Harb Symp Quant Biol 55: 407-418.

Milgroom, A. and E. Ralston (2016). "Clearing skeletal muscle with CLARITY for light microscopy imaging." Cell Biol Int 40(4): 478-483.

Minatel, E., H. S. Neto and M. J. Marques (2003). "Acetylcholine receptor distribution and synapse elimination at the developing neuromuscular junction of mdx mice." Muscle Nerve 28(5): 561-569.

Moens, P., P. H. Baatsen and G. Marechal (1993). "Increased susceptibility of EDL muscles from mdx mice to damage induced by contractions with stretch." J Muscle Res Cell Motil 14(4): 446-451.

Moransard, M., L. S. Borges, R. Willmann, P. A. Marangi, H. R. Brenner, M. J. Ferns and C. Fuhrer (2003). "Agrin regulates rapsyn interaction with surface acetylcholine receptors, and this underlies cytoskeletal anchoring and clustering." J Biol Chem 278(9): 7350-7359.

Moxley, R. T., 3rd, S. Pandya, E. Ciafaloni, D. J. Fox and K. Campbell (2010). "Change in natural history of Duchenne muscular dystrophy with long-term corticosteroid treatment: implications for management." J Child Neurol 25(9): 1116-1129.

Nagel, A., F. Lehmann-Horn and A. G. Engel (1990). "Neuromuscular transmission in the mdx mouse." Muscle Nerve 13(8): 742-749.

Nguyen, Q. T., J. R. Sanes and J. W. Lichtman (2002). "Pre-existing pathways promote precise projection patterns." Nat Neurosci 5(9): 861-867.

Nishimune, H., J. R. Sanes and S. S. Carlson (2004). "A synaptic laminin-calcium channel interaction organizes active zones in motor nerve terminals." Nature 432(7017): 580-587.

Nowak, K. J. and K. E. Davies (2004). "Duchenne muscular dystrophy and dystrophin: pathogenesis and opportunities for treatment." EMBO Rep 5(9): 872-876.

Olguin, H. C., Z. Yang, S. J. Tapscott and B. B. Olwin (2007). "Reciprocal inhibition between Pax7 and muscle regulatory factors modulates myogenic cell fate determination." J Cell Biol 177(5): 769-779.

Ontell, M. (1981). "Muscle fiber necrosis in murine dystrophy." Muscle Nerve 4(3): 204-213.

Ott, M. O., E. Bober, G. Lyons, H. Arnold and M. Buckingham (1991). "Early expression of the myogenic regulatory gene, myf-5, in precursor cells of skeletal muscle in the mouse embryo." Development 111(4): 1097-1107.

Pagel, C. N. and T. A. Partridge (1999). "Covert persistence of mdx mouse myopathy is revealed by acute and chronic effects of irradiation." J Neurol Sci 164(2): 103-116.

Palacios, D., C. Mozzetta, S. Consalvi, G. Caretti, V. Saccone, V. Proserpio, V. E. Marquez, S. Valente, A. Mai, S. V. Forcales, V. Sartorelli and P. L. Puri (2010). "TNF/p38alpha/polycomb signaling to Pax7 locus in satellite cells links inflammation to the epigenetic control of muscle regeneration." Cell Stem Cell 7(4): 455-469.

Passamano, L., A. Taglia, A. Palladino, E. Viggiano, P. D'Ambrosio, M. Scutifero, M. Rosaria Cecio, V. Torre, D. E. L. F, E. Picillo, O. Paciello, G. Piluso, G. Nigro and L. Politano (2012). "Improvement of survival in Duchenne Muscular Dystrophy: retrospective analysis of 835 patients." Acta Myol 31(2): 121-125.

Passos-Bueno, M. R., E. Bakker, A. L. Kneppers, R. I. Takata, D. Rapaport, J. T. den Dunnen, M. Zatz and G. J. van Ommen (1992). "Different mosaicism frequencies for proximal and distal Duchenne muscular dystrophy (DMD) mutations indicate difference in etiology and recurrence risk." Am J Hum Genet 51(5): 1150-1155.

Pastoret, C. and A. Sebille (1993a). "Further aspects of muscular dystrophy in mdx mice." Neuromuscul Disord 3(5-6): 471-475.

Pastoret, C. and A. Sebille (1993b). "Time course study of the isometric contractile properties of mdx mouse striated muscles." J Muscle Res Cell Motil 14(4): 423-431.

Patton, B. L., A. M. Connoll, P. T. Martin, J. M. Cunningham, S. Mehta, A. Pestronk, J. H. Miner and J. R. Sanes (1999). "Distribution of ten laminin chains in dystrophic and regenerating muscles." Neuromuscul Disord 9(6-7): 423-433.

Pavlath, G. K., K. Rich, S. G. Webster and H. M. Blau (1989). "Localization of muscle gene products in nuclear domains." Nature 337(6207): 570-573.

Pichavant, C., P. Chapdelaine, D. G. Cerri, J. C. Dominique, S. P. Quenneville, D. Skuk, J. N. Kornegay, J. C. Bizario, X. Xiao and J. P. Tremblay (2010). "Expression of dog microdystrophin in mouse and dog muscles by gene therapy." Mol Ther 18(5): 1002-1009.

Pichavant, C. and G. K. Pavlath (2014). "Incidence and severity of myofiber branching with regeneration and aging." Skelet Muscle 4: 9.

Porter, G. A., G. M. Dmytrenko, J. C. Winkelmann and R. J. Bloch (1992). "Dystrophin colocalizes with beta-spectrin in distinct subsarcolemmal domains in mammalian skeletal muscle." J Cell Biol 117(5): 997-1005.

Prins, K. W., J. L. Humston, A. Mehta, V. Tate, E. Ralston and J. M. Ervasti (2009). "Dystrophin is a microtubule-associated protein." J Cell Biol 186(3): 363-369.

Reimers, C. D., B. Schlotter, B. M. Eicke and T. N. Witt (1996). "Calf enlargement in neuromuscular diseases: a quantitative ultrasound study in 350 patients and review of the literature." J Neurol Sci 143(1-2): 46-56.

Rich, M. and J. W. Lichtman (1989). "Motor nerve terminal loss from degenerating muscle fibers." Neuron 3(6): 677-688.

Robitaille, R. (1998). "Modulation of synaptic efficacy and synaptic depression by glial cells at the frog neuromuscular junction." Neuron 21(4): 847-855.

Rowe, R. W. (1969). "The effect of senility on skeletal muscles in the mouse." Exp Gerontol 4(2): 119-126.

Ruegg, M. A., K. W. Tsim, S. E. Horton, S. Kroger, G. Escher, E. M. Gensch and U. J. McMahan (1992). "The agrin gene codes for a family of basal lamina proteins that differ in function and distribution." Neuron 8(4): 691-699.

Sacco, A., F. Mourkioti, R. Tran, J. Choi, M. Llewellyn, P. Kraft, M. Shkreli, S. Delp, J. H. Pomerantz, S. E. Artandi and H. M. Blau (2010). "Short telomeres and stem cell exhaustion model Duchenne muscular dystrophy in mdx/mTR mice." Cell 143(7): 1059-1071.

Sadoulet-Puccio, H. M., M. Rajala and L. M. Kunkel (1997). "Dystrobrevin and dystrophin: an interaction through coiled-coil motifs." Proc Natl Acad Sci U S A 94(23): 12413-12418.

Sanes, J. R., Y. R. Johnson, P. T. Kotzbauer, J. Mudd, T. Hanley, J. C. Martinou and J. P. Merlie (1991). "Selective expression of an acetylcholine receptor-lacZ transgene in synaptic nuclei of adult muscle fibers." Development 113(4): 1181-1191.

Sanes, J. R. and J. W. Lichtman (1999). "Development of the vertebrate neuromuscular junction." Annu Rev Neurosci 22: 389-442.

Sasaki, T., K. Mann, J. H. Miner, N. Miosge and R. Timpl (2002). "Domain IV of mouse laminin beta1 and beta2 chains." Eur J Biochem 269(2): 431-442.

Sassoon, D. A., I. Garner and M. Buckingham (1988). "Transcripts of alpha-cardiac and alpha-skeletal actins are early markers for myogenesis in the mouse embryo." Development 104(1): 155-164.

Selchow and Huisken (2013). “Light sheet fluorescence microscopy and revolutionary 3D analyses of live specimens.” Photonik international 17(3): 44-47.

Sheard, P. W. and R. D. Anderson (2012). "Age-related loss of muscle fibres is highly variable amongst mouse skeletal muscles." Biogerontology 13(2): 157-167.

Shioi, G., H. Kiyonari, T. Abe, K. Nakao, T. Fujimori, C. W. Jang, C. C. Huang, H. Akiyama, R. R. Behringer and S. Aizawa (2011). "A mouse reporter line to conditionally mark nuclei and cell membranes for in vivo live-imaging." Genesis 49(7): 570-578.

Simon, A. M., P. Hoppe and S. J. Burden (1992). "Spatial restriction of AChR gene expression to subsynaptic nuclei." Development 114(3): 545-553.

Slater, C. R. (1982). "Postnatal maturation of nerve-muscle junctions in hindlimb muscles of the mouse." Dev Biol 94(1): 11-22.

Smith, I. W., M. Mikesh, Y. Lee and W. J. Thompson (2013). "Terminal Schwann cells participate in the competition underlying neuromuscular synapse elimination." J Neurosci 33(45): 17724-17736.

Snow, M. H. (1977). "Myogenic cell formation in regenerating rat skeletal muscle injured by mincing. I. A fine structural study." Anat Rec 188(2): 181-199.

Son, Y. J. and W. J. Thompson (1995). "Schwann cell processes guide regeneration of peripheral axons." Neuron 14(1): 125-132.

Spiro, A. J., G. M. Shy and N. K. Gonatas (1966). "Myotubular myopathy. Persistence of fetal muscle in an adolescent boy." Arch Neurol 14(1): 1-14.

Stanmore, A., S. Bradbury and A. G. Weddell (1978). "A quantitative study of peripheral nerve fibres in the mouse following the administration of drugs. 1. Age changes in untreated CBA mice from 3 to 21 months of age." J Anat 127(Pt 1): 101-115.

Stone, M. R., A. O'Neill, D. Catino and R. J. Bloch (2005). "Specific interaction of the actin-binding domain of dystrophin with intermediate filaments containing keratin 19." Mol Biol Cell 16(9): 4280-4293.

Stone, M. R., A. O'Neill, R. M. Lovering, J. Strong, W. G. Resneck, P. W. Reed, D. M. Toivola, J. A. Ursitti, M. B. Omary and R. J. Bloch (2007). "Absence of keratin 19 in mice causes skeletal myopathy with mitochondrial and sarcolemmal reorganization." J Cell Sci 120(Pt 22): 3999-4008.

Straub, V. and K. P. Campbell (1997). "Muscular dystrophies and the dystrophin-glycoprotein complex." Curr Opin Neurol 10(2): 168-175.

Studitsky, A. N. (1964). "Free Auto- and Homografts of Muscle Tissue in Experiments on Animals." Ann N Y Acad Sci 120: 789-801.

Sugita, S., L. L. Fleming, C. Wood, S. K. Vaughan, M. P. Gomes, W. Camargo, L. A. Naves, V. F. Prado, M. A. Prado, C. Guatimosim and G. Valdez (2016). "VAChT overexpression increases acetylcholine at the synaptic cleft and accelerates aging of neuromuscular junctions." Skelet Muscle 6: 31.

Susaki, E. A., K. Tainaka, D. Perrin, H. Yukinaga, A. Kuno and H. R. Ueda (2015). "Advanced CUBIC protocols for whole-brain and whole-body clearing and imaging." Nat Protoc 10(11): 1709-1727.

Swash, M. and M. S. Schwartz (1977). "Implications of longitudinal muscle fibre splitting in neurogenic and myopathic disorders." J Neurol Neurosurg Psychiatry 40(12): 1152-1159.

Taetzsch, T., M. J. Tenga and G. Valdez (2017). "Muscle Fibers Secrete FGFBP1 to Slow Degeneration of Neuromuscular Synapses during Aging and Progression of ALS." J Neurosci 37(1): 70-82.

Takada, S., K. L. Stark, M. J. Shea, G. Vassileva, J. A. McMahon and A. P. McMahon (1994). "Wnt-3a regulates somite and tailbud formation in the mouse embryo." Genes Dev 8(2): 174-189.

Talbot, J. and L. Maves (2016). "Skeletal muscle fiber type: using insights from muscle developmental biology to dissect targets for susceptibility and resistance to muscle disease." Wiley Interdiscip Rev Dev Biol 5(4): 518-534.

Tanabe, Y., K. Esaki and T. Nomura (1986). "Skeletal muscle pathology in X chromosome-linked muscular dystrophy (mdx) mouse." Acta Neuropathol 69(1-2): 91-95.

Terada, M., F. Kawano, T. Ohira, N. Nakai, N. Nishimoto and Y. Ohira (2012). "Effects of mechanical over-loading on the properties of soleus muscle fibers, with or without damage, in wild type and mdx mice." PLoS One 7(4): e34557.

Tews, D. S. and H. H. Goebel (1997). "DNA-fragmentation and expression of apoptosis-related proteins in muscular dystrophies." Neuropathol Appl Neurobiol 23(4): 331-338.

Tews, D. S., H. H. Goebel and H. M. Meinck (1997). "DNA-fragmentation and apoptosis-related proteins of muscle cells in motor neuron disorders." Acta Neurol Scand 96(6): 380-386.

Theroux, M. C., A. Olivant and R. E. Akins (2008). "C Histomorphology of neuromuscular junction in Duchenne muscular dystrophy." Paediatr Anaesth 18(3): 256-259.

Thompson, W. (1983). "Synapse elimination in neonatal rat muscle is sensitive to pattern of muscle use." Nature 302(5909): 614-616.

Tomlinson, B. E., J. N. Walton and D. Irving (1974). "Spinal cord limb motor neurones in muscular dystrophy." J Neurol Sci 22(3): 305-327.

Tzartos, S. J., D. E. Rand, B. L. Einarson and J. M. Lindstrom (1981). "Mapping of surface structures of electrophorus acetylcholine receptor using monoclonal antibodies." J Biol Chem 256(16): 8635-8645.

Valdez, G., J. C. Tapia, H. Kang, G. D. Clemenson, Jr., F. H. Gage, J. W. Lichtman and J. R. Sanes (2010). "Attenuation of age-related changes in mouse neuromuscular synapses by caloric restriction and exercise." Proc Natl Acad Sci U S A 107(33): 14863-14868.

van der Pijl, E. M., M. van Putten, E. H. Niks, J. J. Verschuuren, A. Aartsma-Rus and J. J. Plomp (2016). "Characterization of neuromuscular synapse function abnormalities in multiple Duchenne muscular dystrophy mouse models." Eur J Neurosci 43(12): 1623-1635.

Van Horn, R. and M. T. Crow (1989). "Fast myosin heavy chain expression during the early and late embryonic stages of chicken skeletal muscle development." Dev Biol 134(2): 279-288.

van Ruiten, H. J., V. Straub, K. Bushby and M. Guglieri (2014). "Improving recognition of Duchenne muscular dystrophy: a retrospective case note review." Arch Dis Child 99(12): 1074-1077.

Wada, K., S. Katsuta and H. Soya (2008). "Formation process and fate of the nuclear chain after injury in regenerated myofiber." Anat Rec (Hoboken) 291(1): 122-128.

Wada, K. I., S. Katsuta and H. Soya (2003). "Natural occurrence of myofiber cytoplasmic enlargement accompanied by decrease in myonuclear number." Jpn J Physiol 53(2): 145-150.

Weller, T. J., A. Zheng, R. Thompson and F. Tulleners (2012). "Confocal microscopy analysis of breech face marks on fired cartridge cases from 10 consecutively manufactured pistol slides." J Forensic Sci 57(4): 912-917.

Whalen, R. G., J. B. Harris, G. S. Butler-Browne and S. Sesodia (1990). "Expression of myosin isoforms during notexin-induced regeneration of rat soleus muscles." Dev Biol 141(1): 24-40.

Willadt, S., M. Nash and C. R. Slater (2016). "Age-related fragmentation of the motor endplate is not associated with impaired neuromuscular transmission in the mouse diaphragm." Sci Rep 6: 24849.

Williams, M. P. I., M. Rigon, T. Straka, S. J. Horner, M. Thiel, N. Gretz, M. Hafner, M. Reischl and R. Rudolf (2019). "A Novel Optical Tissue Clearing Protocol for Mouse Skeletal Muscle to Visualize Endplates in Their Tissue Context." Front Cell Neurosci 13: 49.

Yue, Y., Z. Li, S. Q. Harper, R. L. Davisson, J. S. Chamberlain and D. Duan (2003). "Microdystrophin gene therapy of cardiomyopathy restores dystrophin-glycoprotein complex and improves sarcolemma integrity in the mdx mouse heart." Circulation 108(13): 1626-1632.

Yumoto, N., N. Kim and S. J. Burden (2012). "Lrp4 is a retrograde signal for presynaptic differentiation at neuromuscular synapses." Nature 489(7416): 438-442.

Zatz, M., D. Rapaport, M. Vainzof, M. R. Passos-Bueno, E. R. Bortolini, C. Pavanello Rde and C. A. Peres (1991). "Serum creatine-kinase (CK) and pyruvate-kinase (PK) activities in Duchenne (DMD) as compared with Becker (BMD) muscular dystrophy." J Neurol Sci 102(2): 190-196.

Zuo, Y., J. L. Lubischer, H. Kang, L. Tian, M. Mikesh, A. Marks, V. L. Scofield, S. Maika, C. Newman, P. Krieg and W. J. Thompson (2004). "Fluorescent proteins expressed in mouse transgenic lines mark subsets of glia, neurons, macrophages, and dendritic cells for vital examination." J Neurosci 24(49): 10999-11009.